Title
HIGH TEMPERATURE SPECTROSCOPY AND THERMODYNAMICS OF TITANIUM OXIDE AND VANADIUM OXIDE

Author
Chang, Shih-Ger.

Publication Date
1972-03-01

LBL-450
c.2

HIGH TEMPERATURE SPECTROSCOPY AND THERMODYNAMICS OF TITANIUM OXIDE AND VANADIUM OXIDE

Shih-Ger Chang
(Ph. D. Thesis)

March 1972

AEC Contract No. W-7405-eng-48

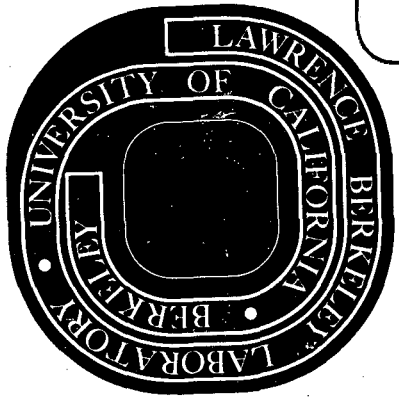

LBL-450
c.2

DISCLAIMER

TABLE OF CONTENTS

LIST OF TABLES

LIST OF FIGURES

HIGH TEMPERATURE SPECTROSCOPY AND THERMODYNAMICS OF TITANIUM OXIDE AND VANADIUM OXIDE

Shih-Ger Chang

Inorganic Materials Research Division, Lawrence Berkeley Laboratory,
and Department of Chemistry; University of California
Berkeley, California 94720

ABSTRACT

Absolute emission measurements of (0,0) band of TiO α-system and VO green system were made on photographic plates. The TiO vapors were in equilibrium with $TiO_{1.6}$ liquid phase at 2140 to 2400°K and VO vapors were in equilibrium with VO solid and liquid phases at 2000 to 2150°K in an electric furnace. The integrated radiance of the band were determined by matching the observed profiles with the profiles determined theoretically.

The radiance measurements and equilibrium partial vapor pressures of TiO and VO from mass spectroscopy and thermodynamic data yield: $f_{em} = 0.144$ for TiO (0,0) band $C^3\Delta$-$X^3\Delta$ transition, and $f_{em} = 0.0058$ for VO (0,0) band $C^4\Sigma^-$-$X^4\Sigma^-$ transition. These correspond to an upper bound of radiative lifetime of 2.82×10^{-8} sec. for v' = 0 $C^3\Delta$ state of TiO and 8.65×10^{-7} sec. for v' = 0 $C^4\Sigma^-$ state of VO.

I. ENERGY LEVEL DIAGRAMS

A. Titanium Monoxide

1. Discovered and Expected Electronic States

The electronic spectrum of TiO has been extensively studied during the past four decades. Eleven band systems containing five triplets and six singlets have been observed. However, only six band systems, three triplets (α, γ, γ') and three singlets (β, δ, ϕ) have been rather thoroughly analyzed.

Among the triplet systems, rotational analysis of (1,0), (0,0) and (0,1) bands of the α-system in the blue-green were carried out by Christy[1] (1929), and assigned to a $^3\Pi$ - $^3\Pi$ transition.

Vibrational analysis of γ-system in the red by Lowater[2] (1929) showed that the lower state of the γ-system is the same as the lower state of the α-system as analyzed by Christy. From the fact that the presence of strong Q branches in the bands of the γ-system that require $\Delta\Lambda = \pm 1$, Lowater concluded that the γ-system was produced by an $A^3\Sigma$ - $X^3\Pi$ transition, since he proposed that the TiO molecule might resemble the electronic configuration with the Ca atom. This implies that O, having gained two electrons from Ti, resembles as an inert Ne atom, while Ti, having lost two electrons, resembles Ca. Rotational analysis on (1,0), (0,0) and (0,1) bands of the γ-system in the red were carried out by Phillips[3] (1951). The fact that the violet, central, and red sub-bands had the combination difference $\Delta_2F_3''(J)$, $\Delta_2F_2''(J)$ and $\Delta_1F_1''(J)$ respectively together with the equations of Budo's[4] for

the terms of a $^3\Pi$ state (i.e., the terms $F_3(J)$ were highest, followed by $F_2(J)$ and $F_1(J)$) led Phillips to suggest that the upper electronic state of the γ-system must have a greater triplet splitting than the ground state $X^3\Pi$. Therefore, it could not be a $^3\Sigma$ state which is a single state for a non-rotating molecule. The transition $A^3\Delta$ - $X^3\Pi$ was then assigned, since the presence of a strong Q branch in each of the sub-bands required that $\Delta = \pm 1$.

Rotational analysis of triplet system of ZrO was carried out by Uhler[5] (1954). The α, β and γ systems were determined to be due to $^3\Delta$ - $^3\Delta$, $^3\Pi$ - $^3\Delta$ and $^3\Phi$ - $^3\Delta$ transitions respectively. He then suggested that the blue-green and red band systems of TiO by analogy to the α and γ systems of ZrO were a $^3\Delta$ - $^3\Delta$ and a $^3\Phi$ - $^3\Delta$ transition respectively.

Rotational analysis of the (0,0) band of the γ'-system in the yellow-red was carried out by Phillips[6] (1969). The lower state was shown to be the same as the lower state of the α and γ system by comparing combination differences. From the fact that neither the α nor the γ system show the Λ-type doubling which could be expected if the common lower state was $^3\Pi$, and the presence of strong Q branches, he assigned the γ'-system to a $B^3\Pi$ - $X^3\Delta$ transition. Transitions producing the α and γ systems were then changed to $C^3\Delta$ - $X^3\Delta$ and $A^3\Phi$ - $X^3\Delta$ respectively.

Among the singlet systems, the (0,0) sequence of the β-system in the orange region was observed by Lowater[2] (1929). From the fact that each band in the sequence has only one very strong Q head and a weaker

R head together with the previously mentioned theory of the similarity between the energy level scheme of the TiO molecule and the Ca atom, Lowater assigned the system to a $^1\Pi$ - $^1\Sigma$ transition. A rotational analysis of the (0,0) band was performed by Phillips[7] (1950) who concluded that the β-system was due to $^1\Phi$ - $a^1\Delta$ transition.

The δ system lies in the infrared region. Dobronravin[8] (1937) made a vibrational analysis of this system using the results of Wurm and Meister[9] (1937) and tried to identify the system as triplet transition, $^3\Sigma$ - $^3\Pi$, with the same lower state as the α-system determined by Christy (1929), while Wurm and Meister had suggested that this system might be associated with a singlet transition. A rotational analysis of (0,0) band was made by Phillips[7] (1950) and the system was assigned to a $^1\Pi$ - $^1\Delta$ transition.

The ø system was first observed by Wurm and Meister[9] (1937). Rotational analysis on (0,0) and (1,0), (2,1) bands were performed by Pettersson et al.[10,11] (1959,1962). Pettersson showed the system to be due to the $^1\Pi$ - $^1\Sigma^+$ transition by comparing the combination difference with δ system and from the fact that the R branch is stronger than P branch that required $\Delta\Lambda = +1$.

Five other band systems were observed recently. Four of them in the ultraviolet region were observed in a flame spectrum by Pathak and Palmer[12] (1970). They identified a triplet-triplet system: D-$X^3\Delta$ at 3000-3260 Å; three singlet-singlet systems: $^1\Sigma$ - $^1\Delta$ at 3286-3545 Å, $^1\Sigma$ - $d^1\Sigma^+$ at 3488-3545 Å and one at 3755-3820 Å with either $^1\Sigma$ or the $^1\Delta$ as the lower state which was proposed simply from

its appearance. A system in the near-infrared region was observed in a neon matrix by Weltner, Jr. et al.[13] (1971) and assigned to an $E^3\Pi - X^3\Delta$ transition. Detailed rotational study on these new bands has not yet been reported.

Prediction of TiO undiscovered electronic energy levels was made by Brewer and Green.[14] They compared the electronic spectra of scandium fluoride, titanium oxide and zirconium oxide. These molecules are isoelectronic in valence electrons. Hence their molecular orbitals are comparable and the trend of electronic energy levels should show similarity. Figure 1 and Table I reproduce their compilation and predictions. In view of the trend of energy levels together with the arguments of MO-ligand field theory relationships given by Jorgensen,[15] we would expect the order of orbitals with increasing energy to be $s\sigma$, $d\delta$, $d\pi$, $d\sigma$, $p\pi$. Hence, for ScF, TiO and ZrO we would expect three molecular states $^3\Sigma^-$, $^1\Sigma^+$, $^1\Gamma$ from the molecular orbital $d\delta^2$ to lie in the infrared region; furthermore, $^3\Sigma^-$, $^1\Sigma^+$, $^1\Delta$ states from the $d\pi^2$ orbital and $^1\Sigma^+$ state from the $d\sigma^2$ orbital to lie somewhere in the visible or ultraviolet region.

Another approach to predicting the undiscovered molecular states is to consider the states which will arise by the combination of the constituent atomic states. The ground state of titanium is ^3F from the $3d^24s^2$ configuration. The lowest excited state is ^5F (~ 0.67 kK) from the $3d^34s$ configuration followed by ^1D (~ 0.73 kK) from $3d^24s^2$, and ^3p (~ 0.85 kK) from $3d^24s^2$. Table II lists the states which arise from the combination of ground state of oxygen (^3P from the $2s^22p^4$

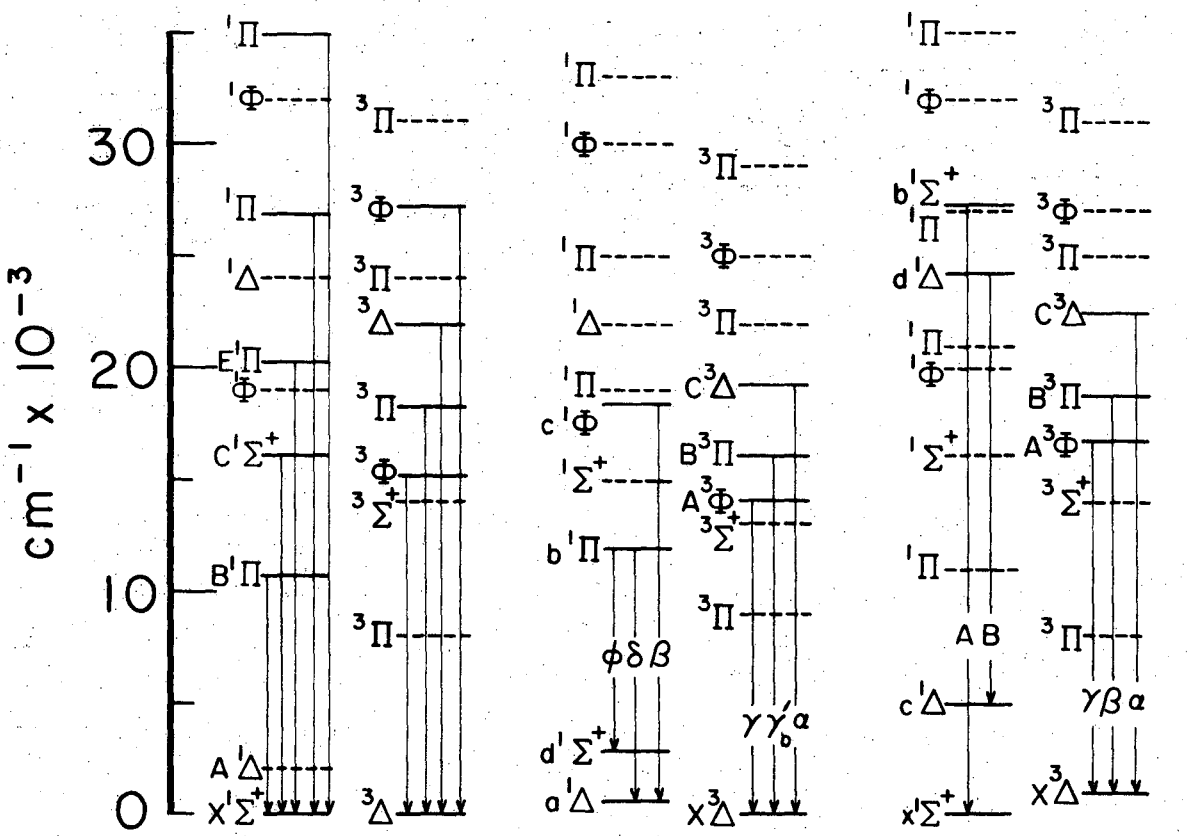

XBL688-3712

Figure 1

Known transitions of ScF, TiO and ZrO and estimates of the absolute energy of the electronic states.

TABLE I

Observed and estimated electronic energy levels of ScF, TiO and ZrO, in $cm^{-1} \times 10^{-3}$

Molecular orbital configuration	Molecular state	ScF	TiO	ZrO
$s\sigma^2$	$^1\Sigma^+$	0.0	2.8	0.0
$s\sigma$ $d\delta$	$^3\Delta$	0.0	0.0	1.0
	$^1\Delta$	2	0.6	5.0
$s\sigma$ $d\pi$	$^3\Pi$	8	9	8
	$^1\Pi$	10.7	11.9	11
$d\delta$ $d\pi$	$^3\Phi$	15.3	14.1	16.7
	$^3\Pi$	18.3	16.2	18.7
	$^1\Phi$	19	18.4	20
	$^1\Pi$	20.3	19	21
$s\sigma$ $d\sigma$	$^3\Sigma^+$	14	13	14
	$^1\Sigma^+$	16.1	15	16
$d\delta$ $d\sigma$	$^3\Delta$	21.9	19.3	22.5
	$^1\Delta$	24	22	24.3
$s\sigma$ $p\pi$	$^3\Pi$	24	22	25
	$^1\Pi$	26.8	25	27
$d\delta$ $p\pi$	$^3\Phi$	27.2	25	27
	$^3\Pi$	31	29	31
	$^1\Phi$	32	30	32
	$^1\Pi$	34.9	33	35

TABLE II

Molecular states of TiO from the combination of the neutral atomic terms

Ti state	O state	Molecular states of TiO	Multiplicities
^3F	^3P	Γ, $\Phi(2)$, $\Delta(3)$, $\Pi(3)$, Σ^-, $\Sigma^+(2)$	1, 3, 5
^5F	^3P	Γ, $\Phi(2)$, $\Delta(3)$, $\Pi(3)$, Σ^-, $\Sigma^+(3)$	3, 5, 7
^1D	^3P	Φ, $\Delta(2)$, $\Pi(3)$, $\Sigma^-(2)$, Σ^+	3
^3P	^3P	Δ, $\Pi(2)$, Σ^-, $\Sigma^+(2)$	1, 3, 5

configuration) with the low-lying states of Ti. As expected, there is a tremendous number of states from just considering the combination of a few low-lying excited states. Because for a transition metal the open shell d electrons gives rise to atomic states of high angular momentum, coupling of these momenta to those of the P states of oxygen would give a large number of molecular states. It is apparent that this approach gives little useful information about the low-lying molecular states of TiO.

Brewer and Rosenblatt[16] calculated the electronic partition functions of a gaseous diatomic oxides of a transition elements by using the low-lying electronic states of the doubly charged gaseous ion as calculated from the energy levels listed by Moore.[17] In the theoretical calculation of heat of formation of metal monoxide, however, Brewer and Mastick[18] showed that a M^+O^- model is more reasonable than $M^{2+}O^{2-}$. Prediction of low-lying molecular states of TiO based on Ti^+ with O^- (^2P) would be still very complicated. Table III lists the states arising from the combination of the ground state of O^{2-} (^1S) with a few low-lying states of Ti^{2+}. They are $3d^2\ ^3F$ (ground state), $3d^2\ ^1D$ ($\sim$8.5 kK), $3d^2\ ^3P$ ($\sim$10.6 kK), $3d^2\ ^1S$ ($\sim$14.0 kK), $3d^2\ ^1G$ ($\sim$14.4 kK), $3d4s\ ^3D$ ($\sim$38.2 kK), and $3d4s\ ^1D$ ($\sim$41.7 kK). It is obvious that the trend of energy levels predicted in this table coincide very well with those obtained from experiments and from the molecular orbital estimation as shown in Table II.

TABLE III

Molecular states of TiO from the combination of the divalent atomic terms

Ti^{2+} state	O^{2-} state	Molecular state of TiO	Multiplicities
^3F	^1S	Φ, Δ, Π, Σ^-	3
^1D	^1S	Δ, Π, Σ^+	1
^3P	^1S	Π, Σ^-	3
^1S	^1S	Σ^+	1
^1G	^1S	Γ, Φ, Δ, Π, Σ^+	1
^3D	^1S	Δ, Π, Σ^+	3
^1D	^1S	Δ, Π, Σ^+	1

2. Permitted Rotational Transitions in the Hund Coupling Case (a) of $^3\Delta$ - $^3\Delta$ Transition

There are three different angular momenta in a molecule, electron spin, electronic orbital and nuclear rotation. In case (a) the resultant electronic angular momentum Ω along the internuclear axis, and the nuclear rotation angular momentum N form the total angular momentum J.[19,20] That means that Ω is the component of J. Hence, J cannot be smaller than its component Ω. Therefore for a given Ω we have

$$J = \Omega, \Omega+1, \Omega+2, \ldots.$$

By considering the quantum numbers and the symmetry properties of the energy levels, the following selection rules can be derived for case (a) $^3\Delta$ - $^3\Delta$ transition.

i) The component of the spin along the internuclear axis does not alter, $\Delta\Sigma = 0$. Therefore there are only three sub-bands: $^3\Delta_1$ - $^3\Delta_1$, $^3\Delta_2$ - $^3\Delta_2$ and $^3\Delta_3$ - $^3\Delta_3$.

ii) For electric dipole radiation, the total angular momentum quantum number must satisfy the rule $\Delta J = 0, \pm 1$, therefore if we disregard Λ-type doubling, each sub-band has a P, a Q and an R branch, hence each band has three heads, but here the Q branch is weak and its intensity decreases rapidly with increasing J, since $\Delta\Lambda = 0$.[19] If we take account of the Λ-type doubling, each line splits into two components. However the Λ-type splitting is negligibly small for not too large J values in Δ states.[21,22]

iii) Positive terms combine only with negative, and vice versa.

$$+ \longleftrightarrow -, \quad + \not\longleftrightarrow +, \quad - \not\longleftrightarrow -$$

According to these rules, permitted rotational transitions of $^3\Delta - {}^3\Delta$ system were drawn in Fig. 2.

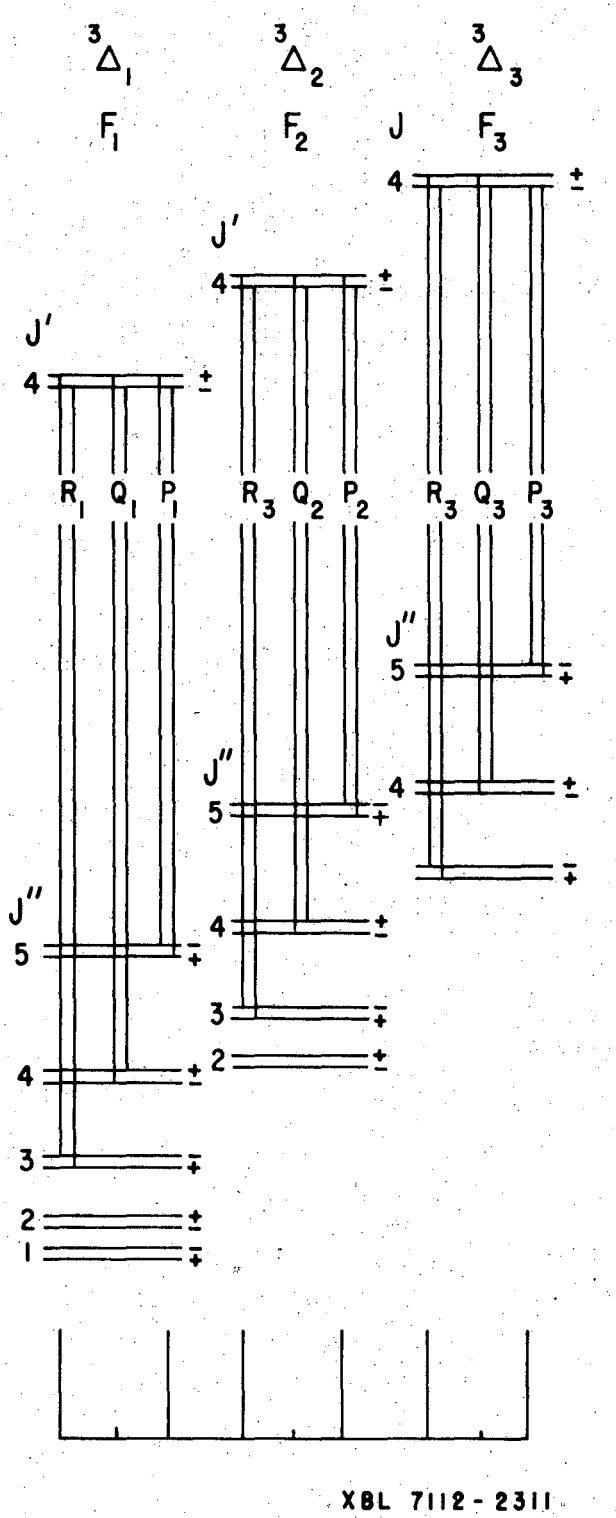

Figure 2

Branches of a $^3\Delta$ (a) - $^3\Delta$ (a) spectrum. The Λ-type doubling is negligible for Δ state; however, it is greatly exaggerated here.

B. Vanadium Monoxide

1. Discovered and Expected Electronic States

The electronic spectrum of VO has been studied less than that of TiO. Only four systems have been observed. They are in the violet, green-yellow, red-infrared and infrared regions (Fig. 3). The green-yellow and red-infrared band systems are better understood. Complete analysis of them, however, has still not been carried out.

Vibrational analysis of VO in the green-yellow region was first undertaken by Mecke[23] (1927) and then by Fergusson[24] (1932). The rotational structure analysis of the bands (0,1), (0,0) and (1,0) was carried out by Mahanti[25] (1935). His analysis revealed that each band consisted of two R, two P as well as short, strong Q branches. Because of this and the fact that none of these branches showed any Λ-type doubling, Mahanti assigned this system to $^2\Delta$ - $^2\Delta$ transition. The rotational analysis was reinvestigated and extended to (2,0), (1,0), (0,0), (0,1) and (0,2) bands by Lagerqvist and Selin[26] (1957). The absence of the Q-branch and the Λ-type splitting and analogy to the transitions of NbO and TaO molecules (determined by Uhler[5] in 1954), molecules isoelectronic to VO in valence electrons, led Lagerqvist and Selin to conclude that the green system was produced by an $^2\Delta$ - $^2\Delta$ transition.

By taking the ligand-field and MO theories into consideration, Jorgensen[15] (1964) pointed out as arbitrary the assigning the ground state of VO as $^2\Delta$ which corresponds to low spin δ^3 or $\sigma^2\delta$. He suggested

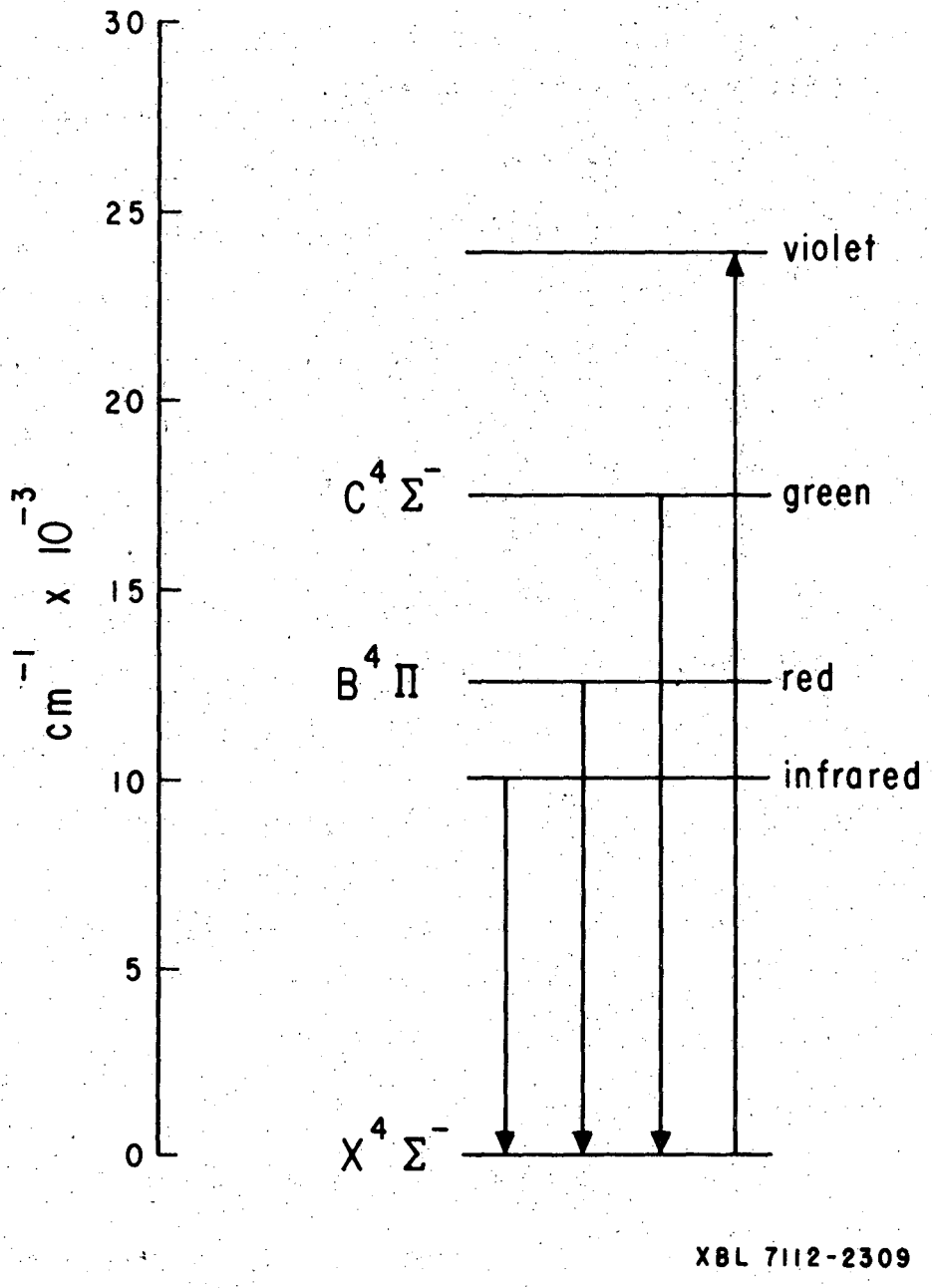

Figure 3

Known transitions of the VO electronic states.

that either $^4\Sigma$ or $^2\Sigma$ arising from the $\sigma\delta^2$ orbital was also possible to be the ground state of VO. The ab initio calculations of VO by Carlson and Moser[27] (1966) showed that the ground state of VO is $^4\Sigma^-$.

In addition to the four branches, two R and two P, analyzed by Lagerqvist and Selin, Richard and Barrow[28,29] (1968) found four more broad line branches, two more R and two more P, in the green system. Rotational analysis of bands were performed. The energy levels were found to be determined by an integral quantum number K rather than half integral J, so that the transition of the green system was reassigned to $^4\Sigma^-$ (case b) - $^4\Sigma^-$ (case b). The ESR spectrum of VO isolated in argon matrix was investigated by Kasai[30] (1968). From his work, the electronic ground state was further proved to be a $^4\Sigma$ state.

Vibrational analysis of the system in the red region was carried out by Keenan and Schroeder[31] (1952). The vibrational constants for the lower levels of this system are almost equal to those of the lower level of the green-yellow system. This indicated that both systems were due to the same lower level. Keenan and Schroeder suggested that the red system might involve quartet terms because of the greater complexity of the bands. Rotational analysis in parts of (1,0) and (0,0) bands were done by Richards and Barrow[28] (1968). Lower state combination differences were found to be in excellent agreement with those observed in the green bands. The upper state energy levels were determined by a half integral quantum number J. The system was concluded to be a $^4\Pi$ - $X^4\Sigma^-$ transition.

Some infrared bands were observed by Lagerqvist and Selin[32] (1957). The high intensity of the system led them to suggest that the transition might be to the ground state.

None of the molecules which are isoelectronic in valence electrons with VO have been well studied so far. Therefore, it would be very difficult to estimate accurately the trend of energy levels of the electronic states of VO as it had been done for TiO by Brewer and Green.[14] However the low-lying electronic states of VO may be predicted from the combination of the low-lying V(I) with O(I) and better yet from the combination of V^{2+} with O^{2-} atomic states.

The electronic ground state of oxygen atom is ^3P and the lowest excited states are ^1D ($\sim$ 15.9 kK) and ^1S ($\sim$ 33.8 kK). They both come from the $2s^2 2p^4$ configuration. The lowest state of the vanadium atom is a $3d^3 4s^2\ ^4F$ term followed by $3d^4 4s\ ^6D$ ($\sim$ 0.2 kK), $3d^4 4s\ ^4D$ ($\sim$ 0.85 kK), and $3d^3 4s^2\ ^4P$ ($\sim$ 0.95 kK). Table IV lists the states which arise from the combination of ground state O with the low-lying states of V. There are thirty-six molecular states arising from ground-state atoms alone. There are, furthermore, many electronic molecular states arising from low-lying excited atomic states. It is difficult to predict the trend of energy levels for these molecular states since molecules in low-lying molecular states may dissociate to excited atoms. In general, the wealth of molecular electronic states suggests the possibility of perturbation, predissociation and many allowed electronic transitions.

TABLE IV

Molecular states of VO from the combination of the neutral atomic terms

V state	O state	Molecular state of VO	Multiplicities
^4F	^3P	Γ, $\Phi(2)$, $\Delta(3)$, $\Pi(3)$, Σ^-, $\Sigma^+(2)$	2, 4, 6
^6D	^3P	Φ, $\Delta(2)$, $\Pi(3)$, $\Sigma^-(2)$, Σ^+	4, 6, 8
^4D	^3P	Φ, $\Delta(2)$, $\Pi(3)$, $\Sigma^-(2)$, Σ^+	2, 4, 6
^4P	^3P	Δ, $\Pi(2)$, Σ^-, $\Sigma^+(2)$	2, 4, 6

As has been discussed by Brewer and Rosenblatt,[16] we may combine the low-lying V^{2+} and O^{2-} atomic states to predict the low-lying molecular electronic states of VO. This method has been very useful for TiO (compare Table I and III). The lowest state of V^{2+} is a $3d^3\ ^4F$ term followed by $3d^3\ ^2P$ ($\sim$ 1.13 kK), $3d^3\ ^4P$ ($\sim$ 1.16 kK), $3d^3\ ^2G$ ($\sim$ 1.20 kK), $3d^3\ ^2D$ ($\sim$ 1.63 kK), $3d^3\ ^2H$ ($\sim$ 1.69 kK), $3d^24s\ ^4F$ ($\sim$ 4.42 kK) and $3d^24s\ ^2F$ ($\sim$ 4.95 kK). Table V lists the predicted VO molecular states which arise from the combination of these low-lying states of V^{2+} with the ground state of O^{2-} which is a $2s^22p^6\ ^1S$ term.

2. Permitted Rotational Transitions in the Hund Coupling Case (b) of $^4\Sigma^- - {}^4\Sigma^-$ Transition

For a $^4\Sigma^-$ term, the electronic orbital angular momentum $\Lambda = 0$. That means that there is no magnetic field in the direction of the internuclear axis, so that the spin vector S is not coupled to the internuclear axis. Therefore Ω is not defined and consequently no splitting occurs as long as the molecules do not rotate. The angular momentum of nuclear rotation, N, is therefore identical with the quantum number K, the total angular momentum apart from spin. K can have all integral values from 0 up. The angular moment K and S then form a resultant J which generally represents the total angular momentum including spin. The possible values of J for a given K are given by

$$J = (K+S), (K+S-1), (K+S-2), \cdots\cdots\cdots |K-S|$$

Since $S = 3/2$ for $^4\Sigma$ state, each level with a given K consists of four

TABLE V

Molecular states of VO from the combination of the divalent atomic terms

V^{2+} state	O^{2-} state	Molecular states of VO	Multiplicities
^4F	^1S	Φ, Δ, Π, Σ^-	4
^2P	^1S	Π, Σ^-	2
^4P	^1S	Π, Σ^-	4
^2G	^1S	Γ, Φ, Δ, Π, Σ^+	2
^2D	^1S	Δ, Π, Σ^+	2
^2H	^1S	H, Γ, Φ, Δ, Π, Σ^-	2
^4F	^1S	Φ, Δ, Π, Σ^-	4
^2F	^1S	Φ, Δ, Π, Σ^-	2

components except for levels with K = 0,1 which contain one and three components respectively.

For a Σ^- state, the parity of the rotational level with even quantum number K is "negative" and the parity of the rotational level with odd quantum number K is "positive". Because the total wavefunctions (including rotational, vibrational and electronic parts) with even K changes its sign and the wavefunction with odd K does not change its sign with respect to a reflection at the origin.

By evaluating the transition matrix elements of the electric dipole moment and considering the quantum numbers and symmetry properties of the initial and final states, the selection rules that hold for $^4\Sigma^-$ - $^4\Sigma^-$ transition can be shown to be the following:

i) Positive terms can only make transition to negative terms, and vice versa.

$$+ \longleftrightarrow -, \quad + \not\longleftrightarrow +, \quad - \not\longleftrightarrow -$$

ii) Since both $^4\Sigma^-$ states belong to case (b), the quantum number of the total angular momentum apart from spin, K, is defined. Therefore $\Delta K = \pm 1$ ($\Delta K = 0$ is forbidden for Σ - Σ transition).

iii) The selection rule for the total angular momentum quantum number $\Delta J = 0, \pm 1$, must also be satisfied.

In the satellite branches for which $\Delta J \neq \Delta K$, the intensity falls off very rapidly with increasing K. These satellite branches always lie very near to the corresponding main branches with the same ΔK but having $\Delta J = \Delta K$. The intensity of the satellite branches is always

small compared to that of the main branches as long as case (b) applies to both states. Therefore, the permitted rotational transitions of $^4\Sigma^- - {}^4\Sigma^-$ system can be drawn, as in Fig. 4. The transitions contain eight main branches and ten satellite branches.

However, for the VO $X^4\Sigma^-$ states, as described by Richards and Barrow,[28,29] and Kasai,[30] because of the nuclear magnetic hyperfine coupling of the unpaired electron spins with the ^{51}V nucleus of spin $I = 7/2$, the total angular momentum is described by quantum number F rather than by J, where

$$F = J+I,\ J+I-1, \cdots\cdots |J-I| .$$

Thus for each of the four multiplet rotational levels there are eight hyperfine components. It seems likely that perturbation might take place among these magnetic hyperfine sublevels provided that the Kronig's selection rules[19] for perturbation are satisfied.

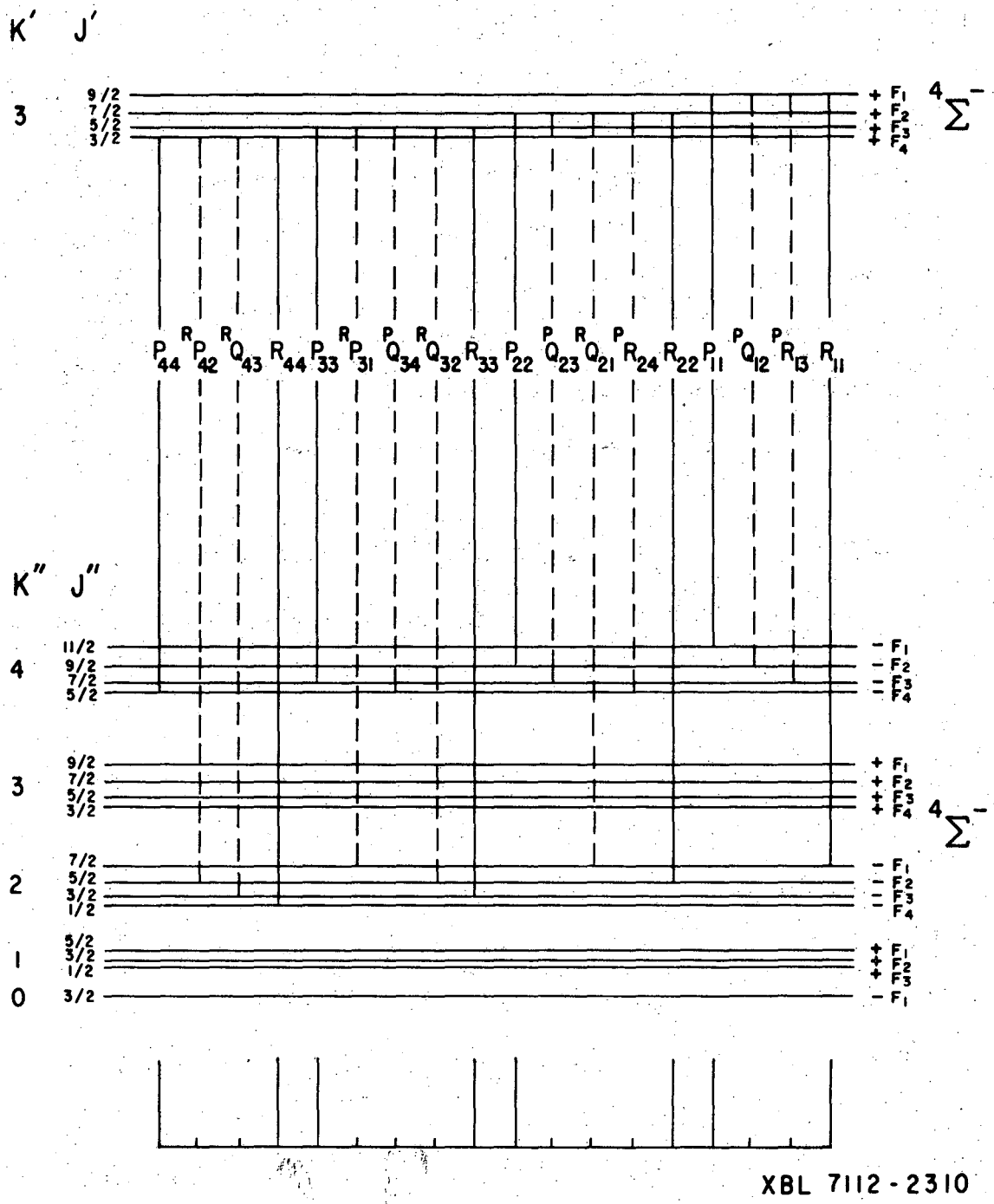

Figure 4

Branches of a $^4\Sigma^- - {}^4\Sigma^-$ spectrum.

II. INTRODUCTION

The TiO bands form the most prominent characteristics of the spectra of the M type stars, reaching their maximum intensity at the M8 type. The VO bands are also present in all the spectra of M-type starts of type M7 or later become very strong in the coolest long-period variables. As the temperature decreases, they increase in strength relative to the adjacent TiO bands. The TiO and VO might also play an important role when the hypersonic vehicles reentry into the atmosphere.

Relative oscillator strengths of bands in the spectra are needed to get the information on the molecular temperatures, and the absolute oscillator strengths of the bands are needed to determine the concentration of molecules in the sources. There are several methods which can be used to determine the oscillator strength of high temperature molecules. Briefly, these methods can be divided into two categories,[33] the methods which are independent of the molecular density N, and the methods which do require the knowledge of N. For experiments of the first category, such as Direct decay and Phase-shift methods, the oscillator strengths are obtained by measuring the radiative lifetime of excited states. Generally, the rate of disappearance of the excited molecules by emission of light is considered to be the first order, and the radiative lifetime of an excited state is defined as the time required for the number of molecules in the excited state to reach 1/e of the initial number excited. Hence, the lifetime is just the inverse of the decay rate constant.

Direct decay method[34,35,36] is the most direct lifetime measurement. It uses a short pulse of radiation (light or electrons) or a continuous supply of excitation energy and a fast switch (such as a Pocket cell, Kerr cell, or thyratron) so that decay of the absorbed radiation, in terms of the fluorescence light intensity, can be observed as close in time as possible to the initial excitation.

Phase shift method[37-41] measures the phase shift between excited pulses of resonance radiation and the corresponding fluorescence radiation pulses. The shift "$\Delta\Phi$" is related to the lifetime τ by $\tan \Delta\Phi = \omega\tau$, where ω is the modulation frequency of the excited radiation.

For experiments of the second category, the oscillator strength is usually determined from absolute intensity of emitted or absorbed radiation. Here, the thermal light sources such as high-current arcs,[42] shock tube[43,44] and furnaces of the King type[45,46] are used.

In principle, methods of the first category should give more accurate results, since they do not need the knowledge of vapor pressures which are always uncertain for high temperature molecules. However, because of many technical difficulties in generating beam of high temperature molecules, the mixing of fluorescence signal with large amount of scattered light due to high-temperature background, the limited intensity of a resonance exciting light source in the optical excitation method, the cascading contribution from many high energy levels in the electron excitation method and many other problems, these first category methods have not been easy to apply. The thermal light source used in the second category method employed in this research was a furnace of the King type.

Relative integrated radiances of bands of the TiO α-system in emission were measured by Phillips[47] (1953), using a King-type furnace and a photoelectric scanning technique to produce the band profiles. Franck-Condon factors of the TiO γ-system were calculated by Fraser, Jarmarin and Nicholls[48] (1953), using Morse potentials to evaluate the overlap integrals of vibrational wave functions. Tawde and Chandratreya[42] (1955) measured the vibrational transition probabilities of the TiO α-system by exciting the TiO in carbon arc in air at atmospheric pressure. The photographic photometry technique was used and the peak values near the band heads were taken for estimation of intensities of bands. Their experimental results were then compared to those calculated from Hutchisson's theory.[49] Ortenberg[50] (1959) calculated the Franck-Condon factors of the α-system of the TiO molecule using the Morse simplified potential method.[51] He then gave the relative transition probabilities of the bands by considering the dependence of the electronic transition moment on the internuclear separation. Prasad[52,53] (1962,1963) also used the Morse potential method of Fraser and Jarmain to calculate the Franck-Condon factors of the TiO α-system. However, his results were different from that calculated by Ortenberg. Morse potential Franck-Condon factors of three singlet systems, β, δ and ø were computed by Linton and Nicholls[54] (1969). The relative intensities of the bands in all three systems were calculated by only considering the populations and frequency dependence of the bands and assuming that the electronic transition moments were constant over the systems. Linton and Nicholls[55] (1970) measured the radiances of the α and β systems of TiO emitted in

a shock tube by driving helium into a mixture containing TiO_2 powder, argon and oxygen gases. The variation of the electronic transition moment of the bands with respect to the (0,0) band were determined by comparing their integrated radiances.

The absolute oscillator strength of TiO molecule has not been investigated until recently. Price, Sulzman and Penner[44] (1971) measured the absolute radiance of α and γ bands of TiO by comparing the radiance of a standard tungsten lamp to that emitted from the shock-heated TiO gas which was produced by reaction between gaseous $TiCl_4$ and O_2 in Ar.

Relative vibrational transition probabilities of the VO green system were measured by Tawde and Chandratreya[42] (1955) using a carbon arc and photographic technique. Their experimental results were compared with those calculated from Hutchisson's theory. Substantial difference between these results led Tawde and Chandratreya to conclude that mass asymmetry of the constituent atoms had to be taken into account when Hutchisson's theory was applied to diatomic molecules. Franck-Condon factors for the VO green-system were calculated by Prasad[56] (1963) and Murthy, Setty and Sumathi[57] (1963) using Morse potential functions. The absolute oscillator strength of the VO molecule has not been determined yet.

The results of the previous work on the relative oscillator strengths of the TiO α-system and the VO green system, relative intensities of the TiO β, δ, and ϕ systems and the absolute oscillator strengths of TiO α and γ system are summarized in the following Tables VI-XI.

TABLE VI

Absoluate oscillator strengths of TiO
α- and γ-system
(Price, Sulzman and Penner, 1971, shock tube)

	v'	v''	Band head (Å)	Center of wavelength observed (Å)	f value
	1	0	4956.85 4955.09 4954.55	4969	0.051 ± 0.011
α SYSTEM	0	0	5169.30 5167.36 5166.86	5183	0.030 ± 0.0056
	0	1	5451.32 5448.86 5448.34	5460	0.052 ± 0.0087
	1	0	6713.9 6680.8 6651.3	6734	0.19 ± 0.071
γ SYSTEM	0	0	7125.5 7087.7 7054.3	7147	0.089 ± 0.036
	0	1	7671.5 7627.7 7589.1	7689	0.17 ± 0.072

TABLE VII

Relative oscillator strengths of TiO α-system

v'	v''	λ (Å)	Phillip 1953 King-furnace expt.	Tawde and Chandratreya 1955 Hutchisson's theory	Arc expt.
3	0	4584		----	----
4	1	4626		0.3333	1.0238
5	2	4669		0.4667	1.1905
2	0	4761	0.652	0.4222	0.5000
3	1	4804	0.829	0.5111	0.5000
4	2	4848	0.757	0.4222	0.6191
1	0	4954	0.962	0.8222	0.8810
2	1	5003	0.740	0.4000	0.2381
0	0	5167	1.000	1.0000	1.0000
1	1	5240	0.162	0.0089	0.1429
2	2	5260		----	----
3	3	5308		0.5556	0.4762
4	4	5359		0.5778	1.0714
0	1	5448	0.877	0.9778	0.4524
1	2	5497	0.550	0.8444	0.2619
2	3	5546		0.3778	0.5714
0	2	5758		0.5889	0.3095
1	3	5810		1.1333	0.8571
2	4	5862		1.2222	0.7857
3	5	5915		1.2222	0.9524
0	3	6105		0.1333	0.4762
1	4	6159		0.4000	0.5000
2	5	6215		0.59	1.4048

(continued on next page)

TABLE VII continued

v'	v''	λ (Å)	Ortenburg 1959 (Morse potential)	Linton and Nicholls 1970* (Morse potential & shock tube)
3	0	4584		0.2287
4	1	4626		0.3952
5	2	4669		0.4767
2	0	4761	0.633	0.5245
3	1	4804	0.649	0.5628
4	2	4848		0.3832
1	0	4954	1.063	0.7814
2	1	5003	0.514	0.4009
0	0	5167	1.000	1.0000
1	1	5240		
2	2	5260		
3	3	5308		
4	4	5359		
0	1	5448	0.781	0.9658
1	2	5497	0.476	0.6106
2	3	5546		
0	2	5758		
1	3	5810		
2	4	5862		
3	5	5915		
0	3	6105		
1	4	6159		
2	5	6215		

TABLE VIII

Relative intensities of TiO β-system

v'	v''	λ R head (Å)	Linton and Nicholls 1969 Iv'v'' (calc.) (at 4000°K)	Iv'v'' (abs.) (shock tube)
1	0	5326.8	0.071	0.13
2	1	5358.0	0.098	0.20
3	2	5389.7	0.100	0.19
4	3	5422.1	0.091	0.16
5	4	5455.1	0.075	
6	5	5488.7	0.059	
0	0	5597.6	1.000	1.00
1	1	5629.3	0.591	0.57
2	2	5661.6	0.341	0.47
3	3	5694.5	0.191	0.28
4	4	5728.0	0.103	0.16
5	5	5762.2	0.052	
6	6	5798.1	0.025	
0	1	5932.6	0.062	
1	2	5965.4	0.083	
2	3	5998.8	0.082	
3	4	6032.9	0.072	
4	5	6067.7	0.058	
5	6	6103.1	0.045	

TABLE IX

Relative intensities of TiO δ-system

v'	v''	λ R head (Å)	Linton and Nicholls 1969 Iv'v'' (at 4000°K) (calc.)
1	0	8198	0.231
2	1	8269	0.229
3	2	8341	0.188
4	3	8414	0.135
5	4	8488	0.089
6	5	8563	0.054
0	0	8860	1.000
1	1	8937	0.429
2	2	9015	0.169
3	3	9095	0.058
4	4	9174	0.016
0	1	9729	0.147
1	2	9815	0.166
2	3	9901	0.139
3	4	9989	0.102
4	5	10077	0.069
5	6	10168	0.044

TABLE X

Relative intensities of TiO ø-system

v'	v''	Band origin (Å)	Linton and Nicholls 1969 Iv'v'' (at 4000°K) (calc.)
2	0	9198	0.145
3	1	9299	0.195
4	2	9401	0.171
5	3	9504	0.122
6	4	9607	0.075
1	0	10032	0.507
2	1	10145	0.373
3	2	10258	0.190
4	3	10373	0.076
5	4	10487	0.023
0	0	11042	1.000
1	1	11169	0.175
2	2	11298	0.009
0	1	12436	0.323
1	2	12582	0.263
2	3	12731	0.153
3	4	12879	0.075
4	5	13027	0.031
0	2	14212	0.042
1	3	14386	0.063
2	4	14559	0.063
3	5	14734	0.052
4	6	14908	0.039

TABLE XI

Relative oscillator strengths of VO green-system

v'	v''	λ (Å)	Tawde and Chandretreya 1955 Hutchisson's theory	Arc expt.
2	0	5228	5.0909	0.6571
3	1	5276	0.3636	1.1714
1	0	5469	3.0909	1.1714
2	1	5517	2.3636	0.4857
0	0	5737	1.0000	1.0000
1	1	5786	3.9091	0.1714
2	2	5837	0.0091	1.1429
3	3	5889	----	----
4	4	5942	1.4546	0.7143
0	1	6086	2.4546	1.0286
1	2	6139	2.9091	0.4000
0	2	6478	6.0909	1.2857
1	3	6531	0.1818	1.4571
2	4	6589	2.3636	0.6857
0	3	6919	8.9091	1.3714
1	4	6976	0.9091	0.8857
2	5	7035	0.6364	1.1143
0	4	7418	4.3636	0.5714
1	5	7477	4.5455	1.7429
0	5	7986	3.9091	----

III. THEORY

In the classical electron theory of dispersion,[58] the oscillator strength is used to measure the effective number of electrons whose oscillations give rise to a particular transition. For each single rotational line in the transition of a molecule, the oscillator strength of emission and absorption, $f^{n'v'J'M_{J'}}_{n''v''J''M_{J''}}$ and $f^{n''v''J''M_{J''}}_{n'v'J'M_{J'}}$, respectively, can be expressed as the number per cm^3 of vibrating dispersion electrons, N_{el} (derived from the inetnsity of the emission or absorption lines) divided by the number of the molecules able to emit or absorb radiation corresponding to this individual line (derived from the Boltzmann distribution in the thermal equilibrium condition). Here, primes refer to the upper state and double primes to the lower state, M_J is the magnetic quantum number, J is the rotational quantum number, v is the vibrational quantum number, and n represents the remainder of the quantum numbers of the electronic state.

In the Einstein radiation theory, the mechanism of light absorption and emission was discussed.[59] The probability per second that a molecule in an upper magnetic sublevel, $M_{J'}$, will spontaneously decay to a lower magnetic sublevel, $M_{J''}$, with emission of a quantum of light, is represented by the coefficient $A^{n'v'J\,M_{J'}}_{n''v''J''M_{J''}}$. The probability per second that a molecule in a lower magnetic sublevel will jump to an upper magnetic sublevel under the action of light is represented by $B^{n''v''J''M_{J''}}_{n'v'J'M_{J'}}\,E_\nu$, where E_ν is the radiant photon flux which is expressed in quanta/sec/cm^2/unit frequency interval in cm. The relationship of the Einstein coefficients $A^{n'v'J'M_{J'}}_{n''v''J''M_{J''}}$ and $B^{n''v''J''M_{J''}}_{n'v'J'M_{J'}}$ to the classical emission and

absorption oscillator strengths of a rotational line of a molecular transition $f^{n'v'J'M_{J'}}_{n"v"J"M_{J"}}$ and $f^{n"v"J"M_{J"}}_{n'v'J'M_{J'}}$, respectively,[60,61] are

$$\frac{g_e{}'S_{J'J"}}{2J'+1} f^{n'v'J'M_{J'}}_{n"v"J"M_{J"}} = \frac{\lambda^2 mc}{8\pi^2 e^2} \frac{g_e{}'S_{J'J"}}{2J'+1} A^{n'v'J'M_{J'}}_{n"v"J"M_{J"}} =$$

$$\frac{mc}{\pi e^2} \frac{g_e{}"S_{J"J'}}{2J"+1} B^{n"v"J"M_{J"}}_{n'v'J'M_{J'}} = \frac{g_e{}"S_{J"J'}}{2J"+1} f^{n"v"J"M_{J"}}_{n'v'J'M_{J'}} \qquad (1)$$

where e and m are the charge and mass of an electron, c is the velocity of light in vacuum and λ is the wavelength in cm. $g_e{}'$ is the electronic statistical weight of the emitting state (equals $(2 - \delta_{o,\Lambda})(2S+1)$. $(2 - \delta_{o,\Lambda})$ and $(2S+1)$ take into account the Λ-type splitting and spin multiplicity respectively). $S_{J'J"}$ is the line strength.

In the wave mechanics, the commonly used intensity parameters of emission can be related to the transition matrix element of the molecule by[20,62]

$$A^{n'v'J'M_{J'}}_{n"v"J"M_{J"}} = \frac{64\pi^4\nu^3}{3h} \frac{\sum_{M_{J'}} \left| R^{n'v'J'M_{J'}}_{n"v"J"M_{J"}} \right|^2}{g_{J'}} \qquad (2)$$

$$f^{n'v'J'M_{J'}}_{n"v"J"M_{J"}} = \frac{8\pi^2 me\nu}{3he^2} \frac{\sum_{M_{J'}} \left| R^{n'v'J'M_{J'}}_{n"v"J"M_{J"}} \right|^2}{g_{J'}} \qquad (3)$$

$$\int L^{n'v'J'M_{J'}}_{n"v"J"M_{J"}} \, d\nu = \frac{\ell}{4\pi} N_{n'v'J'M_{J'}} A^{n'v'J'M_{J'}}_{n"v"J"M_{J"}} \qquad (4)$$

where $\int L^{n'v'J'M_{J'}}_{n"v"J"M_{J"}} \, d\nu$ is the total radiance emitted from a magnetic sublevel of rotational level in the upper state (in photons/cm^2/sec/solid angle/frequency interval in cm), ℓ is the length of a column of

gaseous molecules (in cm), $N_{n'v'J'M_{J'}}$ is the number of molecules in the emitting magnetic sub-state/cm^3, h is Planck's constant (in erg-sec), v is the wave number (in cm^{-1}) of the spectral line emitted in the transition and $g_{J'}$ is the rotational statistical weight of the emitting state (equals 2J'+1, since the angular momentum J' of the molecule can be oriented in 2J'+1 ways in the presence of an external magnetic field). $\sum_{M_{J'}} \left| R^{n'v'J'M_{J'}}_{n''v''J''M_{J''}} \right|$ is the sum of the squares of transition matrix elements. The summation is to be extended over all magnetic sublevels involved in the transition. The rotational wave functions in the transition matrix can be factored out if the interaction of rotation and electronic motion is negligible since the rotational wave functions do not depend on the internuclear distance r. Hence, the transition matrix term can be written as:

$$\sum_{M_{J'}} \left| R^{n'v'J'M_{J'}}_{n''v''J''M_{J''}} \right|^2 = S_{J'J''} \left| R^{n'v'}_{n''v''} \right|^2$$

Here, $S_{J'J''} = \sum_{M_{J'}=-J'}^{+J'} \left| R^{J'M_{J'}}_{J''M_{J''}} \right|^2$ is the rotational line strength, commonly called the Hönl-London factor which determines the relative intensities of the branches within a band. It represents that part of the transition matrix element due to overlap of the rotational wave functions. The rest of the transition matrix $\left|R^{n'v'}_{n''v''}\right|^2$ is commonly called the band strength $S_{v'v''}$. The transition moment $R^{n'v'}_{n''v''}$ can be expressed as:

$$R^{n'v'}_{n''v''} = \langle \psi_{e'}^{*} \psi_{v'}^{*} \left| M \right| \psi_{e''} \psi_{v''} \rangle \qquad (6)$$

Here, the ψ_e's are the electronic wave functions, the ψ_v's are the vibrational wave functions and M is the transition moment $\sum_i e_i v_i$. Separation of the transition moment into two parts, one depending only on the positions of the nuclei, M_n, and one depending only on the coordinates of the electrons, M_e, yields:

$$R^{n'v'}_{n''v''} = \langle \psi_{e'}{}^* \mid \psi_{e''} \rangle \langle \psi_{v'}{}^* \mid M_n \mid \psi_{v''} \rangle + \langle \psi_{v'}{}^* \mid R^{n'}_{n''} \mid \psi_{v''} \rangle \quad (7)$$

where $R^{n'}_{n''} = \langle \psi_{e'}{}^* \mid M_e \mid \psi_{e''} \rangle$

For a transition between two different electronic states, the first term goes to zero due to the orthogonality of the electronic wave functions. $R^{n'}_{n''}$ is called the electronic transition moment. Since the electronic wave functions, under the Born-Oppenheimer approximation[63] are only slightly dependent on the internuclear distance, the electronic transition moment is often removed from the second integral and is considered to take on an average value, $\overline{R^{n'}_{n''}}$, thus yielding

$$\left|R^{n'v'}_{n''v''}\right|^2 = \left|\overline{R^{n'}_{n''}}\right|^2 \langle \psi_{v'}{}^* \mid \psi_{v''} \rangle^2 \quad (8)$$

The squared integrals $\langle \psi_{v'}{}^* \mid \psi_{v''} \rangle^2 = \int \psi_{v'}{}^* \psi_{v''} r^2 \, dr = \left|R^{v'}_{v''}\right|^2$ are the well known Franck-Condon factors which determine the relative strength of the bands within a system. In view of the foregoing considerations, therefore,

$$A^{n'v'J'M_{J'}}_{n''v''J''M_{J''}} = \frac{64\pi^4 \nu^3 \left|\overline{R^{n'}_{n''}}\right|^2 \left|R^{v'}_{v''}\right|^2 S_{J'J''}}{3h\,(2J'+1)} \quad (9)$$

$$f^{n'v'J'M_{J'}}_{n''v''J''M_{J''}} = \frac{8\pi^2 mc\nu \left|\overline{R^{n'}_{n''}}\right|^2 \left|R^{v'}_{v''}\right|^2 S_{J'J''}}{3he^2(2J'+1)} \qquad (10)$$

In order to calculate the oscillator strength of an emitting state, it is necessary to sum all the line strengths of the possible downward transitions allowed by the selection rules. Although the line strength $S_{J'J''}$ is different for a P, Q or R rotational line, the sum of $S_{J'J''}$ values for all rotational lines from a given level totals 2J'+1 (compare to the Burger-Dorgelo-Ornstein sum rule for atoms).[64] Therefore, from Eq.(10) it is apparent that different rotational levels belonging to the same vibrational level of an electronic state have the same magnitude of oscillator strength, if the ν dependence is neglected. Since the Franck-Condon factor satisfied the sum rule $\sum_{v''} \left|R^{v'}_{v''}\right|^2 = 1$, it is also true that the rotational levels belonging to an electronic state have an oscillator strength of the same magnitude provided that the ν dependence is negligible and the Born-Oppenheimer approximation is valid.

From Eqs. (4), (9) and (10), the radiance emitted from a magnetic sublevel of a rotational level in the upper state can be expressed as:

$$\int L^{n'v'J'M_{J'}}_{n''v''J''M_{J''}} d\nu = \left(\frac{2\pi e^2 \ell}{mc}\right) \frac{\nu^2 N_{n'v'J'M_{J'}} f^{n'v'J'M_{J'}}_{n''v''J''M_{J''}}}{(2J'+1)} \qquad (11)$$

Hence, the total radiance for a band can be written as:

$$\int L^{n'v'}_{n''v''} d\nu = \left(\frac{2\pi e^2 \ell}{mc}\right) f^{n'v'} \sum_{J'} \frac{\nu^2(2-\delta_{o,\Lambda})(2S+1)(2J'+1)N_{n'v'J'M_{J'}} S_{J'J''}}{(2J'+1)}$$

$$= \left(\frac{2\pi e^2 \ell}{mc}\right) f^{n'v'} \sum_{J'} \nu^2(2-\delta_{o,\Lambda})(2S+1)\, N_{n'v'J'M_{J'}}\, S_{J'J''} \qquad (12)$$

The emission oscillator strength, $f^{n'v'}$ or f_{em}, is assumed to be the same for all the magnetic sublevels within the vibrational level in question. Since all the population terms of $N_{n'v'J'M_{J'}}$ can be expressed in terms of $N_{n'v'J_o'M_{J_o'}}$ which is the number of molecules per cm^3 in a magnetic sublevel of the lowest rotational level J_o', of the vibrational level v', of the electronic state, n',

$$N_{n'v'J'M_{J'}} = N_{n'v'J_o'M_{J_o'}} e^{-hcF_{J'}/kT} \qquad (13)$$

$F_{J'}$ is the rotational energy of the J'th rotational level relative to the lowest rotational level J_o'. Substituting Eq.(13) into (12), gives

$$\int L^{n'v'}_{n''v''} d\nu = \left(\frac{2\pi e^2 \ell}{mc}\right) N_{n'v'J_o'M_{J_o'}} f^{n'v'} \cdot \sum_{J'} (2-\delta_{o,\Lambda})(2S+1) S_{J'J''} \nu^2 e^{-hcF_{J'}/kT} \qquad (14)$$

Here the summation term must include all the lines involved in the transition between the upper and the lower rotational levels.

In this experiment, the quantity measured is the ratio

$$\frac{\int L^{n'v'}_{n''v''} d\nu}{L_\nu \Delta\lambda}$$

where the radiance of a band is compared to that of a black body in the same wavelength interval. The absolute radiance of the band can be computed, since the absolute radiance of a black body can be calculated from the Planck equation,

$$L_\nu = \frac{2c}{\lambda^4} \frac{1}{e^{hc/\lambda kT} - 1}$$

L_ν is the radiance emitted by a black body of temperature T(°K) at wavelength λ (cm), in quanta/sec/cm^2/solid angle/unit frequency interval, and hc/k is the second radiation constant.

The lifetime of an excited state is the reciprocal of the sum of all transition rates which depopulate the state.[65] It should be noted that in addition to the first order spontaneous radiative decay there are many other processes which may depopulate the excited state. First-order decay process such as spontaneous predissociation and auto-ionization and second-order decay process such as collisional quenching and stimulated emission contribute to make the lifetime shorter than it would be if the spontaneous radiative decay process were the only mode of decay.

The following relationships among the lifetime, wavelength and oscillator strength or Einstein A coefficient are restricted to purely spontaneous radiative decay. From the definition of lifetime:

$$\tau^{n'v'J'M_{J'}} = \frac{1}{\sum_{n''v''J''M_{J''}} A^{n'v'J'M_{J'}}_{n''v''J''M_{J''}}} \qquad (16)$$

where the sum is over the entire lower level. From Eq.(1) or Eqs.(9) and (10):

$$f^{n'v'J'M_{J'}}_{n''v''J''M_{J''}} = \frac{\lambda^2 mc}{8\pi^2 e^2} A^{n'v'J'M_{J'}}_{n''v''J''M_{J''}}$$

$$= 1.499\ \lambda^2\ A^{n'v'J'M_{J'}}_{n''v''J''M_{J''}} \qquad (17)$$

Substituting Eq. (17) into Eq. (16) gives:

$$\tau^{n'v'J'M_{J'}} = 1.499 \Big/ \sum_{n''v''J''M_{J''}} \left(\frac{f^{n'v'J'M_{J'}}_{n''v''J''M_{J''}}}{\lambda^2} \right) \tag{18}$$

Generally, the emission oscillator strength can be assumed to be equal for all the sublevels of a vibrational level and so can the lifetime. If λ represents the average wavelength of the rotational lines involved in each vibronic transition, then we have the following expression for the lifetime of an excited vibrational level.

$$\tau^{n'v'} = 1.499 \Big/ \sum_{n''v''} \left(\frac{f^{n'v'}_{n''v''}}{\lambda^2} \right) \tag{19}$$

The summation is over all vibrational levels of the lower electronic states.

IV. EXPERIMENTAL

A. Description of Furnace

The King-type furnace used in this work was identical to the one described by Brewer, Gilles and Jenkins.[66] The furnace consists of a hollow graphite resistance heating tube, which is similar to that described by Hagen.[67] The tubes have a $\frac{1}{2}$ inch bore drilled uniformly through the length of the tube. A 6-inch heating zone in the center of the tube was machined with an outside diameter tapered from 0.865 inch at the center to 0.750 inch at the constrictions which were located $3\frac{1}{4}$ inches from either end. The outside diameter of these $3\frac{1}{4}$ inch end sections is 0.877 inch. The insides of the graphite tubes were lined with 1 mil thick tantalum foil followed by 1 mil thick tungsten foil. $TiO_{1.6}$ or VO powder was placed on the tungsten foil in the hot zone inside the tube to prevent eutectic formation between Ti-Ta, Ti-C, V-Ta, V-C, or W-C. To further define the hot zone, $\frac{1}{4}$-inch I.D. $\frac{1}{2}$-inch long buffles made of graphite were placed at each end of the tapered region. The buffles were also used to reduce the amount of wall radiation reaching the spectrograph and minimize diffusion of the gaseous species from the hot zone. The tube was fitted snugly into split graphite bushings which were in turn fitted into the copper electrodes so as to give good electrical contact (Fig. 5). This arrangement permits longitudinal thermal expansion and contraction of the graphite tube without destroying the electrical contact.

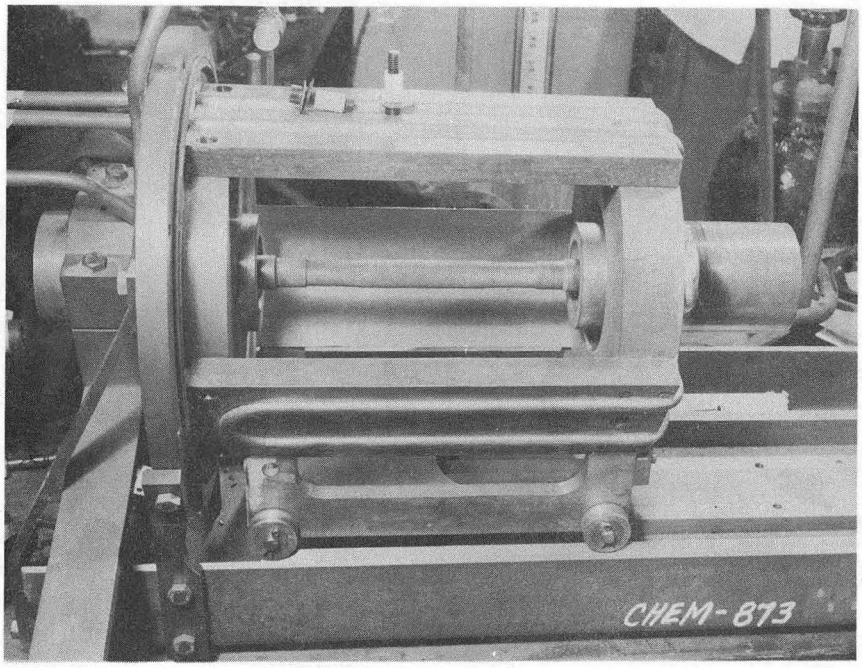

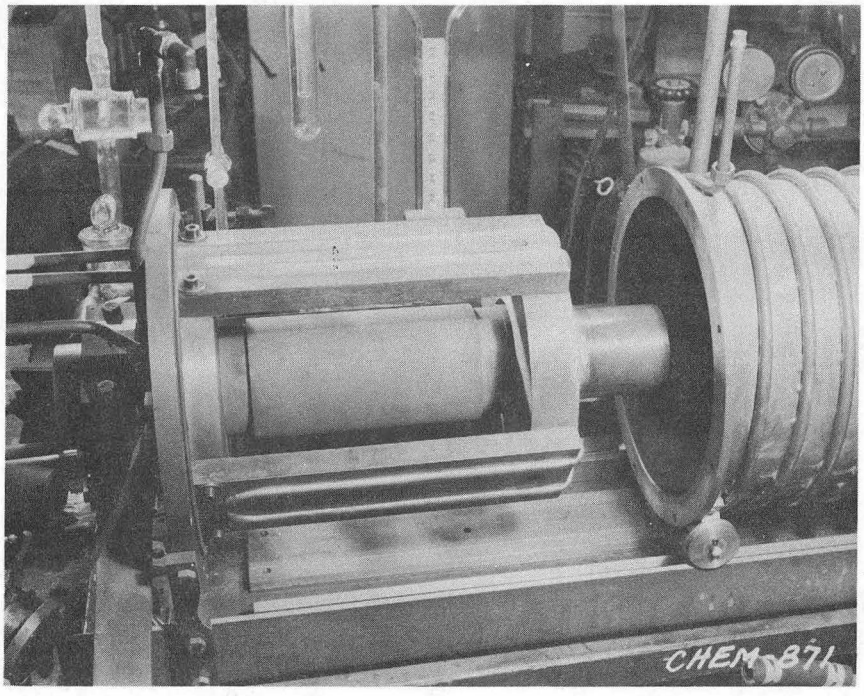

Figure 5

Internal view of the King furnace.

Quartz windows at either end of the furnace tube make possible the focusing of the hot zone on the spectrograph slit from one end, and the reading of the temperature with a Leads and Northrup optical pyrometer at the other end. Surrounding the heater tube is a graphite spool which holds five concentric graphite cylinders as radiation shields. The spool is insulated from the grounded outer brass drum by quartz rods that fasten one end of the spool into the disk cavity in one of the copper blocks. On the other end, teflon is used to insulate the inner metal support from the other chambers. The assembly is surrounded by a brass drum so that the entire system may be evacuated. Water is circulated as a coolant through brass tubing around the brass drum and the electrodes (Fig. 6). The tube was heated by low voltage alternating current from a 100 amp., 440 volts, 120-cycle source through a 200 kVA stepdown transformer with multiple connections providing the temperature range selection. Fine temperature adjustment was obtained with a Buck-boost variable transformer. The circuit of the power source for the King furnace is shown in Fig. 7.

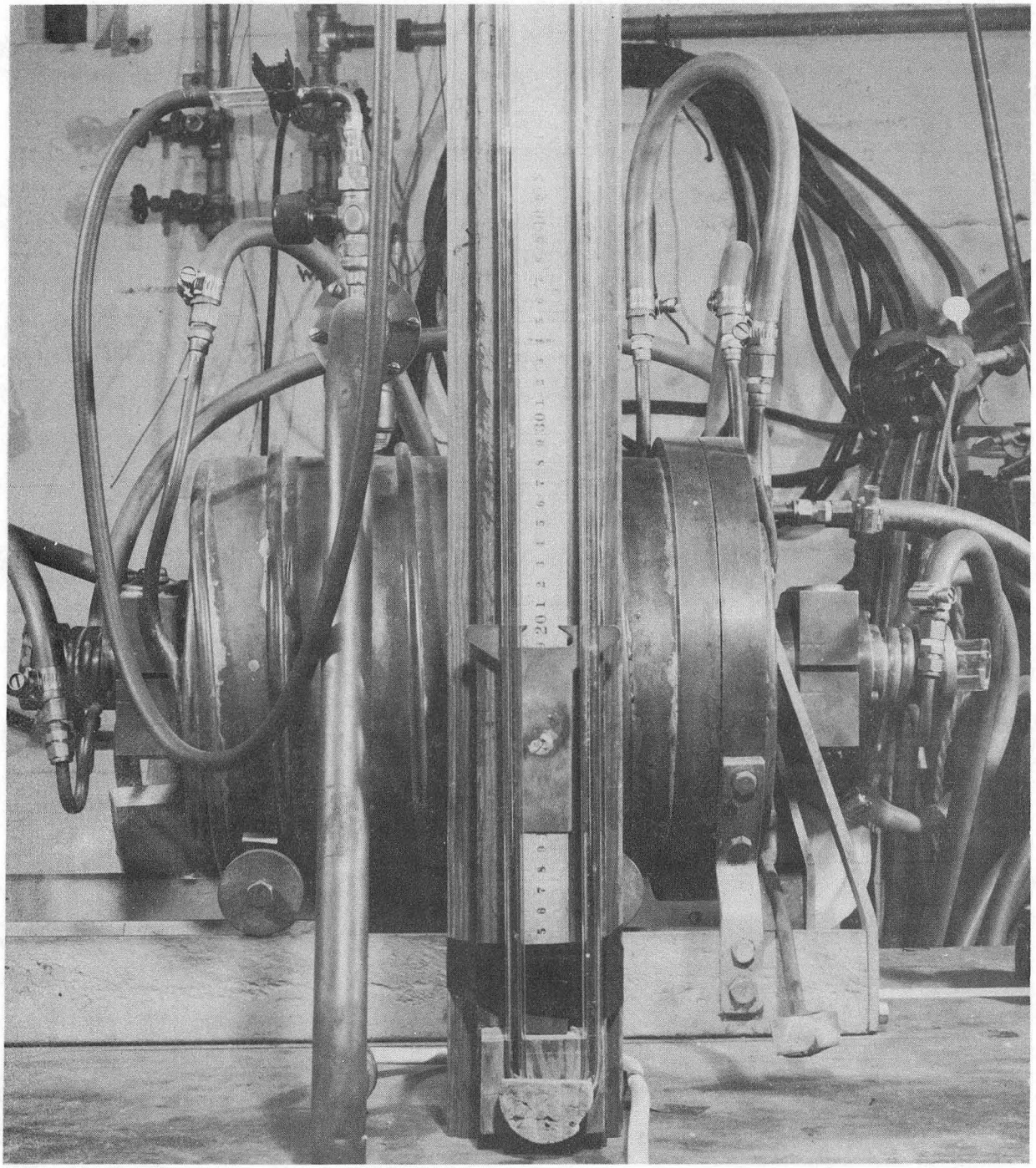

Figure 6

External view of the King furnace.

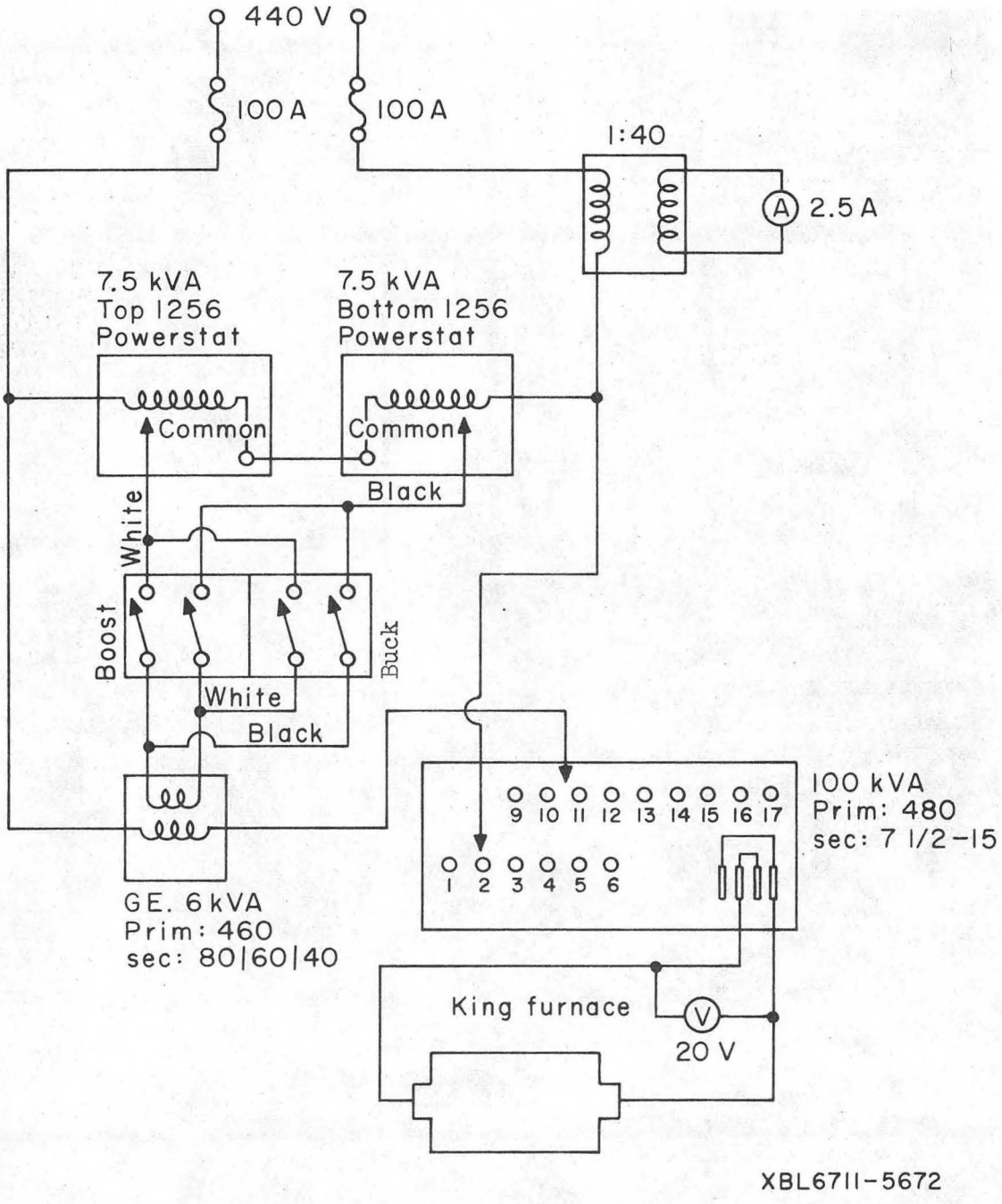

Figure 7

Wiring diagram of the power supply for the King furnace.

B. Optical Arrangement

The graphite tube is an extended source. Thus, in order to obtain the most effective slit illumination of gas emission and to prevent the wall light from falling on the slit, a spherical lens L_1 with focal length f_1 equal to or greater than the length of the furnace was adjusted to focus on the back of the hot zone of the tube and to diverge the light from the tube. A cardboard light stop and an aperture stop with orifice diameter smaller than the tube diameter were used to eliminate the black body radiation and the scattering light coming from the tube. A vertical cylindrical lens L_2 with focal length f_2 was used to image the gas emission light on the slit and to fill the whole grating horizontally with emission light. The focal lengths of the lenses required to fill the numerical aperture of the grating are $f_1 = 16.7$ cm and $f_2 = 6.67$ cm (Fig. 8).

The measurement of absolute intensity of emission requires consideration of the effect of the geometry of the King-furnace tube on the intensity of light arriving at the slit. It is necessary to compare the intensity from the gas in the tube to that of the reference black body light from the wall of the tube. The detailed calculation and experiments were performed by Hagen.[67] The results show that the difference in geometry between the reference source and the gas did not affect the measurements within the limits of error of the experimental data.

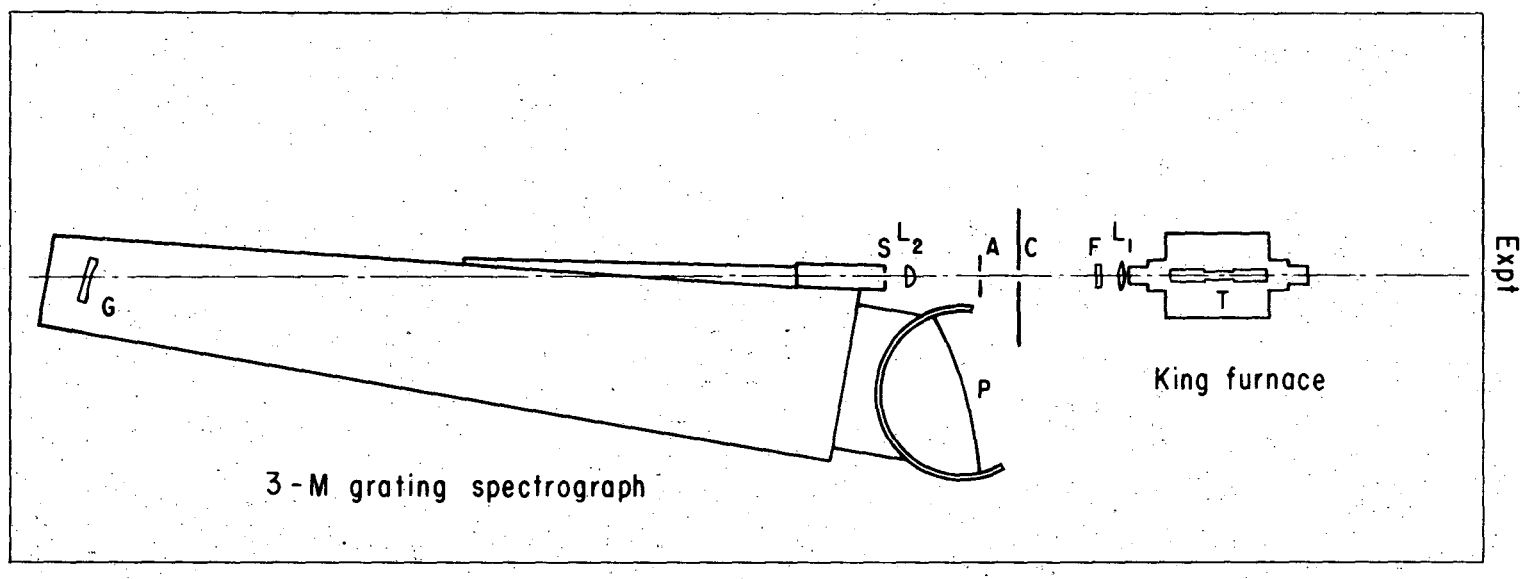

Figure 8

Schematic diagram of apparatus for King furnace emission experiment, top view, drawn approximately to scale with 25 to 1 reduction along optical axis. T, graphite tube; L_1, 23-cm spherical focal-length lens; F, neutral density filter; C, cardboard light stop; L_2, 6-cm focal-length cylindrical lens; S, 15μ-25μ slit; P, photographic plate; G, 6 x 14 cm grating with 6,000 lines per cm.

C. Spectrograph

A 3-m concave grating spectrograph with Eagle mount was used. Just like most of the other kinds of mountings of the concave grating, the Eagle mounting follows the principle, originally described by Rowland in 1883, that the slit and the plate lie on a circle, called the Rowland circle, to which the grating is tangent. The diameter of the circle has the radius of curvature of the grating blank. The slit and plate holder are mounted close together on one end of a rigid bar, and on the other end of the bar the concave grating is mounted (Fig. 8). The plate holder is pivoted around the center of gravity of the plate holder, so that the angle of incidence will change slightly for different settings. The grating is mounted on a turntable which slides in accurate ways in the direction of the slit. It is necessary to rotate the grating around its vertical axis, and at the same time to move it along the rigid bar in order to adjust for different ranges of spectrum. The dispersion on the plate is variable for the Eagle type mounting, it increases toward longer wavelengths; further, it changes from one setting to another, increasing toward longer wavelengths. The 3x5 inch grating has 15,000 lines per inch and the reciprocal linear dispersion is about 5.5 Å per mm in the first order and about 2.75 Å per mm in the second order at around 5,000 Å. A slit opening of 0.015 to 0.025 mm was used. The instrumental broadening was about 0.60 Å in the first order and about 0.35 Å in the second order.

D. Procedures

TiO powder was prepared by mixing proper amounts of titanium powder (m3N) from ALFA Inorganic, Ventron Corp., Beverly, Massachusetts, with purified titanium dioxide powder from Allied Chemical Co., Morriston, New Jersey. VO powder was prepared by mixing proper amounts of vanadium powder (99.5%) with vanadium dioxide powder (99+%), both from Research Organic/Inorganic Chemical Corp., Sun Valley, California.

The $TiO_{1.6}$ powder or VO powder was placed on the tungsten foil within the hot zone inside the graphite tube. The system was evacuated to around 150 μ which was read on a Hasting thermocouple gauge. Argon inert gas was added to the furnace through a valve to the atmosphere pressure and the system was evacuated again. The procedure was repeated several times to dispel atmospheric oxygen from the inside of the tube. Finally the argon gas at about 15 cm Hg was introduced in and remained inside the furnace. The gas pressure was measured on a manometer. The tube was heated to around 500-800°K for a couple of minutes to out-gas the system. The system was then evacuated after turning off the heating power. Before taking the spectra, argon gas at a pressure of 15 cm Hg was again introduced into the furnace, and power was turned on and adjusted until the desired temperature was reached. The inert gas in the tube reduced the rate of diffusion of the TiO or VO molecules out the ends of the tube and effects a sufficient number of collisions with the TiO or VO molecules to establish thermal equilibrium with the walls. It also prevents the excitation of the species under study brought about by substantial acceleration of free electrons due to the potential difference across the graphite tube.

A temperature of about 2,000°C was obtained when there was a potential drop of 12 to 14 volts along the graphite resistance heating tube with a current of approximately 1,000 amperes. The temperature was read on the brightest part inside the hot zone (i.e., metal oxide), on the tungsten wall and on the graphite buffle inside the tube.

The gas emission and then the radiation from the wall of the tube passing through the calibrated Corning neutral density filters were focused for same length of time on the slit of the 3-m concave-grating spectrograph. The images of the slit were then formed on the photographic plates. To relate plate-darkening to intensity, a calibrated-step weakner from Jarrell-Ash Company was mounted on the spectrograph behind the plate just before the exposure to the wall radiation. Plates were developed in Kodak D-19 developer for 4 minutes. During development the plates were lightly brushed with cotton to minimize the Eberhard effect. The plates were then rinsed for 30 sec and placed in Kodak rapid fixer for 5 min. The temperature of the solutions was approximately 20°C. The plates were then rinsed for 30 min. in running water. Plates were removed and dried for at least 24 hours at room temperature before scanning.

The characteristic curve for the spectrogram was fed into the Jarrell-Ash Direct-Intensity Microphotometer through the 24 dial knobs. A computer code converted photographic densities into relative intensities.

E. Temperature Corrections

Tow optical pyrometers were used in this work. The #1 pyrometer with Leeds and Northrup serial no. 749235 was used for all the experimental measurements. The #2 pyrometer with Leeds and Northrup serial no. 1532547 which had been calibrated by the U. S. National Bureau of Standards in Washington, D.C. was used as a standard to calibrate the readings taken by #1 pyrometer. The correlation of temperature readings from #1 to those from #2 is shown in Fig. 9. The #2 pyrometer was standardized on the basis of the International Practical Temperature Scale 1948 (IPTS-48). Its scale correction amounted to ±8°C when the pyrometer reads 1750°C and ±18°C when it reads 2540°C according to the NBS corrections. The IPTS-68 was adopted in 1968 as a replacement for the IPTS-48.[68,69] The IPTS-68 scale extends the temperature range downward (from approximately 90°K in the IPTS-48 to approximately 14°K in the IPTS-68). The IPTS-68 scale is also closer to the thermodynamic temperature scale. Hence, the temperatures measured, based on IPTS-48, must be converted to IPTS-68 scale before using thermodynamic functions to calculate the vapor pressures of the species under study. Differences between the IPTS-68 and IPTS-48 at a few temperatures are the following:

T_{68} (°K):	273.16	298.15	1000	1500	2000	3000
$T_{68}-T_{48}$ (°K):	0.0000	-0.0085	+0.464	+1.70	+2.65	+5.1

In addition to these pyrometer scale and temperature scale corrections, the temperatures read through the window of the King furnace

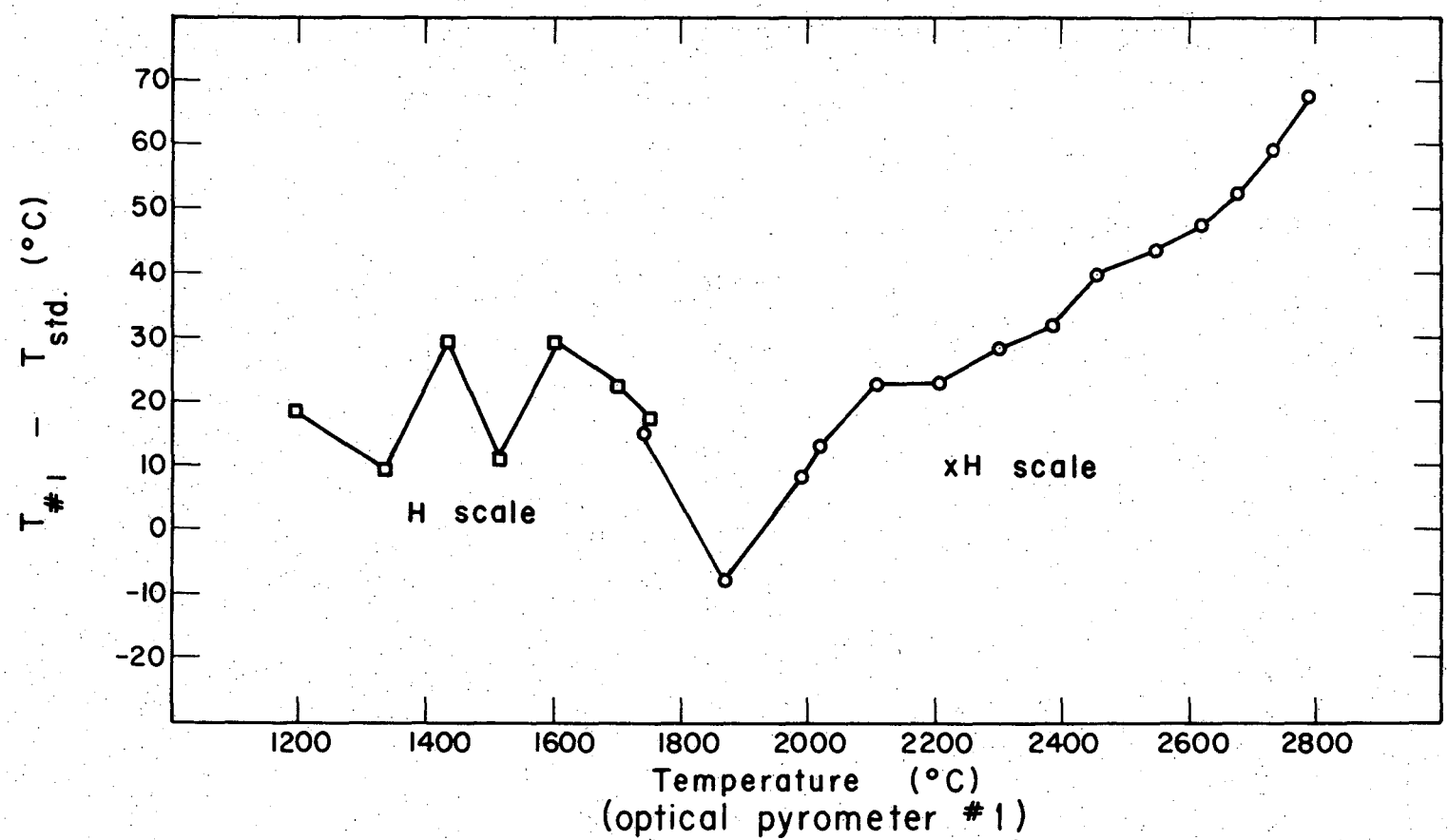

Figure 9

The correlation of temperature readings between #1 and standard optical pyrometer.

were corrected for transmission losses according to Wien's law: $1/T_1 - 1/T_2 = K$, where K is a transmission constant which was determined experimentally to be $0.060 \pm 0.003 \times 10^{-4}$ deg^{-1} (Fig. 10). This accounts for a difference of 25°K at about 2,000°K.

The emissivity correction must also be made for the substance on which the temperature was measured. The emissivity of metal oxides is closer than that of the tungsten wall to the black body radiation. Hence, the temperature taken by viewing metal oxide is closer to the true temperature. However, the $TiO_{1.6}$ and the VO still did not act as perfect black-body radiators even in a long narrow cylinder. To test how it approached a black body radiator, the metal oxide and a piece of ZrC were placed inside the hot zone of the graphite tube. Both the temperatures of metal oxide and the ZrC were read and compared (Fig. 11). Since the emissivity of ZrC was reported to be 0.96,[70] the temperature of ZrC could be taken as the temperature of a black body radiator without introducing substantial error in a long narrow cylinder; meanwhile, the temperature during the experiments stayed below 2,500°K. The temperatures of the metal oxides can thus be correlated to the true temperatures.

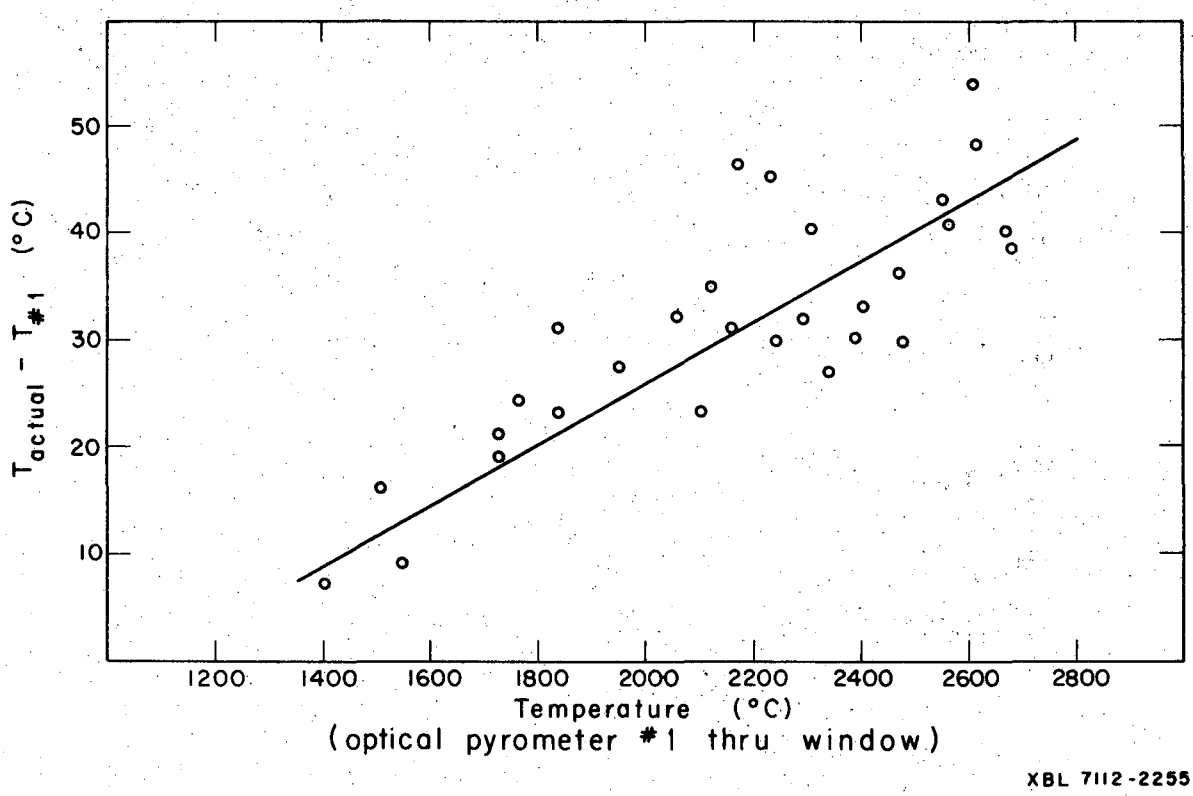

Figure 10

Temperature correction for the transmission loss of window.

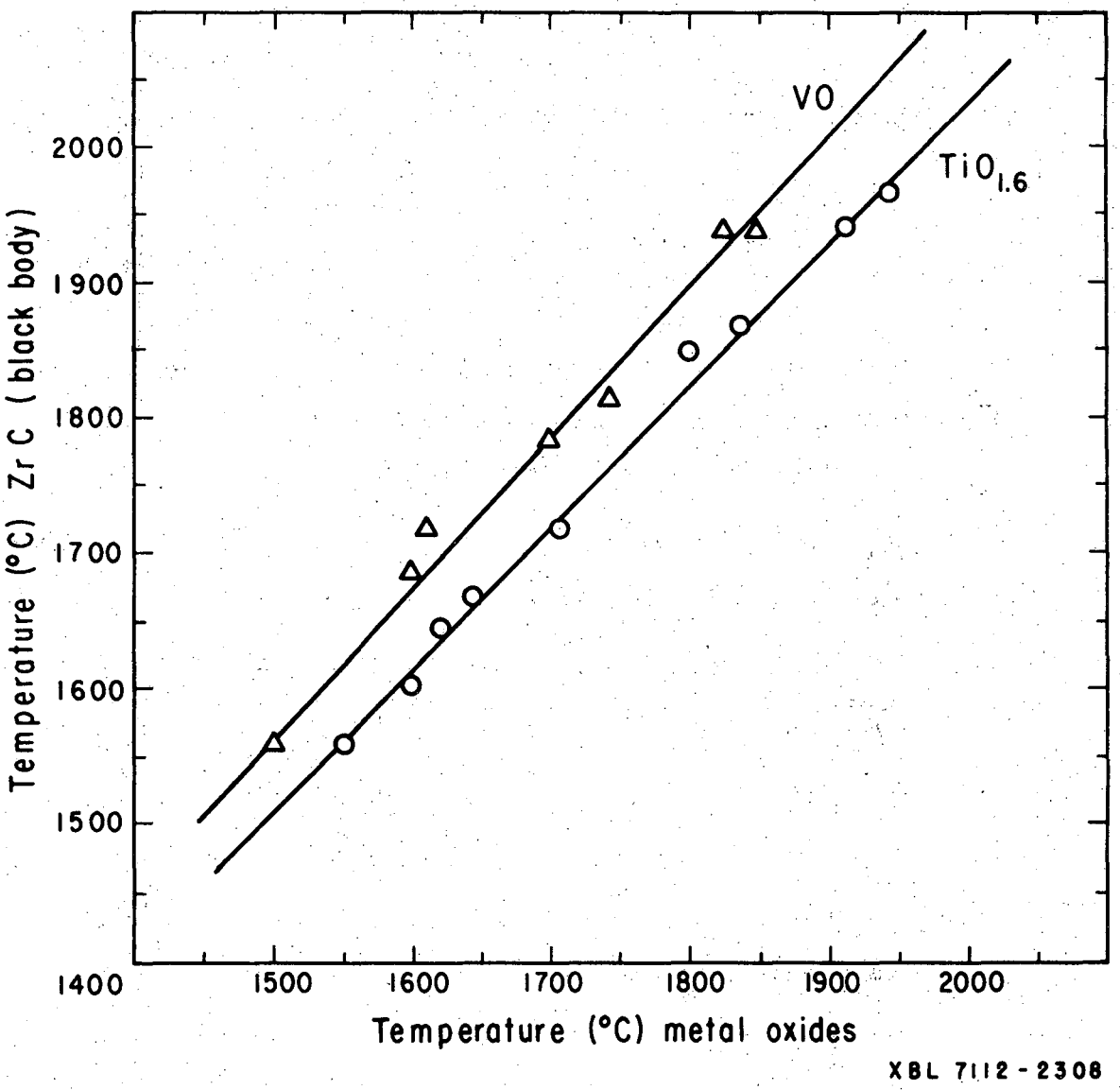

Figure 11

Temperature correction for the emissivity of metal oxides.

V. CALCULATION OF RESULTS

Equation (14) was used to calculate the absolute oscillator strengths of TiO and VO bands. The total absolute amount of radiation emitted in the bands, integrated over all wavelengths, $\int L_{n''v''}^{n'v'} d\nu$, was obtained experimentally by comparing the area under the gas emission profile to that under the profile of black body radiation over the same wavelength interval. The measured emitted radiance, however, was not directly proportional to the concentration of the molecules in the upper state since the emitted light could be reabsorbed by molecules in the lower state before leaving the gas. Brewer, Hick and Krikorian[71] had shown that the measured radiance could be corrected for self-absorption.

Computer programs were written to calculate the summation term $\sum_{J_i}^{J'} S_{J'J''} \nu^2 e^{-hcF_{J'}/kT}$, which is summed over each individual rotational line of the (0,0) band of the TiO α-system and the (0,0) band of the VO green system. The programs which also plotted the theoretical emission profile of the bands in $^3\Delta$ - $^3\Delta$ and $^4\Sigma$ - $^4\Sigma$ transition are listed in Appendix B.

In these experiments the emission spectra of gaseous TiO were taken over liquid phase of $TiO_{1.6}$ and the emission spectra of gaseous VO were taken over the solid and liquid phases of VO. The vapor pressure of TiO and VO over solid phases at certain tamperatures were measured by mass spectroscopy.

The vapor pressure of VO over the VO solid and liquid phases can be calculated by using the free energy functions or heat contents and

molal entropies. The vapor pressure of TiO over $TiO_{1.6}$ liquid phase can be calculated by using the free energy functions coupled with the titanium-oxygen phase diagram to extrapolate those experimental values of vapor pressure known for the solid phase to the liquid phase of desired temperatures.

The number densities of TiO and VO molecules in the state $N_{n'v'J'M_{J'}}$, can then be computed from these calculated vapor pressures and taking statistical distribution law into consideration.

A. Titanium Monoxide

1) Vapor Pressures

The partial vapor pressures of TiO over TiO, Ti_2O_3, Ti_3O_5 and Ti_4O_7 solid phases have been extensively studied by Johnston et al.,[72] Berkowitz et al.,[73] and Gilles et al.,[74] using the mass spectrometer to analyze the vapors effusing from a Knudsen cell. Some of their experimental results are listed in Table XII. Their results can be used to estimate the TiO vapor pressure over $TiO_{1.6}$ liquid phase. The phase diagram of the titanium-oxygen system was investigated by Wahlbeck and Gilles.[75] A portion of the phase diagram taken from Gilles' work is shown in Fig. 12. The diagram shows only that part of the diagram with O/Ti ranging from 1.0 to 2.0.

The solid phases are in equilibrium with liquid phases at A, B and C shown in Fig. 12. These three points correspond to the melting points of compositions $TiO_{1.29}$, $TiO_{1.5}$ and $TiO_{1.71}$ at 1993°K, 2120°K and 2050°K respectively. The change of free energy in going from solid to liquid phases is zero at these points since the free energy of a compound in solid phase equals that in liquid phase at its melting point.

Extrapolation using any two of these three points to the liquid phase would give us the TiO vapor pressures over $TiO_{1.6}$ liquid phase. The vapor pressures used in the following f-value calculations are based on the extrapolation of B and C points. Point A was also used to check the results.

TABLE XII

Partial Vapor Pressures of TiO, TiO_2 and Ti
Obtained from Experimental Results

Composition	Vapor pressure (atm)			Reference
	P_{TiO}	P_{TiO_2}	P_{Ti}	
metal-rich Ti_2O_3(s) phase (Ti_2O_3 + TiO phases) at 2000°K	$10^{-5.9}$	$10^{-8.2}$	$10^{-6.0}$	Berkowitz, Chupka, Ingram
congruent Ti_2O_3(s) phase at 2000°K	$10^{-6.5}$	$10^{-7.6}$	$10^{-7.0}$	
metal-rich Ti_3O_5(s) phase (Ti_2O_3 + Ti_3O_5 phases) at 2000°K	$10^{-6.75}$	$10^{-7.3}$	$10^{-8.8}$	Hampson, Gilles Fig. 1 MS-3(K)
congruent Ti_3O_5(s) phase at 2000°K	$10^{-7.30}$	$10^{-7.03}$	$10^{-10.14}$	Hampson, Gilles Fig. 4
oxygen-rich Ti_3O_5(s) phase (Ti_3O_5 + Ti_4O_7 phases) at 1891°K	$10^{-8.2}$	$10^{-7.76}$		Hampson, Gilles

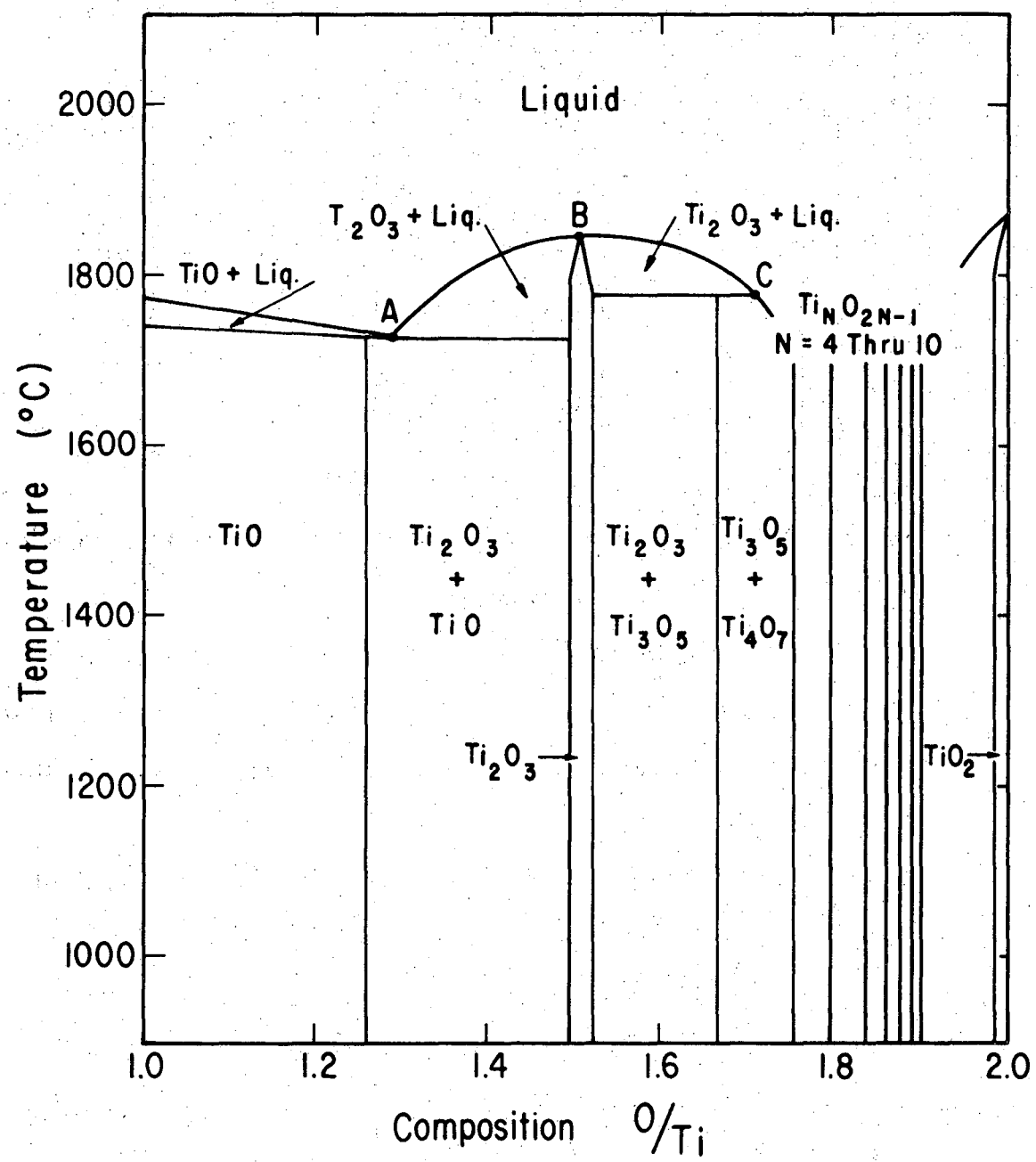

Figure 12

Phase diagram of titanium-oxygen system.

The free energy functions of Ti_2O_3 (i.e., $TiO_{1.5}$) for both solid and liquid phases are available from JANAF table.[76] However data are also needed for $TiO_{1.29}$ and $TiO_{1.71}$. Table XIII gives free energy function per gram-atom of $TiO_{1.67}$, $TiO_{1.71}$ and TiO_2 in solid phase. Table XIV shows the free energy function per gram-atom of TiO, $TiO_{1.29}$, $TiO_{1.5}$ and $TiO_{1.67}$, $TiO_{1.71}$, TiO_2 in liquid phase. These values were calculated by using the free energy function of TiO, Ti_2O_3, Ti_3O_5 and TiO_2 in solid as well as liquid phases provided from JANAF table. Molal entropies of Ti, TiO and TiO_2 in gas phase at several experimental temperatures are listed in Table XV. They are also taken from JANAF table.

The vapor pressures of TiO, TiO_2 and Ti at different temperatures can then be calculated from the equation $\Delta F_T^\circ = -RT \ln K$, and by assuming that $\Delta C_P = 0$ over a small range of temperature variation, so that

$$\Delta F^\circ_{T_2} = \Delta F^\circ_{T_1} - \left[T_2\left(\frac{\Delta F^\circ_{T_2} - \Delta H^\circ_{298}}{T_2}\right) - T_1\left(\frac{\Delta F^\circ_{T_1} - \Delta H^\circ_{298}}{T_1}\right)\right]$$

The results of the calculation are shown in Table XVI. The vapor pressure of TiO over $TiO_{1.6}$ phase can be estimated at the desired temperature by interpolation of these data. The result of these interpolation are shown in Fig. 13.

2) The Population Analysis

The number densities of TiO at $J' = 1$, $v' = 0$ levels of the $C^3\Delta_1$ state were computed first by calculating the number densities of TiO

TABLE XIII

Free Energy Function of Titanium Oxides (solid)
($-(F^\circ - H^\circ_{298})/T$ in cal deg^{-1} gram-atom^{-1})

Temperature (°K)	$TiO_{1.667}$ (Ti_3O_5) JANAF	$TiO_{1.714}$	TiO_2 JANAF
1891	10.410	10.258	9.332
2050	10.845	10.688	9.736

TABLE XIV

Free Energy Function of Titanium Oxides (liquid)
($-(F^\circ - H^\circ_{298})/T$ in cal deg^{-1} gram-atom^{-1})

Temp. (°K)	TiO JANAF	$TiO_{1.292}$	$TiO_{1.5}$ (Ti_2O_3) JANAF	$TiO_{1.667}$ (Ti_3O_5) JANAF	$TiO_{1.714}$	TiO_2 JANAF
1993	15.512	13.730	12.460			
2050				12.347	12.308	12.073
2120			12.856			
2141	16.001	14.201	12.919	12.608	12.565	12.302
2152	16.036	14.235	12.952	12.639	12.595	12.329
2184	16.139	14.334	13.048	12.729	12.684	12.408
2193	16.168	14.362	13.075	12.754	12.708	12.430
2237	16.305	14.493	13.203	12.874	12.826	12.536
2292	16.474	14.657	13.363	13.022	12.972	12.668
2314	16.541	14.721	13.425	13.080	13.030	12.724
2323	16.567	14.747	13.450	13.104	13.053	12.740
2328	16.582	14.761	13.464	13.117	13.065	12.752
2406	16.813	14.984	13.681	13.319	13.264	12.932

TABLE XV

Free Energy Function of Titanium Oxides (gas) *

($-(F^\circ - H^\circ_{298})/T$ in cal deg^{-1} $mole^{-1}$)

Temperature (°K)	Ti(g) JANAF	TiO(g) JANAF	TiO_2(g) JANAF
1891	48.440	64.515	69.056
1993	48.676	64.908	69.672
2000	48.692	64.935	69.714
2050	48.804	65.120	70.004
2120	48.958	65.375	70.406
2141	49.004	65.450	70.523
2152	49.027	65.489	70.585
2184	49.096	65.603	70.764
2193	49.116	65.635	70.814
2210	49.152	65.694	70.907
2237	49.208	65.787	71.052
2292	49.323	65.976	71.349
2314	49.368	66.049	71.465
2323	49.387	66.079	71.512
2328	49.397	66.096	71.538
2406	49.555	66.353	71.943

* The data of this table are interpolated from those listed in JANAF.

TABLE XVI

Calculated vapor pressures of Ti, TiO and TiO_2 *

	Ti_2O_3 congruent								
	$(TiO_{1.292})_{liq}$			$(TiO_{1.5})_{liq}$			$(TiO_{1.715})_{liq}$		
Temp. (°K)	P_{TiO} ($\times 10^6$)	$PTiO_2$ ($\times 10^8$)	P_{Ti} ($\times 10^6$)	P_{TiO} ($\times 10^6$)	P_{TiO_2} ($\times 10^7$)	P_{Ti} ($\times 10^7$)	P_{TiO} ($\times 10^7$)	P_{TiO_2} ($\times 10^7$)	P_{Ti} ($\times 10^9$)
2141	6.75	3.38	5.38	2.35	1.87	7.43	2.34	7.74	3.24
2152	7.64	3.83	6.07	2.68	2.12	8.46	2.66	8.81	3.70
2184	10.9	5.45	8.64	3.88	3.08	12.3	3.88	12.9	5.38
2193	12.0	6.0	9.50	4.30	3.42	13.6	4.34	14.4	6.03
2210	14.4	7.18	11.4	5.20	4.14	16.5	5.29	17.5	7.35
2237	19.6	10.	15.6	7.44	5.91	23.6	7.20	23.8	10.
2292	33.0	16.5	26.2	12.6	10.	39.8	13.1	43.4	18.2
2314	40.8	20.4	32.4	15.7	12.5	49.8	16.6	54.8	23.0
2323	44.5	22.3	35.3	17.4	13.8	54.9	18.2	60.2	25.2
2328	46.6	23.4	37.0	18.1	14.4	57.4	19.2	63.4	26.6
2406	94.6	47.5	75.3	38.4	30.5	122.	43.6	138.	57.8

* All pressures in atm.

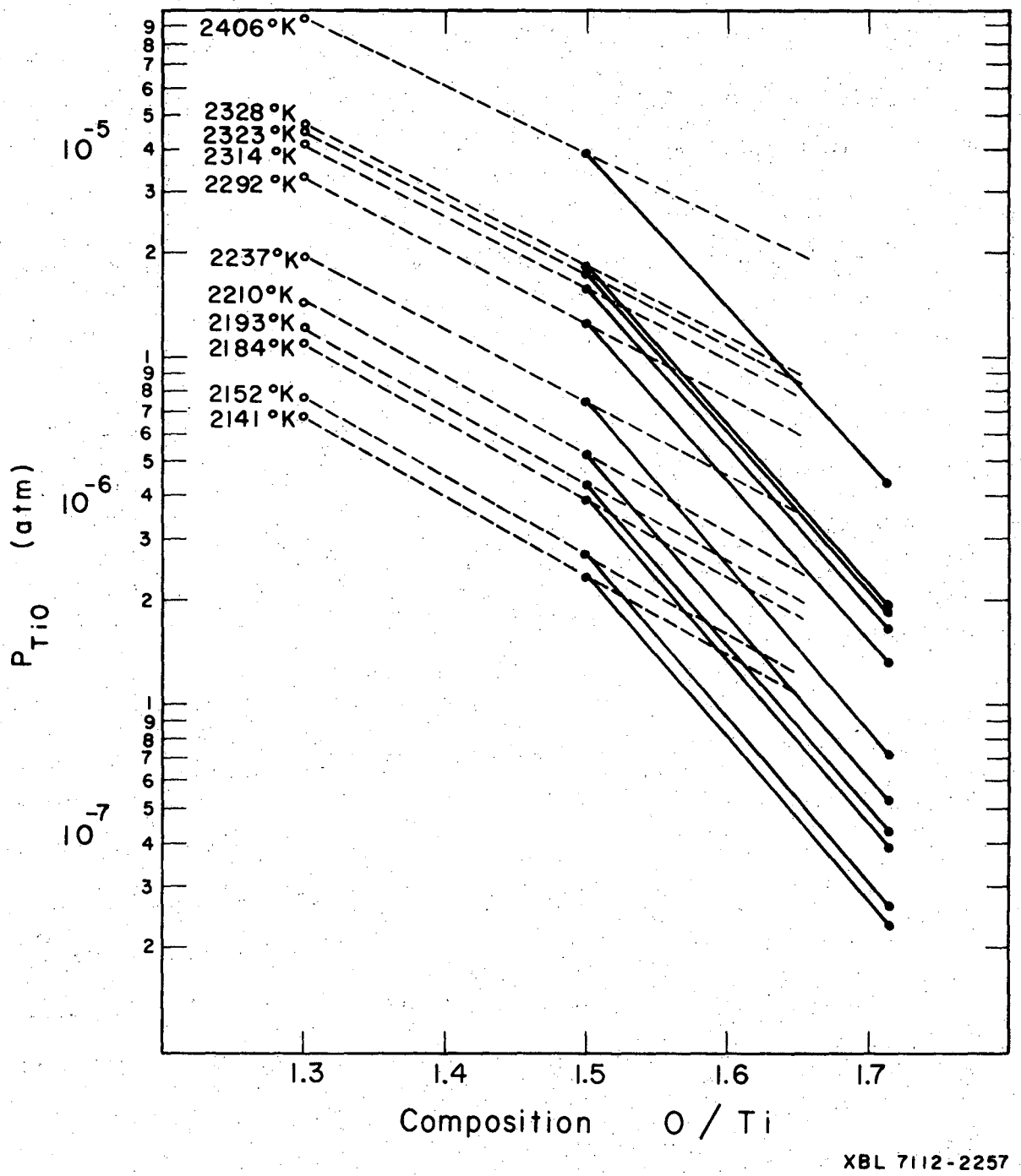

Figure 13

Interpolated vapor pressure of TiO over $TiO_{1.6}$ phase.

at J" = 1, v" = 0 levels of the ground electronic state $X^3\Delta_1$ using the extrapolated vapor pressure and then by considering the Boltzmann distribution law. The energy difference between these two levels was taken from that given by Christy.[1]

Rotational partition function, Q_r, is calculated from the equation:

$$\ln Q_r = - \ln y - \ln \sigma + \frac{y}{3} + \frac{y^2}{90} + \ldots . \qquad (20)$$

where the dimensionless quantity is defined as $y = \frac{hcB}{kT}$, B is the rotational constant and σ, the symmetry number, is 1 for the unsymmetrical TiO.

Vibrational partition function, Q_{vib} is calculated from the equation:

$$Q_{vib} = \sum_v e^{-uv} = \frac{1}{1 - e^{-u}} \qquad (21)$$

where $u = \frac{h\nu}{kT} = \frac{hc\omega}{kT} = 1.4387 \frac{\omega}{T}$, ω is the frequency of the vibration in units of reciprocal centimeters. The discussion of these equations can be found in the text of thermodynamics by Pitzer and Brewer.[77]

The contribution to the free energy function of TiO due to the electronic part was calculated from the electronic levels of TiO given by Brewer and Rosenblatt.[16] The electronic partition function, Q_{el} can be calculated from the equation:

$$- \left(\frac{F^\circ - H^\circ}{T} \right)_{el} = R \ln Q_{el} \qquad (22)$$

The calculated partition functions Q_r, Q_{vib} and Q_{el} are summarized in Table XVII.

TABLE XVII

Partition Functions of TiO

Temperature (°K)	$Q_{rot} \times 10^{-3}$	Q_{vib}	Q_{el}
2141	2.775	2.033	8.37
2152	2.785	2.041	8.39
2184	2.825	2.062	8.40
2193	2.840	2.070	8.41
2210	2.854	2.083	8.42
2237	2.90	2.101	8.42
2292	2.97	2.137	8.45
2314	2.995	2.151	8.46
2323	3.005	2.160	8.47
2328	3.015	2.162	8.47
2406	3.120	2.217	8.53

Fraction of population in a specific rotational level can be calculated by using the equation:

$$q = \frac{(2 - \delta_{o,\Lambda})(2S + 1)(2J + 1)}{Q_{el}\, Q_{vib}\, Q_{rot}} \tag{23}$$

where $(2 - \delta_{o,\Lambda})(2S+1)$ takes into account the degeneracy of the electronic state, $(2 - \delta_{o,\Lambda})$ accounts for the spin multiplicity, and $(2J+1)$ accounts for the rotational degeneracy. The desired quantity is the number density of only one of the magnetic sublevels of the lowest rotational level of the state in using Eq.(14) as mentioned previously. Both states of the α system of TiO transition belong to $^3\Delta$. The energy diagram of the $^3\Delta$ - $^3\Delta$ transition was shown in Fig. 2. The lowest rotational level is the $J'' = 1$, $v'' = 0$ of $^3\Delta_1$ substate. The rotational level of $^3\Delta_2$ and $^3\Delta_3$ substates begin with $J = 2$ and $J = 3$ respectively. Therefore Eq.(23) is reduced to the following form for the calculation of fractional population of one of the magnetic sublevels of $J'' = 1$, $v'' = 0$ level of the $X^3\Delta_1$ state. (Here, the sublevels with magnetic quantum number M_J and $-M_J$ are considered as two different levels.)

$$q'' = \frac{1}{Q_{el}\, Q_{vib}\, Q_{rot}} \tag{24}$$

Fraction population of TiO of one of the magnetic sublevels of the $J' = 1$, $v' = 0$ level of the $C^3\Delta_1$ state, q', can be calculated by the following equation:

$$q' = q'' \, e^{hc\Delta E/kT} \tag{25}$$

where ΔE is the energy difference in cm^{-1} between $J'' = 1$, $v'' = 0$ of the $X^3\Delta_1$ state and $J' = 1$, $v' = 0$ of the $C^3\Delta_1$ state.

The total number density, n, in molecules/cm^3 can be obtained from the equation $n = P/RT$, where P is the vapor pressure in mm Hg and R is the gas constant, equal to 10.4×10^{-20} cm^3-mmHg/molecules-deg.

The vapor pressure of TiO over $TiO_{1.6}$ phase interpolated from the vapor pressures over $TiO_{1.5}$ and $TiO_{1.71}$ phases is used to calculate the total number density, the number density of one magnetic sublevel of $J' = 1$, $v' = 0$ level of the $C^3\Delta_1$ state and of one magnetic sublevel of $J'' = 1$, $v'' = 0$ level of the $X^3\Delta_1$ state. These results are given in Table XVIII.

3) The Band Intensities

To obtain the total amount of radiation emitted in a band, integrated over all wavelengths, care must be taken to exclude the contribution of radiation due to the impurity lines. One must also consider the fact that the bands of a system might fall into close sequences, so the "tails" of the band might be blended with the following bands of the sequences.

In the case of (0,0) band of the α-system of TiO, the rotational constants are known. The true location of each individual rotational line was determined experimentally by Christy and later improved upon by Phillips.[78] Hence the intensity profile of this band without blending with any other spectral feature can be computed according to the following equation:

TABLE XVIII

Population analysis of TiO vapor over $TiO_{1.6}$ liquid phase

True temperature (°K)	Total number density (molecules/cm^3) ($x10^{-12}$)	Fraction of population of one magnetic sublevel of $J''=1,v''=0,X^3\Delta$ ($x10^5$)	Number density of one magnetic sublevel of $J''=1,v''=0,X^3\Delta$ (molecules/cm^3) ($x10^{-7}$)	Fraction of population of one magnetic sublevel of $J'=1,v'=0,C^3\Delta$ ($x10^{11}$)	Number density of one magnetic sublevel of $J'=1,v'=0,C^3\Delta$ (molecules/cm^3) ($x10^{-2}$)
2141	2.765	2.117	5.856	4.145	1.423
2152	3.124	2.098	6.553	5.496	1.717
2184	4.484	2.044	9.163	6.469	2.901
2193	4.998	2.022	10.106	6.744	3.370
2210	5.952	1.990	11.843	7.302	4.347
2237	8.330	1.948	16.230	8.320	6.929
2292	14.19	1.865	26.470	10.726	15.219
2314	17.69	1.835	32.452	11.834	20.935
2323	19.19	1.820	34.927	12.286	23.586
2328	20.09	1.812	36.412	12.538	25.178
2406	42.22	1.695	71.576	17.291	72.996

$$I_{em} \propto \nu^4 S_{J'J''} e^{-B'J'(J'+1)hC/kT} \tag{26}$$

where ν is the wave number, B' is the rotational constant, and I_{em} is the intensity of an emission line. The α-system of TiO is produced by the $C^3\Delta - X^3\Delta$ transition. Both the electronic states are good examples of Hund case (a) type coupling. For such a transition the following equation derived theoretically by Hönl and London[79] can be used for the line strength.

$$\begin{aligned} S_J^P &= \frac{(J' + 1 + \Omega')(J' + 1 - \Omega')}{(J' + 1)} \\ S_J^Q &= \frac{(2J' + 1)\Omega'^2}{J'(J' + 1)} \\ S_J^R &= \frac{(J' + \Omega')(J' - \Omega')}{J'} \end{aligned} \tag{27}$$

The parameter Ω in these equations takes the values 1, 2 and 3 for the $^3\Delta_1 - {}^3\Delta_1$, $^3\Delta_2 - {}^3\Delta_2$ and $^3\Delta_3 - {}^3\Delta_3$ subbands respectively. It is obvious from the equations that, for all but the smallest values of J, the intensities of lines of the Q-branch must be very low relative to the intensities of lines of the R- and P-branches. Hence one can ignore the Q-branch in the computation of the intensity profile, without making any detectable error.

The profile of spectral lines must be known before the theoretical band profile can be drawn. A detailed quantitative description of the spectral line profiles requires consideration of various line-broadening mechanisms[65] which include the natural line broadening, Doppler broadening, pressure broadening and the instrumental broadening.

The natural line width arises from the Uncertainty Principle. Each of the two energy levels between which a transition occurs, is not indefinitely sharp but has a finite width of ΔE_1 and ΔE_2. The line shape due to the natural line broadening is Lorentzian. The half-width (in cm^{-1}) of a transition line is made up by the term widths of the two levels:

$$\Delta\nu_N = \Delta E_1 + \Delta E_2 = \frac{1}{2\pi C}\left(\frac{1}{\tau_1} + \frac{1}{\tau_2}\right) \tag{28}$$

The Doppler line width comes from the thermal motion of the molecules (atoms) of a gas. The effect of its own thermal motion broadens the lines statistically. The form of the line shape is Gaussian. The half-width (in cm^{-1}) of a transition line is:

$$\Delta\nu_D = \frac{2\sqrt{2R \ln 2}}{C} \nu_o \sqrt{\frac{T}{M}} \tag{29}$$

The pressure broadening is often called the collision broadening. The essential cause of line broadening lies in the interaction of long-range van der Waals force between the radiating molecules (atoms), in the initial and final states involved in the radiation process, and a colliding molecule (atom). The long-range van der Waals force commonly includes four types of forces: i) electrostatic forces (such as those between electric dipoles), ii) induction forces (such as those between a polarizable nonpolar molecule and an electric dipole), iii) dispersion forces (such as those between nonpolar molecules) and iv) resonance forces (exchange of excitation energy between molecules of the same

kind). The interaction causes a perturbation on the molecule. The energy levels of the molecule are, therefore, shifted. The line shape due to the collision broadening is Lorentzian. The half-width (in cm^{-1}) of a transition line is:

$$\Delta\nu_P = \frac{2}{\pi}\sigma^2 N\left[2\pi RT\left(\frac{1}{M_1}+\frac{1}{M_2}\right)\right]^{\frac{1}{2}} \qquad (30)$$

M_1 and M_2 are the molecular weights of the colliding molecules, σ^2 is the effective cross-section and N is the number of the foreign gas molecules per cm^3.

The instrumental broadening is due to astigmatism of the concave grating. The astigmatic broadening can be calculated from the relation given by Sawyer[80] and by Beutler.[81] It can also be measured experimentally. The atomic Ar and Ti lines were tested for the 3-m-grating spectrograph. The optical arrangement was identical to that used for this research. The lines were broadened to a width of 1 to 2 cm^{-1}. Krikorian[82] measured the atomic line profile of Zr on the 3-m-grating using an interferometric technique. He found that the atomic line was Doppler-shaped (i.e. Gaussian).

The TiO or VO vapor with 15 cm Hg of Ar gas was at about 2500°K during the experiment. If the radiative lifetime of the excited state is 10^{-8} sec, the natural line broadening: $\Delta\nu_N = 5 \times 10^{-4}$ cm^{-1}. The Doppler line broadening (due to the thermal motion): $\Delta\nu_D = 9 \times 10^{-2}$ cm^{-1}. The pressure line broadening for 15 cm Hg Ar gas: $\Delta\nu_P = 3 \times 10^{-2}$ cm^{-1}. The instrumental line broadening: $\Delta\nu_I = 1$ cm^{-1}. Apparently, the instrumental broadening is the main factor that determines the line half-width. The profile of each rotational line can be assumed to be a Gaussian:

$$g(\nu-\nu_o) = \frac{2\sqrt{\ln 2}}{\sqrt{\pi}\,\Delta\nu} e^{-4(\ln 2)(\nu-\nu_o)^2/(\Delta\nu)^2}$$

$$= \frac{0.93952}{\Delta\nu} e^{-2.77309(\nu-\nu_o)^2/(\Delta\nu)^2} \qquad (31)$$

Here, the center of the line is located at ν_o (in cm^{-1}) and the line half-width is $\Delta\nu$.

The resultant band profile can be obtained by summing over the individual line profile, using Eq.(26). A computer program, PROTIO, was written for this purpose. The program is listed in Appendix B.

The computed theoretical profiles are fitted into the observed profiles. Some of the results are shown as samples on Figs. 15, 16 and 17 for the first order and on Figs. 18, 19 and 20 for the second order spectrographic exposures (pp. 90-107). The dashed lines in these figures indicate the theoretical profiles which have been shifted vertically upward relative to the solid lines which are the observed experimental profiles. The broken lines indicate the reference intensities due to the radiation of the tungsten wall.

It can be seen from these figures that the theoretical curves match the experimental ones nicely. Several Ti atomic lines at 5174 Å, 5193 Å, 5210 Å and 5220 Å mix in the band. Meanwhile, the (1,1) band of the TiO α-system starts to blend at 5240 Å. Hence, only that part of radiation emitted by those rotational lines from band head at 5167 Å to 5240 Å is considered in the calculation. The radiation due to Ti lines is excluded from the experimental profiles according to the shape of the theoretical profiles. An OTT-planimeter is used to integrate

the areas, and the accuracy is within 1%. The absolute radiance due to the emission of TiO vapor can be calculated by comparing it with that of the tungsten wall radiation which, after making the emissivity correction, can be calculated by using the Planck equation (Eq. 15).

The ratio of the integrated areas of the TiO emission profile to that of the tungsten radiation profile, $\int L_{em}\, d\nu / L_\nu \Delta\lambda$; the absolute radiance of the tungsten wall between the frequency interval 5176 Å to 5240 Å, $L_\nu \Delta\lambda$; the absolute intensities of the gas emission, $\int L_{em}\, d\nu$ and the factor, $\sum_{J'_o}^{J} S_{J'J''}\, \nu^2\, e^{-hCF_{J'}/kT}$ calculated by the computer together with $N_{n'v'J'_o M_{J''}} f_{em}$ and f_{em} values are summarized in Table XIX (first order photographic exposure) and Table XX (second order photographic exposure).

TABLE XIX

Summary (TiO First Order Photographic Exposure)

Plate	True temperature (°K)	Brightness temperature (W wall) (°K)	$L_\nu \Delta\lambda$ ($\times 10^{-15}$)	$\frac{\int L_{em}\, d\nu}{L_\nu \Delta\lambda}$ (explt.)	$\int L_{em}\, d\nu$ ($\times 10^{-14}$)	$\sum \frac{S_J}{\lambda^2} e^{-hcF_{J'}/kT}$ * ($\times 10^{-12}$)	$N'f_{em}$ ($\times 10^{-1}$)	f_{em}
I-30-2	2141	2012	6.350	0.01475	0.937	2.779	2.121	0.149
I-30-3	2152	2022	6.829	0.01618	1.105	2.788	2.494	0.145
I-32-3	2148	2050	8.206	0.01508	1.238	2.816	2.767	0.095
I-32-4	2193	2058	8.625	0.02013	1.736	2.823	3.870	0.115
I-26-1	2210	2073	9.525	0.02615	2.491	2.838	5.524	0.127
I-26-2	2237	2096	11.08	0.03146	3.486	2.860	7.670	0.111
I-34-2	2323	2172	17.50	0.04951	8.664	2.930	18.608	0.079
I-34-3	2323	2172	17.50	0.04975	8.706	2.930	18.698	0.079
I-34-1	2328	2176	17.91	0.05350	9.582	2.934	20.552	0.082

* The lines includes in the computation of this term were only resolved for the multiplet terms, i.e. (2S+1), but were not resolved for the magnetic sublevels due to the Λ-type doubling. Therefore, this term must be multiplied by $(2 - \delta_{o,\Lambda})$ in using Eq.(14) to calculate the f_{em} values.

Average of f_{em} = 0.109

TABLE XX

Summary (TiO Second Order Photographic Exposure)

Plate	True temperature (°K)	Brightness temperature (W wall) (°K)	$L_\nu \Delta\lambda$ ($\times 10^{-16}$)	$\frac{\int L_{em}\, d\nu}{L_\nu \Delta\lambda}$ (exptl.)	$\int L_{em}\, d\nu$ ($\times 10^{-15}$)	$\sum \frac{S_J}{\lambda^2} e^{-hcF_J/kT}$ * ($\times 10^{-12}$)	$N' f_{em}$ ($\times 10^{-2}$)	f_{em}
II-22-1	2292	2145	1.492	0.11246	1.667	2.9051	3.633	0.239
II-22-2	2314	2164	1.671	0.12231	2.044	2.9228	4.401	0.210
II-23-2	2328	2176	1.791	0.16236	2.908	2.9340	6.237	0.248
II-24-1	2328	2176	1.791	0.06095	1.091	2.9340	2.340	0.093
II-24-2	2328	2176	1.791	0.08828	1.581	2.9340	3.391	0.135
II-25-1	2328	2176	1.791	0.10620	1.902	2.934	4.075	0.162
II-20-1	2406	2244	2.636	0.21179	5.583	2.9952	11.730	0.161

* The lines included in the computation of this term were only resolved for the multiplet terms, i.e. (2S+1), but were not resolved for the magnetic sublevels due to the Λ-type doubling. Therefore, this term must be multiplied by $(2 - \delta_{o,\Lambda})$ in using Eq.(14) to calculate the f_{em} values.

Average of f_{em} = 0.178

B. Vanadium Monoxide

1) Vapor Pressures

Neither the partial vapor pressures nor the phase diagrams of vanadium-oxygen system have been as extensively studied as those of titanium-oxygen system. The melting point of VO(s) was determined to be 2075°K by Rostoker and Yamamoto[83] using microscopic and X-ray techniques. The partial vapor pressures of VO, V and VO_2 over VO solid phase were studied by Berkowitz, Chupka and Ingram.[84] It was found that the partial vapor pressures of VO over the solid phase changed very slowly when the heating proceeded at 1900°K. The congruent composition or compositions of this system have not been determined. Heat contents and entropies of VO(s) were reported from 298°K to 1698°K by Orr.[85] These data were used in "Contribution to the Data on Theoretical Metallrugy", Bulletin 584, Bureau of Mines 1960 to extrapolate the heat contents and entropies to higher temperatures, which were tablulated at 100°K intervals from 400°K to 2000°K. The values for the temperatures between the intervals were interpolated according to these data (Fig. 14). The free energy function can be calculated by using the equation:

$$\frac{F^\circ_T - H^\circ_{298}}{T} = \frac{H^\circ_T - H^\circ_{298}}{T} - (S^\circ_T - S^\circ_{298}) - S^\circ_{298} \qquad (27)$$

The free energy function of liquid phase of VO has not been reported. However, the free energy of liquid phase of VO can be estimated from the following equation:

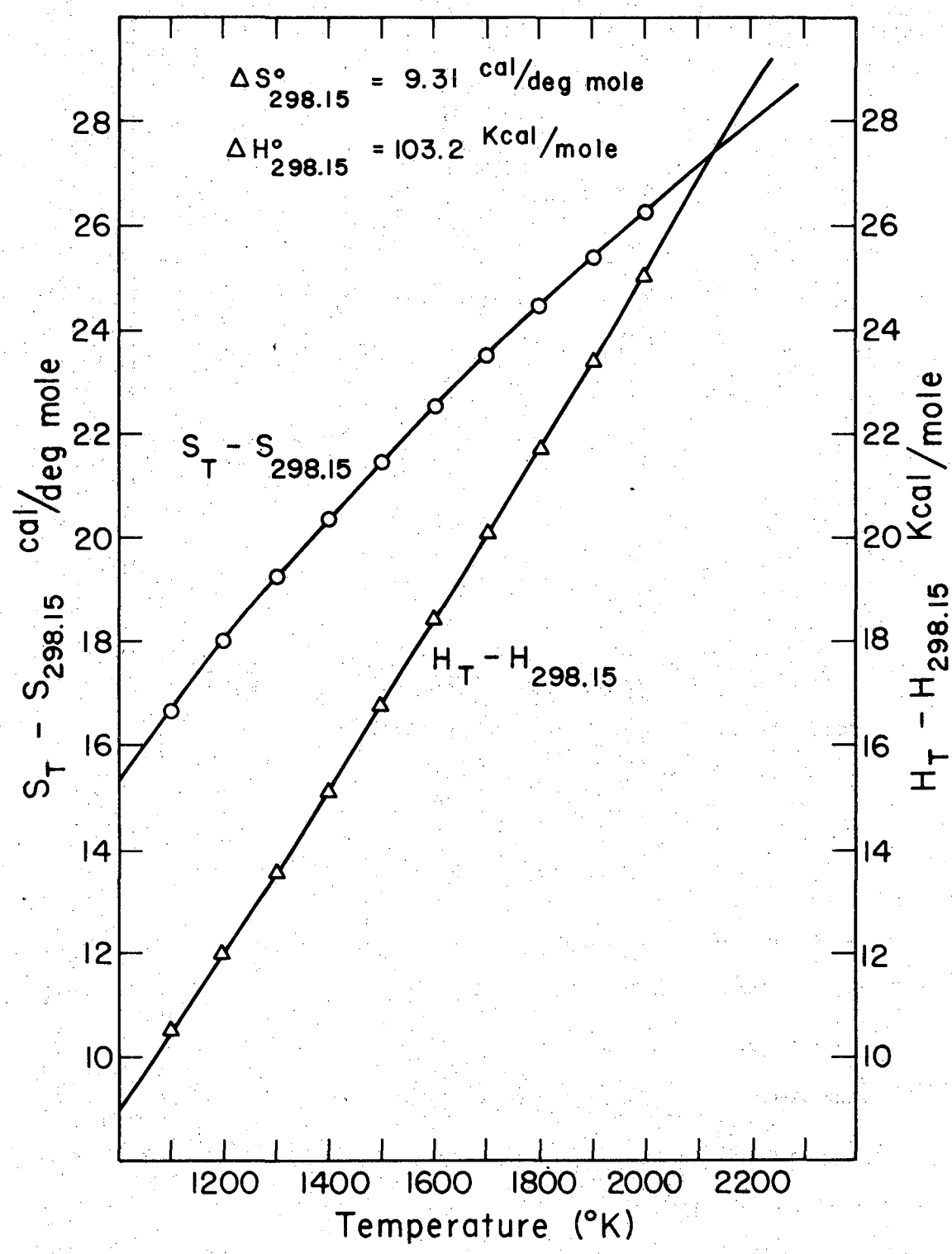

Figure 14

Heat content and entropy of VO (solid).

$$\left(\frac{F^\circ_T}{T}\right)_{liq} = \left(\frac{F^\circ_T - H^\circ_{298}}{T}\right)_{solid} + \frac{H^\circ_{298}}{T} + \frac{H_f}{T} - \frac{H_f}{T_m} \qquad (28)$$

H_f is the heat of fusion of VO(s) which is taken to be 5 kcal/deg.mole. T_m is the melting point of VO(s).

The free energy function of VO in gas phase was given by Brewer and Rosenblatt.[16] The vapor pressures of VO over the solid and liquid phases thus calculated are shown in Table XXI.

2) The Population Analysis

Rotational, vibrational partition functions of the VO $X^4\Sigma^-$ state were calculated in exactly the same way as for TiO. Equation 20 was used to calculate the rotational partition function Q_{rot}; Eq. 21 was used to calculate the vibrational partition function Q_{vib}. Here, the rotational constant B and the frequency of the vibration ω are 0.5463 cm^{-1} and 1011.56 cm^{-1} respectively. Equation 22 was used to claculate the electronic partition function. The contribution to the free energy function of VO due to the electronic part was given by Brewer and Rosenblatt.[16] The calculated results of these partition functions Q_{rot}, Q_{vib} and Q_{el} are summarized in Table XXII.

The fractional population of the k" = 0, v" = 0 level of the $X^4\Sigma^-$ state of VO, q", and that of the k' = 0, v' = 0 level of the $C^4\Sigma^-$ state, q', were calculated by using Eq.(23) and Eq.(25) respectively. Here, $q = 1/Q_{el} \times Q_{vib} \times Q_{rot}$. Since the Λ-type doubling does not occur for a Σ state and there is only one lowest rotational level instead of four

TABLE XXI

Calculated free energy functions and vapor pressures of VO

True Temperature (°K)	$-\frac{F^\circ_T - H^\circ_{298}}{T}$ VO solid	$-\frac{F^\circ_T - H^\circ_{298}}{T}$ VO gas	$-\frac{\Delta F^\circ - \Delta H^\circ_{298}}{T}$	$\frac{\Delta H^\circ_{298}}{T}$	$P_{VO\ gas}$ (atm.)
1994	23.00	67.31	44.31	66.27	1.59×10^{-5}
2030	23.23	67.44	44.21	65.12	2.70×10^{-5}
2055	23.39	67.53	44.14	64.33	3.89×10^{-5}
2075	23.50	67.60	44.10	63.71	5.18×10^{-5}
2130	23.87	67.81	43.94	62.07	1.09×10^{-4}

TABLE XXII

Partition functions of VO

True Temperature (°K)	Q_{rot} $v''=0$, $X^4\Sigma^-$	Q_{vib} $X^4\Sigma^-$	Q_{el}
1995	2.54×10^3	1.9305	22.32
2030	2.58×10^3	1.9531	22.42
2055	2.60×10^3	1.9685	22.48
2075	2.63×10^3	1.9802	22.51
2130	2.70×10^3	2.0202	22.65

on k = 0, v = 0 of the $^4\Sigma^-$ state, as can be seen from the energy level diagram of the $^4\Sigma^-$ - $^4\Sigma^-$ transition (Fig. 4).

The total number densities and the number densities of the K" = 0, v" = 0 of the $X^4\Sigma^-$ state of VO and of the K' = 0 and v' = 0 of the $C^4\Sigma^-$ state in molecules/cm^3 are presented in Table XXIII.

3) The Band Intensities

The detailed rotational analysis of VO $C^4\Sigma^-$ - $X^4\Sigma^-$ transition has not been carried out. Two P and two R branches were analyzed by Mahanti,[25] and by Lagerqvist and Selin[26] which they thought was due to a $^2\Delta$ - $^2\Delta$ transition. Barrow[28,29] pointed out that the four branches of this system analyzed by Lagerqvist and Selin were correct. However, in addition to these four branches, four more broad lines branches, two R and two P, were discovered in this green system. The line strength for the $^4\Sigma$ - $^4\Sigma$ transition were given by Rao[86] and are as follows:

$$S_J^{P_1} = \frac{(2J-3)(2J+1)}{4(J-1)} \quad ; \quad S_J^{R_1} = \frac{(2J-1)(2J+3)}{4J} \tag{29}$$

$$S_J^{P_2} = \frac{(J+1)(2J-3)(2J+1)}{4J} \quad ; \quad S_J^{R_2} = \frac{(J+2)(2J-1)(2J+3)}{4(J+1)} \tag{30}$$

$$S_J^{P_3} = \frac{(J-1)(2J-1)(2J+3)}{4J} \quad ; \quad S_J^{R_3} = \frac{J(2J+1)(2J+5)}{4(J+1)} \tag{31}$$

$$S_J^{P_4} = \frac{(2J-1)(2J+3)}{4(J+1)} \quad ; \quad S_J^{R_4} = \frac{(2J+1)(2J+5)}{4(J+2)} \tag{32}$$

The generalized formulas for the line strength given by Herzberg[19] were used to calculate the theoretical profile of the (0,0) band green

TABLE XXIII

Population analysis of VO vapor over VO solid and liquid phases

True Temperature (°K)	Total number density (molecules/cm^3)	Fraction of population on $K''=0,v''=0,X^4\Sigma^-$	Number density on $K''=0,v''=0,X^4\Sigma^-$ (molecules/cm^3)	Fraction of population on $K'=0,v'=0,C^4\Sigma^-$	Number density on $K'=0,v'=0,C^4\Sigma^-$ (molecules/cm^3)
1995	5.824×10^{14}	9.137×10^{-6}	5.321×10^{9}	3.198×10^{-11}	1.863×10^{4}
2030	9.720×10^{14}	8.852×10^{-6}	8.604×10^{9}	3.842×10^{-11}	3.374×10^{4}
2055	1.376×10^{15}	8.692×10^{-6}	1.196×10^{10}	4.381×10^{-11}	6.028×10^{4}
2075	1.824×10^{15}	8.530×10^{-6}	1.556×10^{10}	4.837×10^{-11}	8.823×10^{4}
2130	3.740×10^{15}	8.094×10^{-6}	3.027×10^{10}	6.265×10^{-11}	2.343×10^{5}

system of VO spectrum since the location of the rotational lines of the completed eight branches were still unavailable. These generalized formulas for $\Delta\Lambda = 0$ transition are:

$$S_J^P = \frac{(J'+1+\Lambda')(J'+1-\Lambda')}{J'+1} \; ; \quad S_J^R = \frac{(J'+\Lambda')(J'-\Lambda')}{J'} \tag{33}$$

Only the four branches determined by Lagerqvist and Selin were used. The location of the rotational lines was taken from their results but the rest of the lines with rotational quantum numbers K = 0 to 13 were not given by them. Equation 34 was used to calculate the location of these lines.[19] Rotational and vibrational constants determined by them were also used.

$$\nu = \nu_e + \left\{\omega_e'(v'+\tfrac{1}{2}) - \omega_e'x_e'(v'+\tfrac{1}{2})^2 + \omega_e'y_e'(v'+\tfrac{1}{2})^3 - \omega_e'z_e'(v'+\tfrac{1}{2})^4\right\} - \left\{\omega_e''(v''+\tfrac{1}{2}) - \omega_e''x_e''(v''+\tfrac{1}{2})^2 + \omega_e''y_e''(v''+\tfrac{1}{2})^3 - \omega_e''z_e''(v''+\tfrac{1}{2})^4\right\} + F'(J') - F''(J'') \tag{34}$$

where $F(J) = BJ(J+1) - DJ^2(J+1)^2$, $D = 4B^3/\omega^2$.

The method for plotting the VO band profile is the same as that used for the TiO profile. The computer program, PROVO, is listed in Appendix B. The computed theoretical profiles were matched to the observed profiles. Some of these results are shown in Figs. 21, 22 and 23. The dashed theoretical profiles were shifted vertically upward relative to the solid observed ones. They correspond fairly well.

The ratio of the integrated areas of the VO emission profile to that of the tungsten radiation profile, $\frac{\int L_{em}\, d\nu}{L_\nu\, \Delta\lambda}$; the absolute

radiance of the tungsten wall between the frequency interval 5736 Å to 5822 Å, $L_\nu \Delta\lambda$; the absolute intensities of the gas emission, $\int L_{em}\, d\nu$ and the factor, $\Sigma S_{K'K''} \nu^2 e^{-hCF_{K'}/kT}$ calculated by the computer together with $N_{n'v'J'M_{J'}} f_{em}$ and f_{em} value are summarized in Table XXIV.

TABLE XXIV

Summary (VO results)

Plate	True temperature (°K)	Brightness temperature (W wall) (°K)	$L_v \Delta\lambda$ ($\times 10^{-16}$)	$\frac{\int L_{em}\, d\nu}{L_v \Delta\lambda}$ (exptl.)	$\int L_{em}\, d\nu$ ($\times 10^{-14}$)	$\frac{S_K}{\lambda^2} e^{-hcF_{K'}/kT}$ ($\times 10^{-12}$)	$N' f_{em}$ ($\times 10^{-2}$)	f_{em}
2-1	1995	1882	1.0901	0.02323	2.5323	1.2998	2.4520	0.0132
2-3	1995	1882	1.0901	0.02475	2.698	1.2998	2.6125	0.0140
21-3	2030	1914	1.3538	0.01067	1.4445	1.3150	1.3825	0.0041
21-4	2030	1914	1.3538	0.01192	1.6137	1.3150	1.5445	0.0046
21-5	2030	1914	1.3538	0.01021	1.3822	1.3150	1.3229	0.0039
15-1	2055	1936	1.5693	0.02167	3.4007	1.3258	3.2217	0.0054
15-2	2055	1936	1.5693	0.02509	3.9374	1.3285	3.7302	0.0062
17-2	2075	1953	1.7610	0.01456	2.5640	1.3244	2.4366	0.0028
17-3	2075	1953	1.7610	0.01528	2.6908	1.3244	2.5571	0.0029
17-4	2075	1953	1.7610	0.01403	2.4707	1.3244	2.3479	0.0027
19-1	2130	2002	2.4019	0.02220	5.3322	1.3480	4.9785	0.0021
19-2	2130	2002	2.4019	0.02498	6.0000	1.3480	5.6020	0.0024
19-3	2130	2002	2.4019	0.02379	5.7141	1.3480	5.3351	0.0023
19-4	2130	2002	2.4019	0.02498	6.0000	1.3480	5.6020	0.0024
19-5	2130	2002	2.4019	0.02312	5.5532	1.3480	5.1849	0.0022

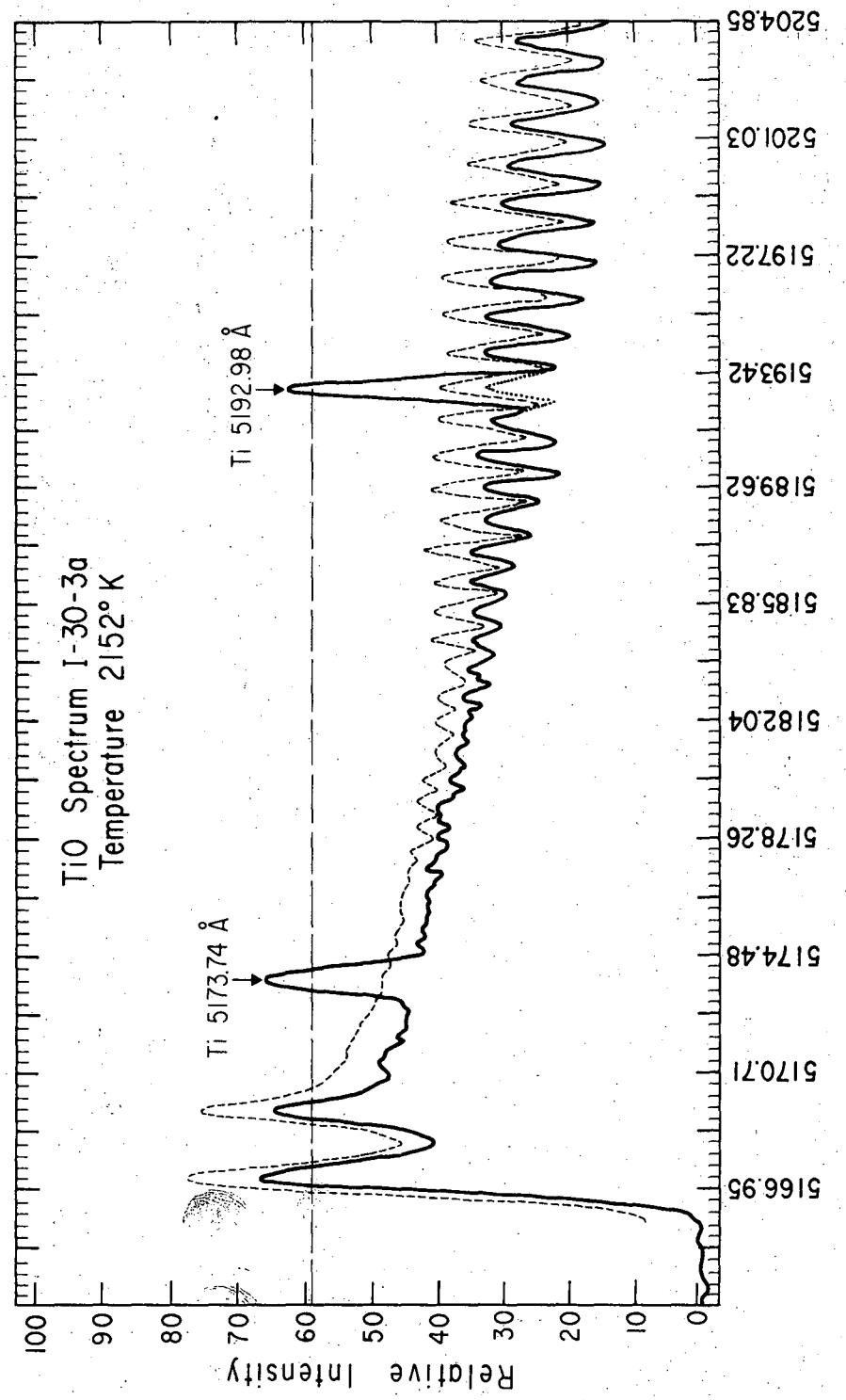
TiO Spectrum I-30-3a
Temperature 2152° K
Ti 5192.98 Å
Ti 5173.74 Å
Relative Intensity
Wavelength (Å)
5166.95
5170.71
5174.48
5178.26
5182.04
5185.83
5189.62
5193.42
5197.22
5201.03
5204.85
XBL 7112-2231

Figure 15

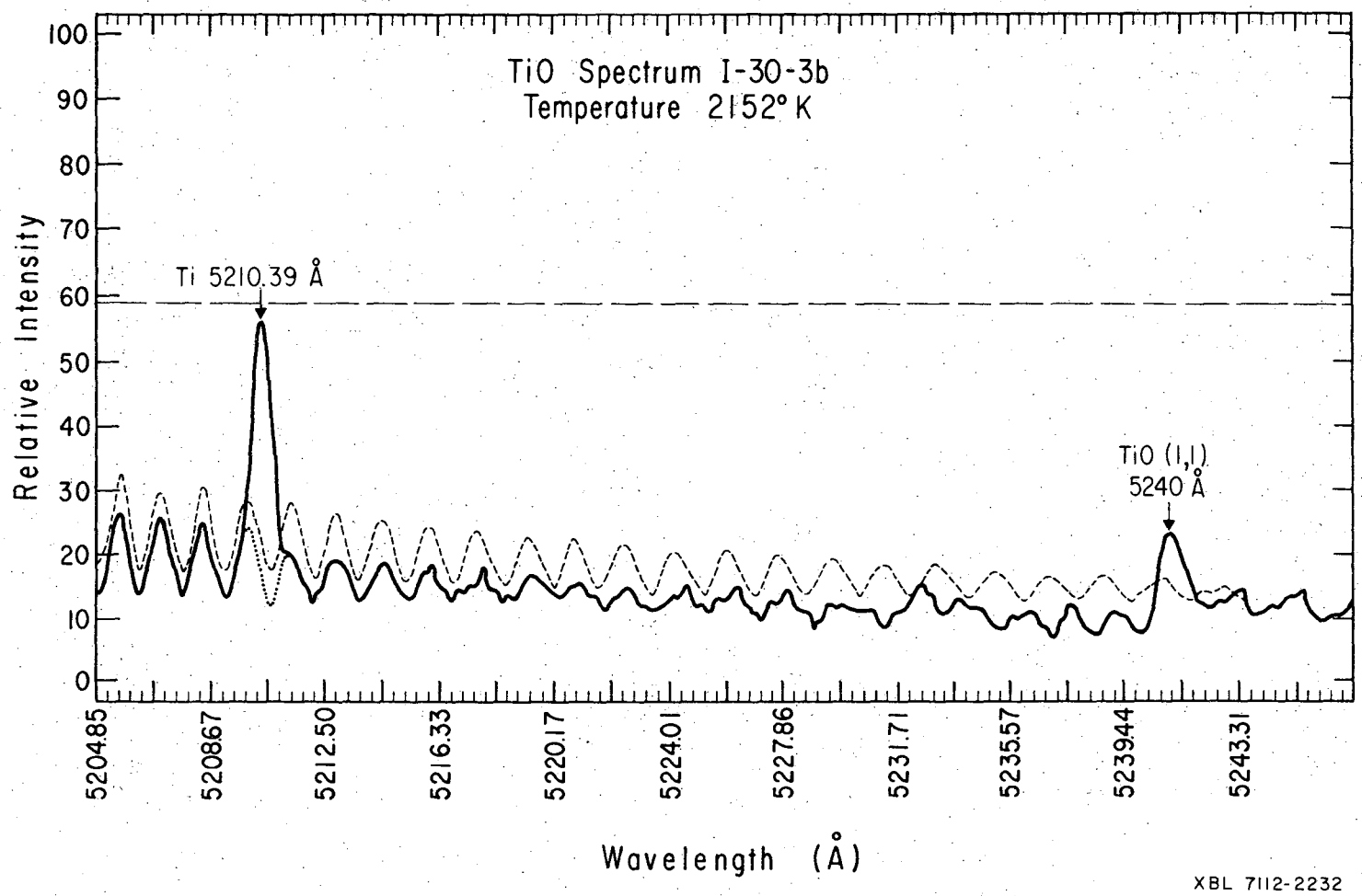

Figure 15 (continued)

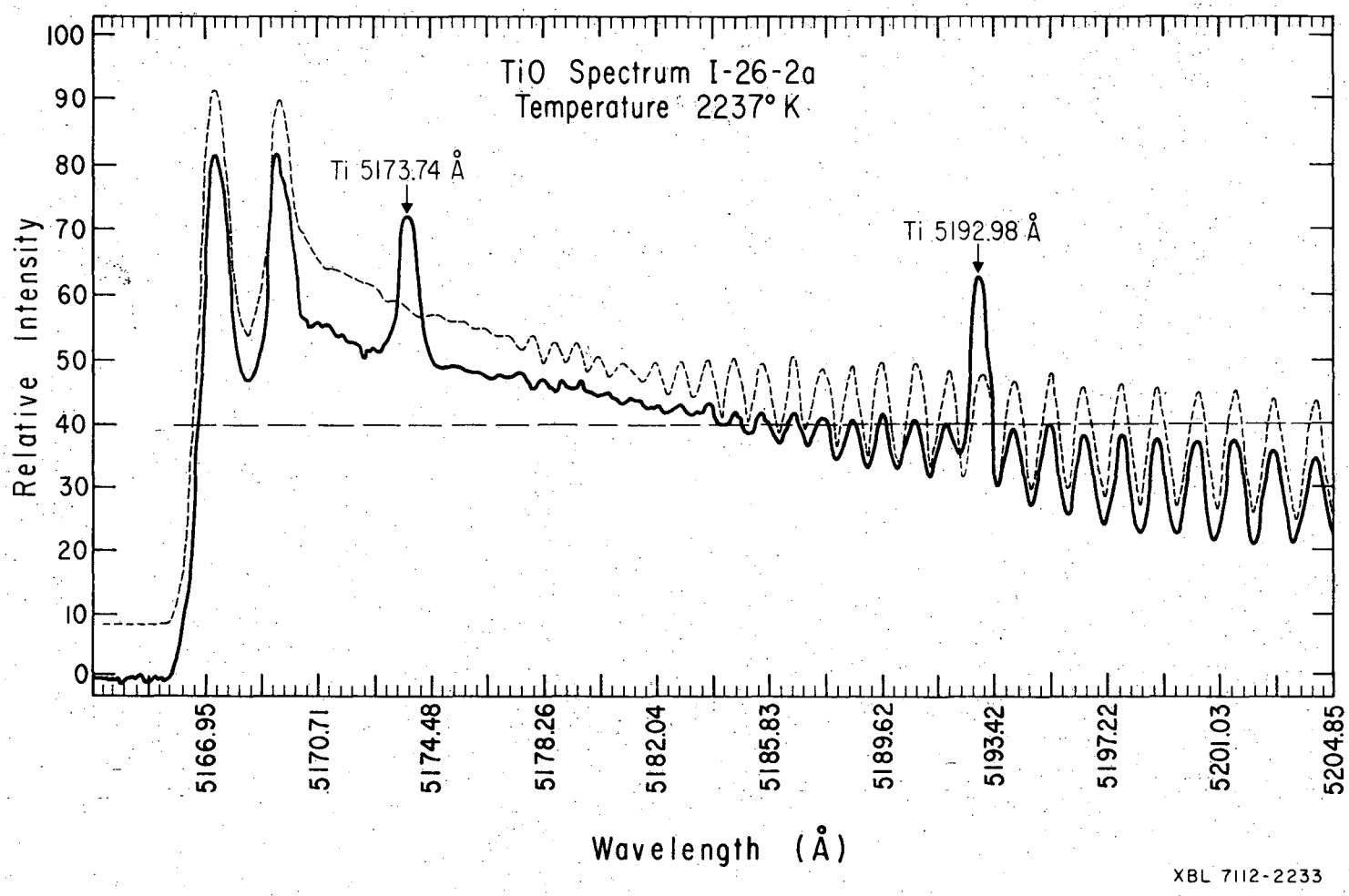
TiO Spectrum I-26-2a
Temperature 2237° K
Ti 5173.74 Å
Ti 5192.98 Å
Relative Intensity
100
90
80
70
60
50
40
30
20
10
0
5166.95
5170.71
5174.48
5178.26
5182.04
5185.83
5189.62
5193.42
5197.22
5201.03
5204.85
Wavelength (Å)
XBL 7112-2233

Figure 16

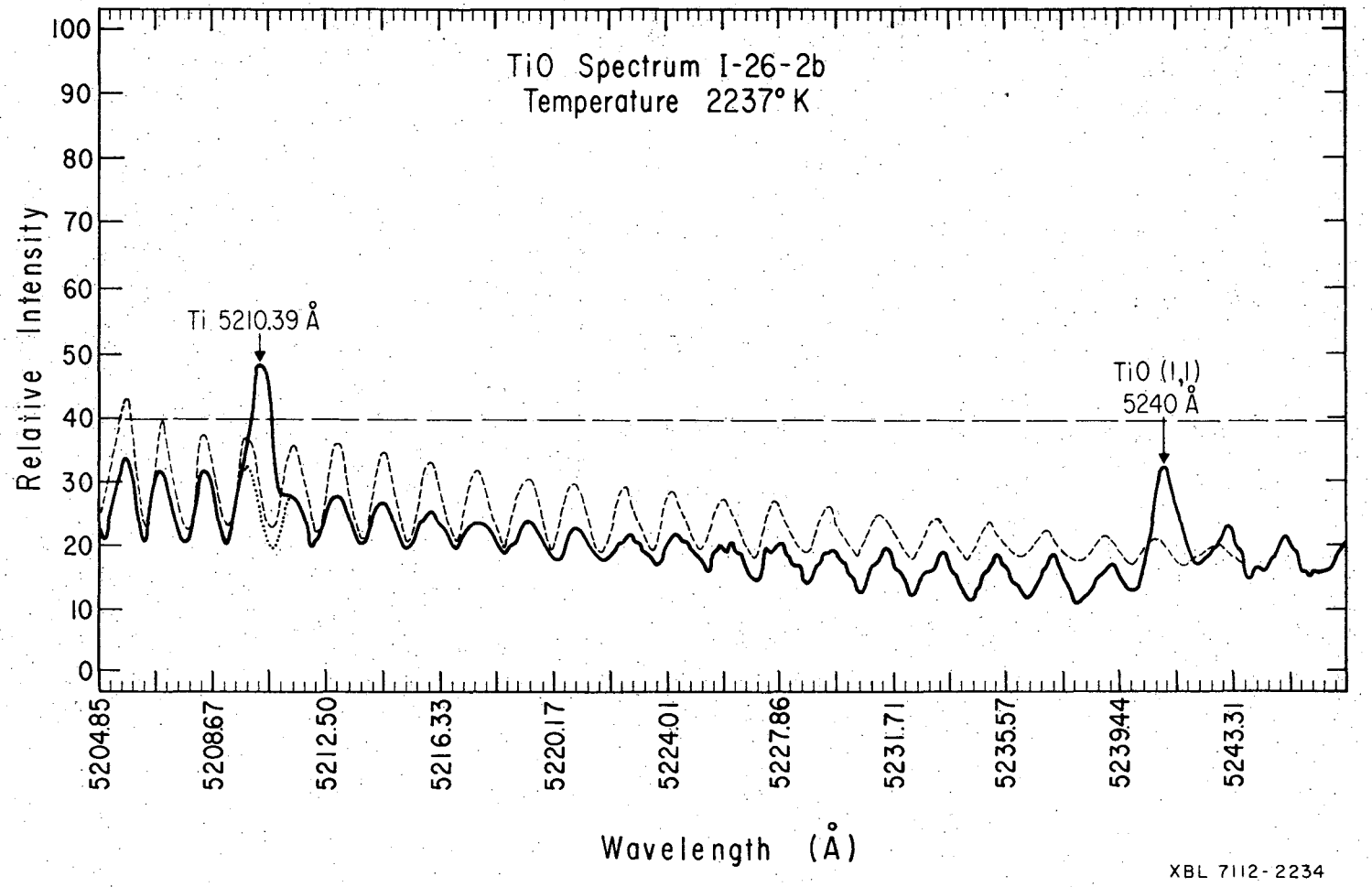

Figure 16 (continued)

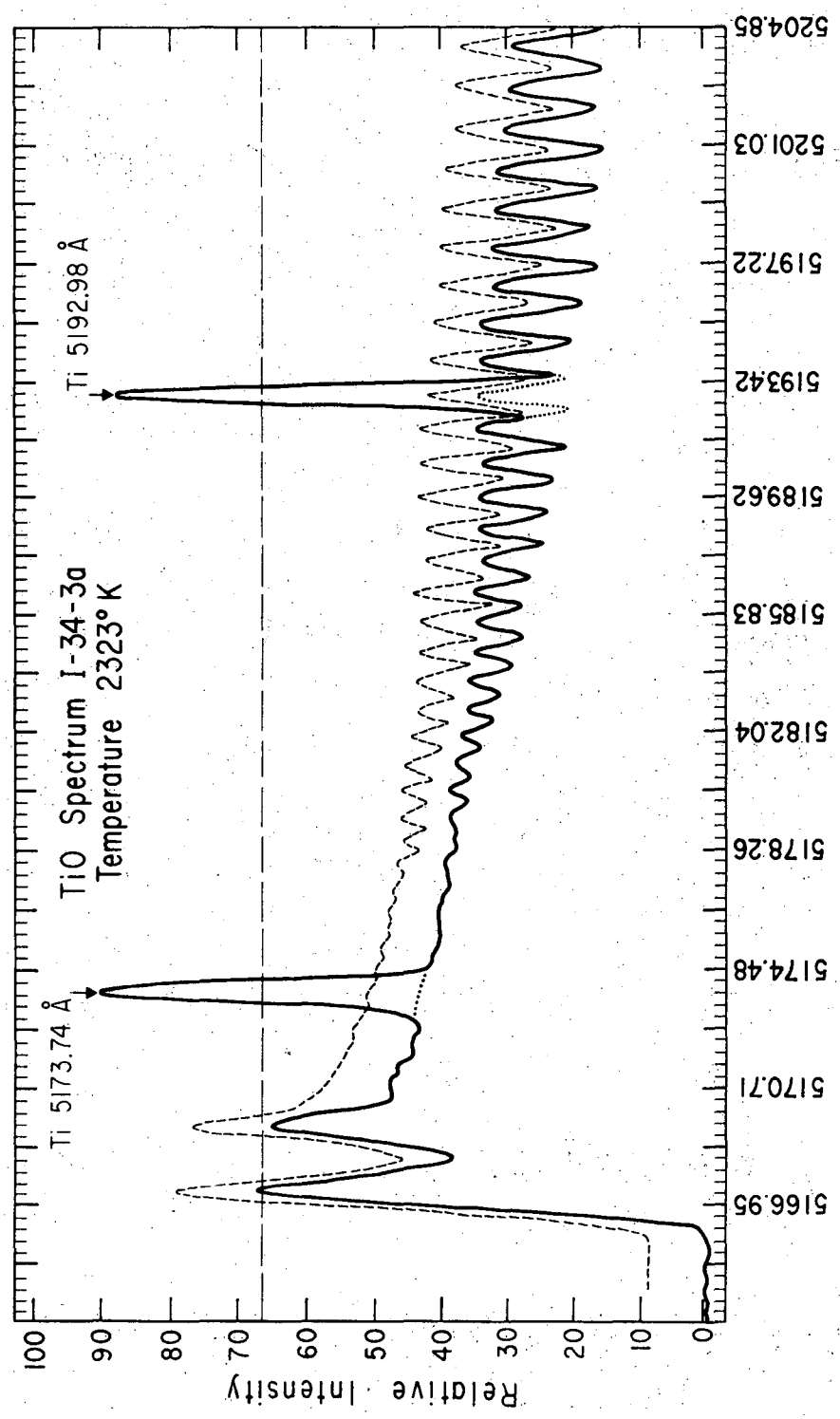
TiO Spectrum I-34-3a
Temperature 2323° K
Ti 5173.74 Å
Ti 5192.98 Å
Relative Intensity
100
90
80
70
60
50
40
30
20
10
0
5166.95
5170.71
5174.48
5178.26
5182.04
5185.83
5189.62
5193.42
5197.22
5201.03
5204.85
Wavelength (Å)
XBL 7112-2229

Figure 17

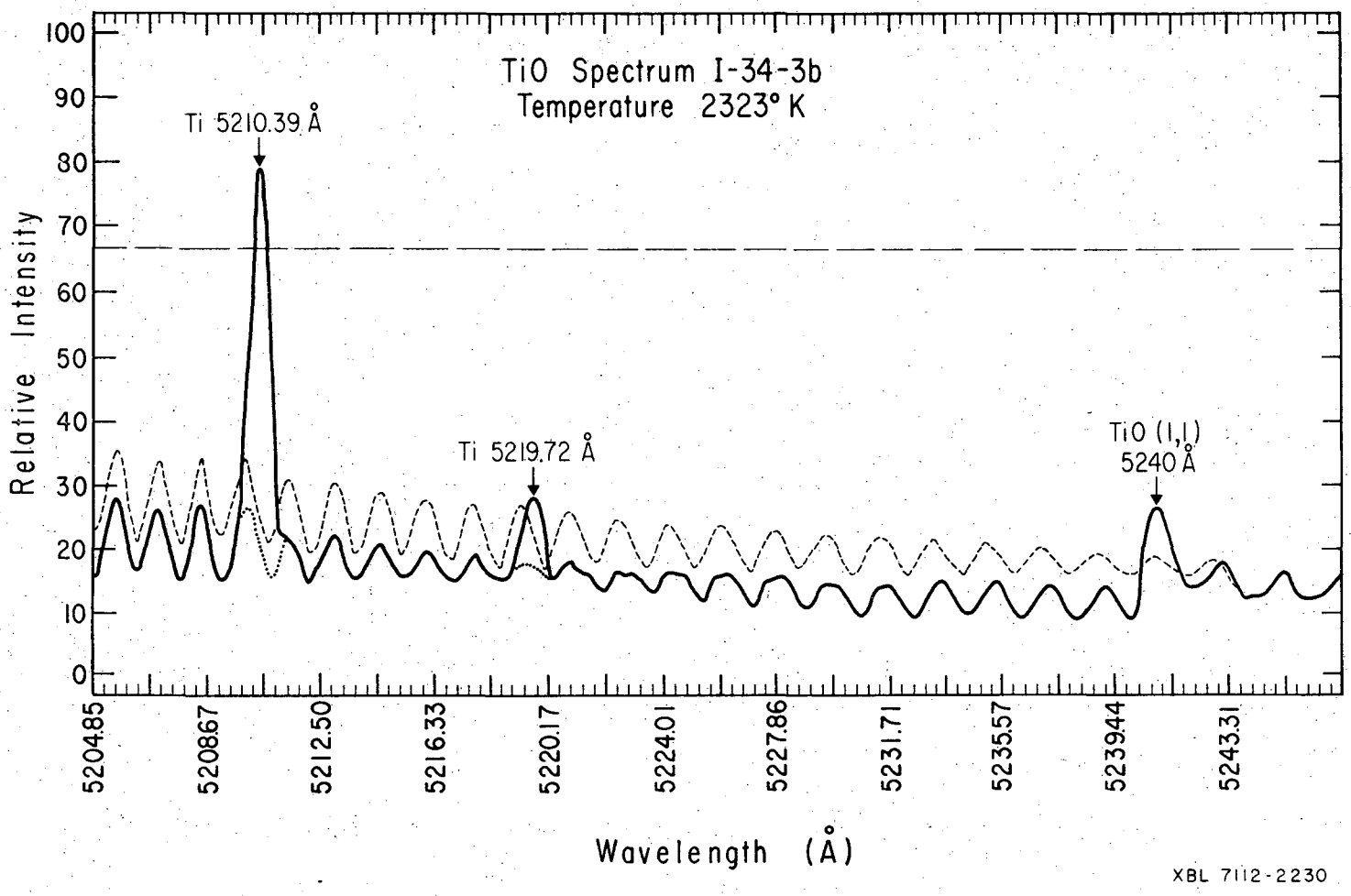

Figure 17 (continued)

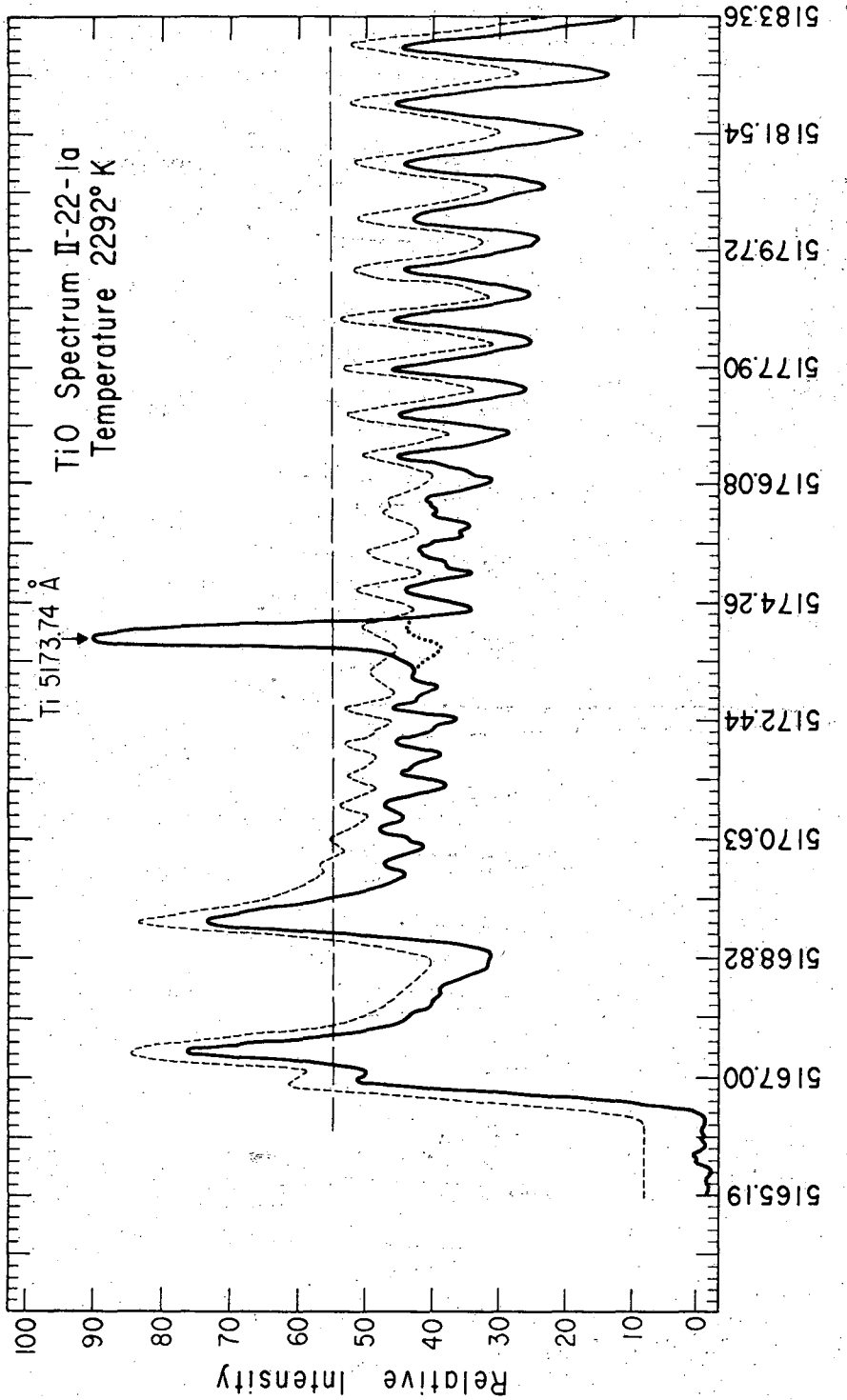
TiO Spectrum II-22-Ia
Temperature 2292° K
Ti 5173.74 Å
Relative Intensity
0
10
20
30
40
50
60
70
80
90
100
5165.19
5167.00
5168.82
5170.63
5172.44
5174.26
5176.08
5177.90
5179.72
5181.54
5183.36
Wavelength (Å)
XBL 7112-2239

Figure 18

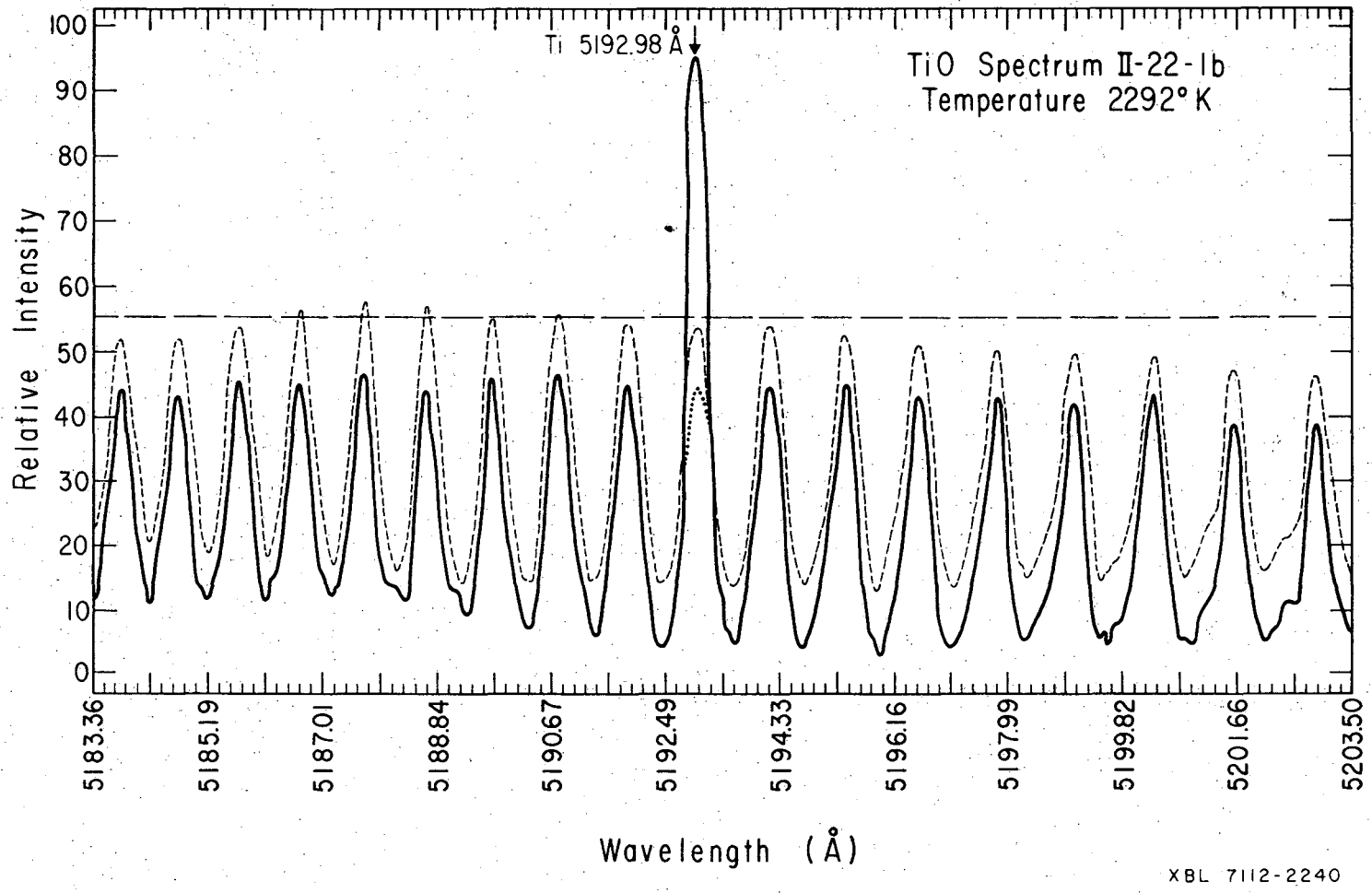

Figure 18 (continued)

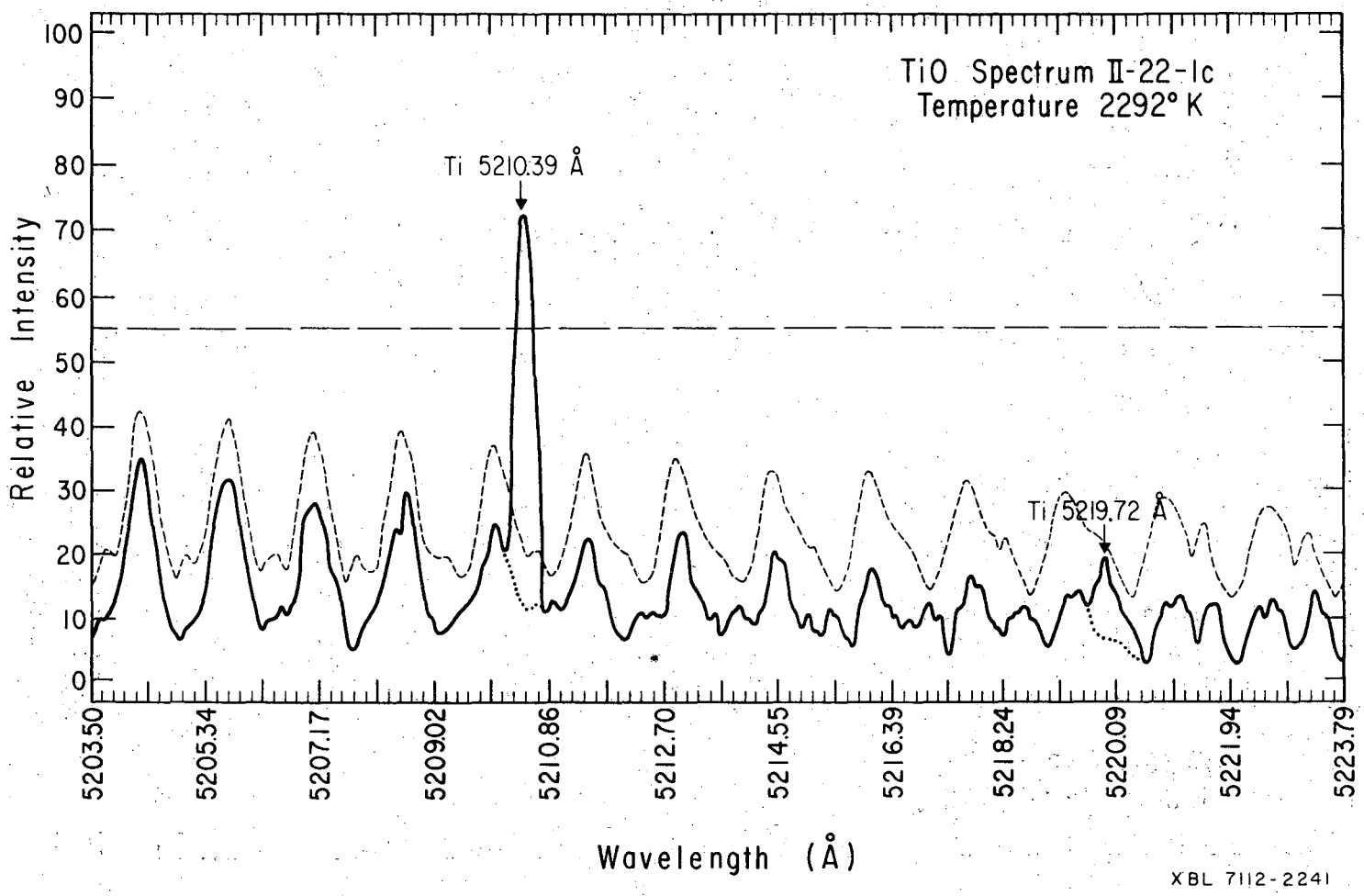

Figure 18 (continued)

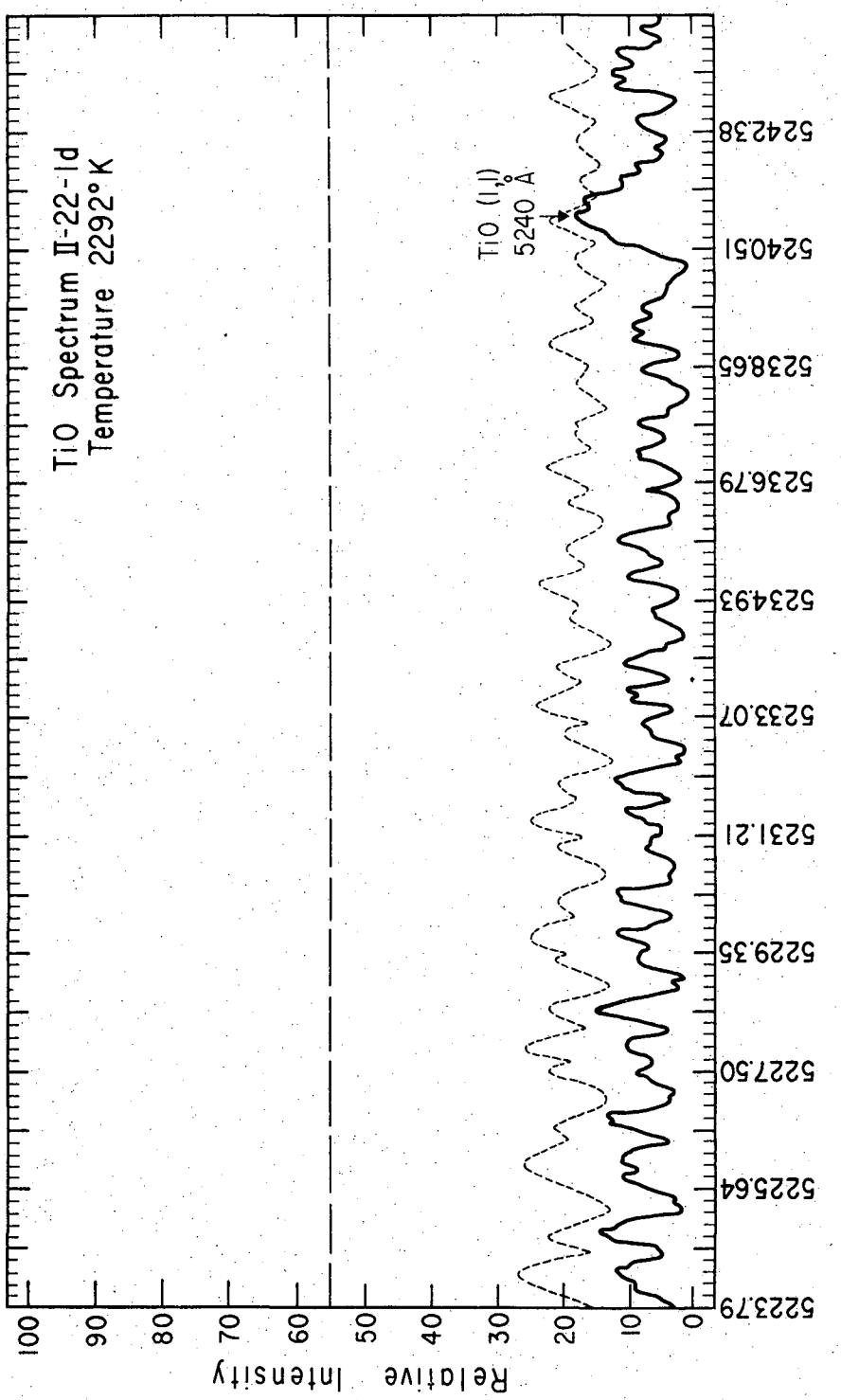

XBL 7112-2242

Figure 18 (continued)

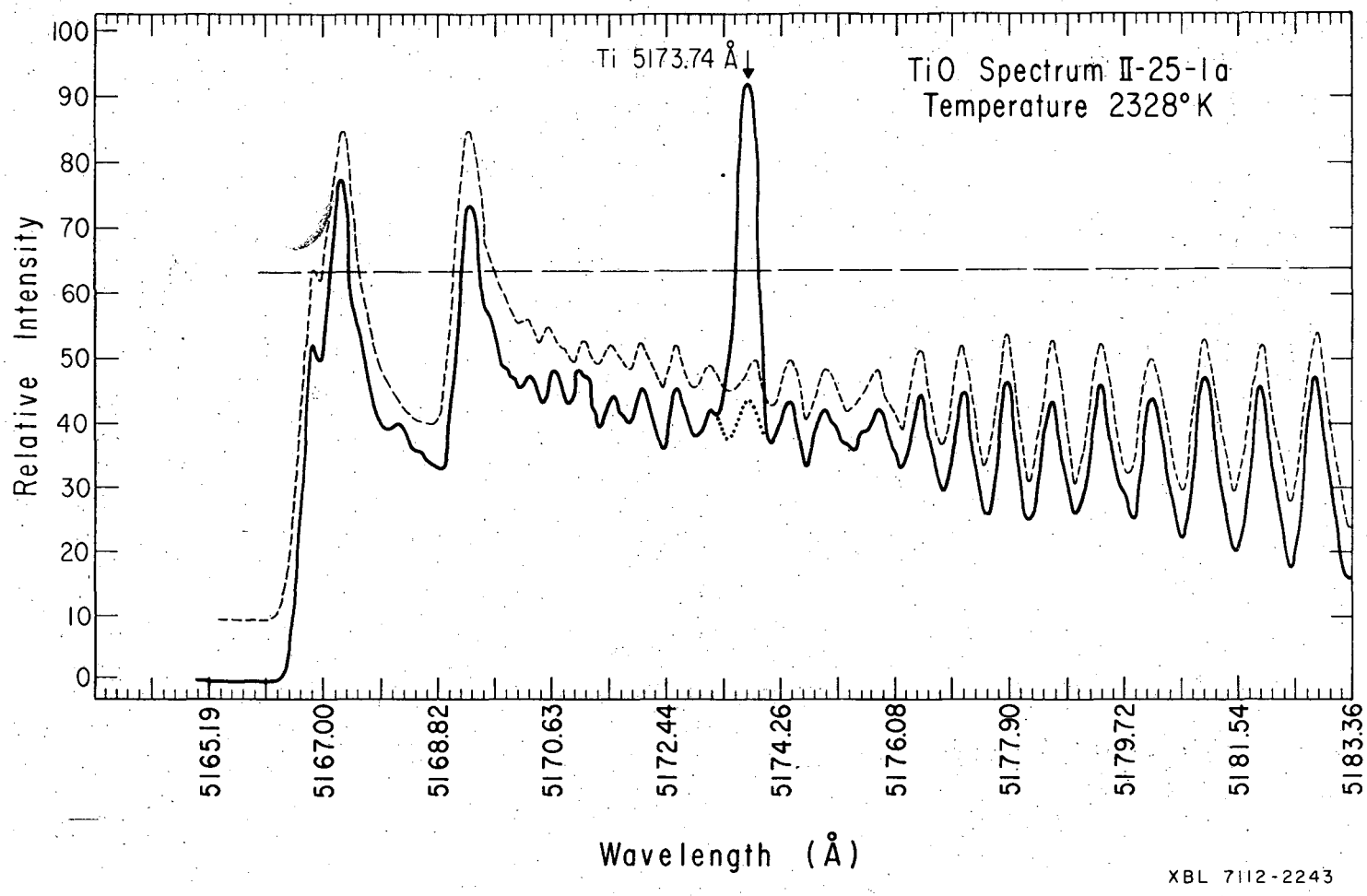
Ti 5173.74 Å
TiO Spectrum II-25-1a
Temperature 2328°K
Relative Intensity
100
90
80
70
60
50
40
30
20
10
0
5165.19
5167.00
5168.82
5170.63
5172.44
5174.26
5176.08
5177.90
5179.72
5181.54
5183.36
Wavelength (Å)
XBL 7112-2243

Figure 19

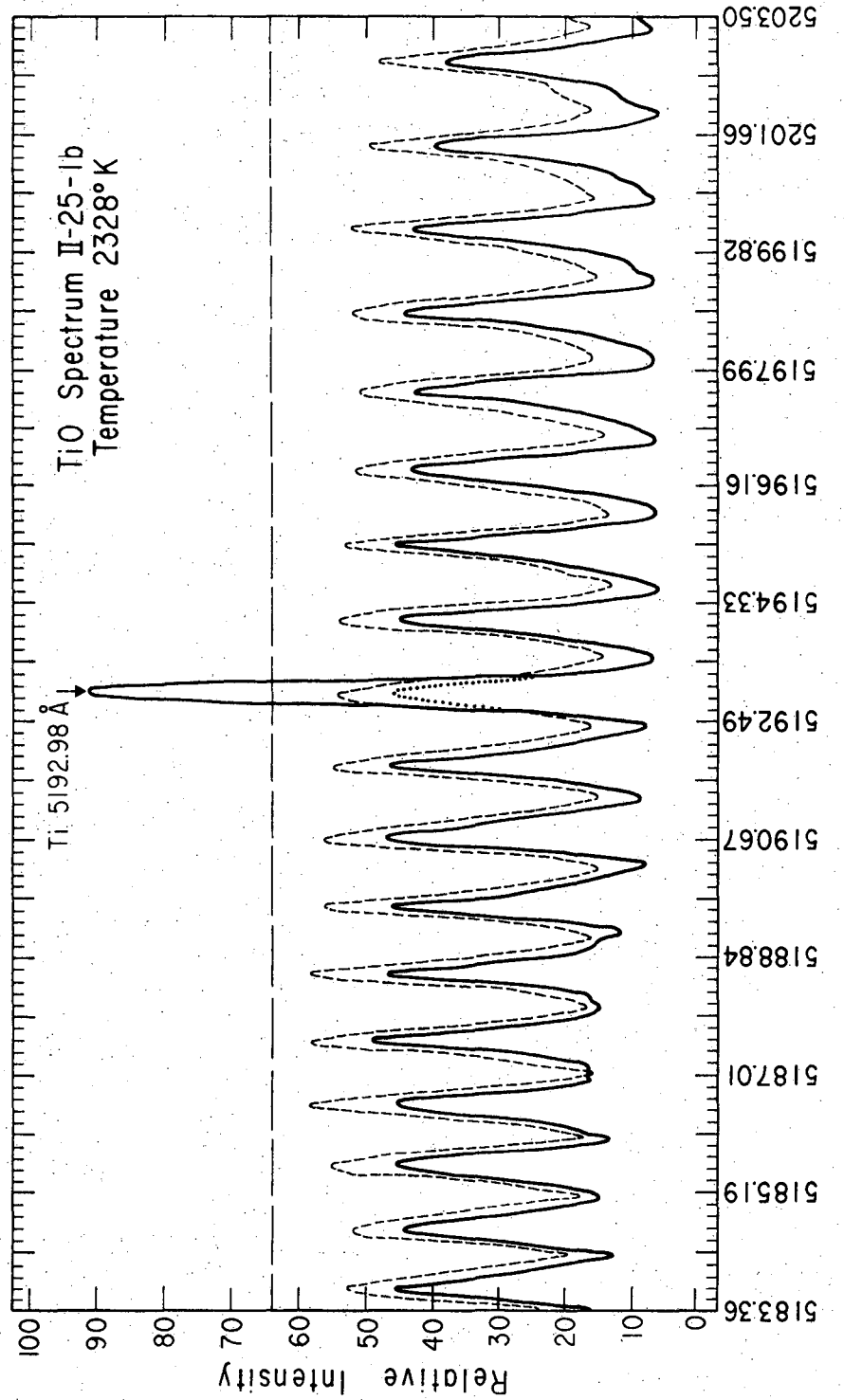

Figure 19 (continued)

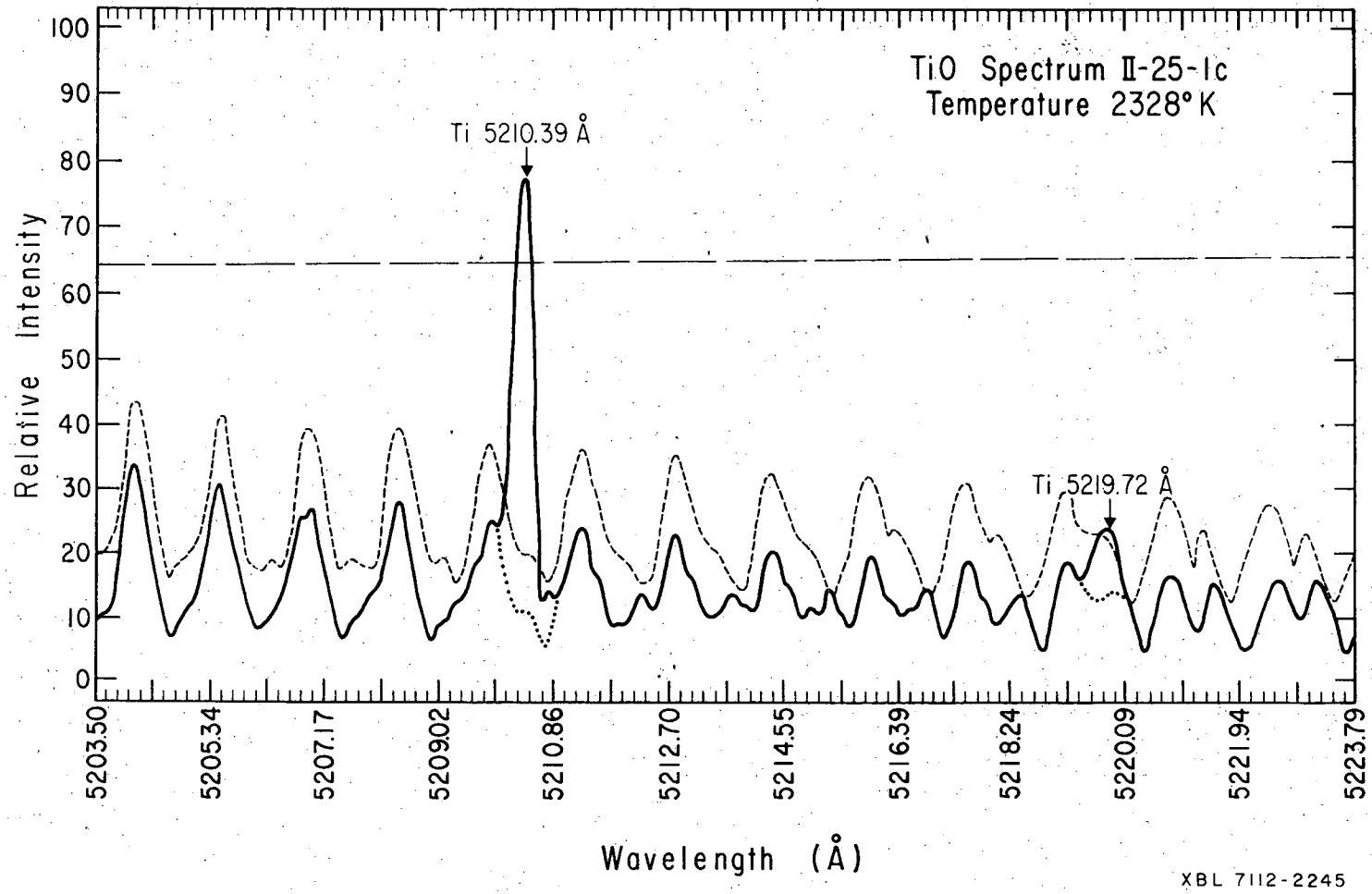

Figure 19 (continued)

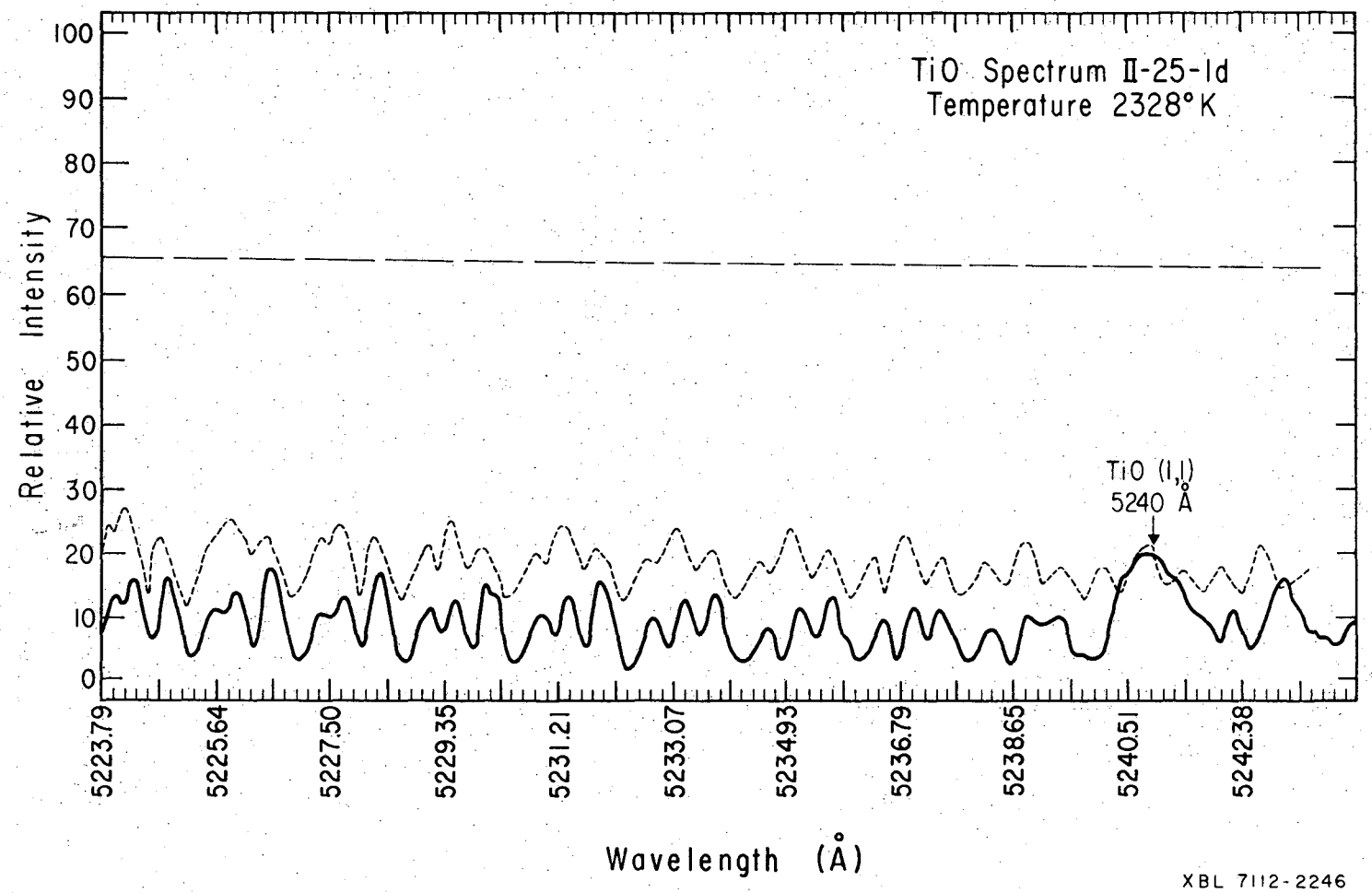

Figure 19 (continued)

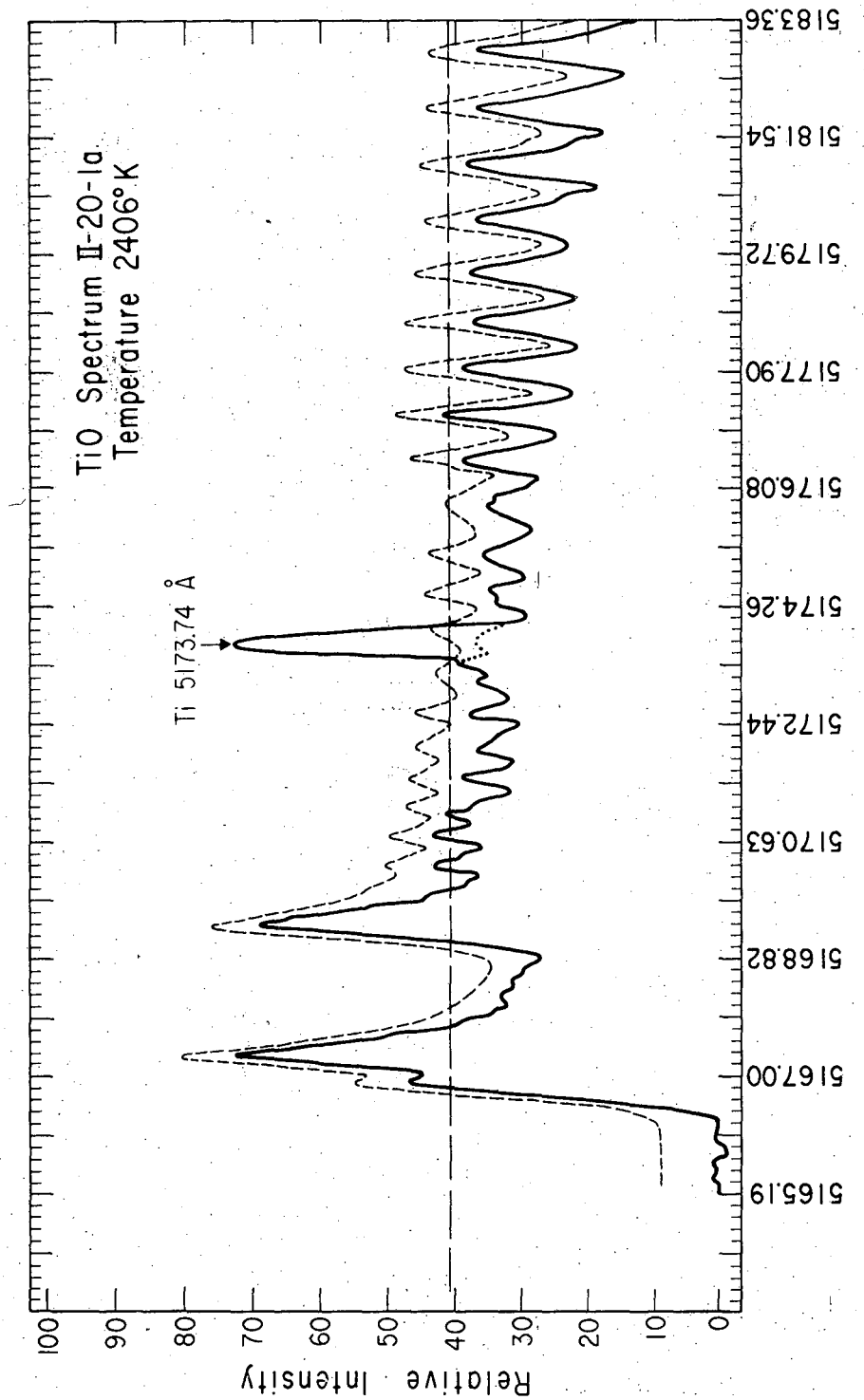
TiO Spectrum II-20-1a
Temperature 2406°K
Ti 5173.74 Å
Relative Intensity
0
10
20
30
40
50
60
70
80
90
100
5165.19
5167.00
5168.82
5170.63
5172.44
5174.26
5176.08
5177.90
5179.72
5181.54
5183.36
Wavelength (Å)
XBL 7112-2235

Figure 20

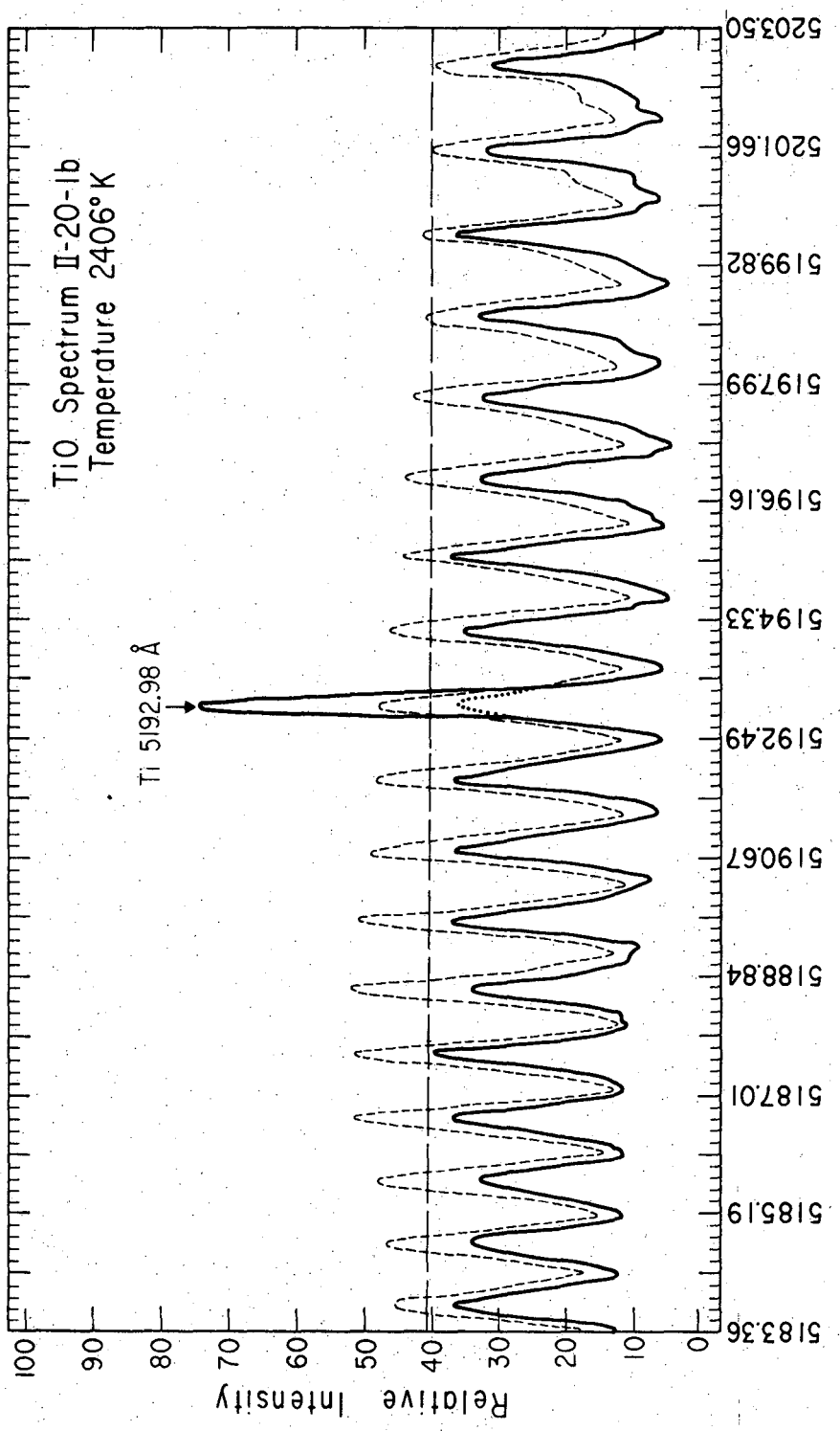

XBL 7112-2236

Figure 20 (continued)

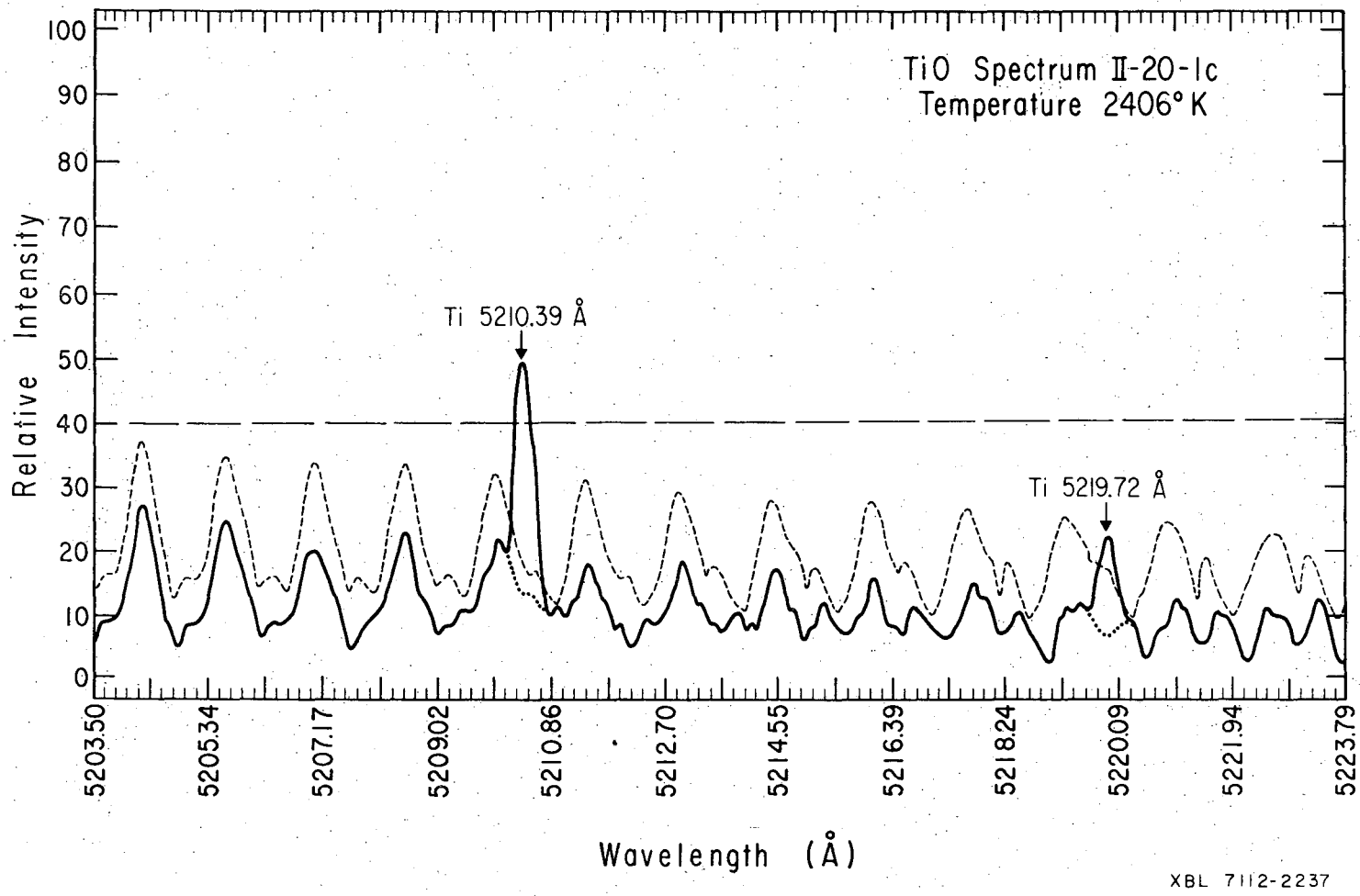

Figure 20 (continued)

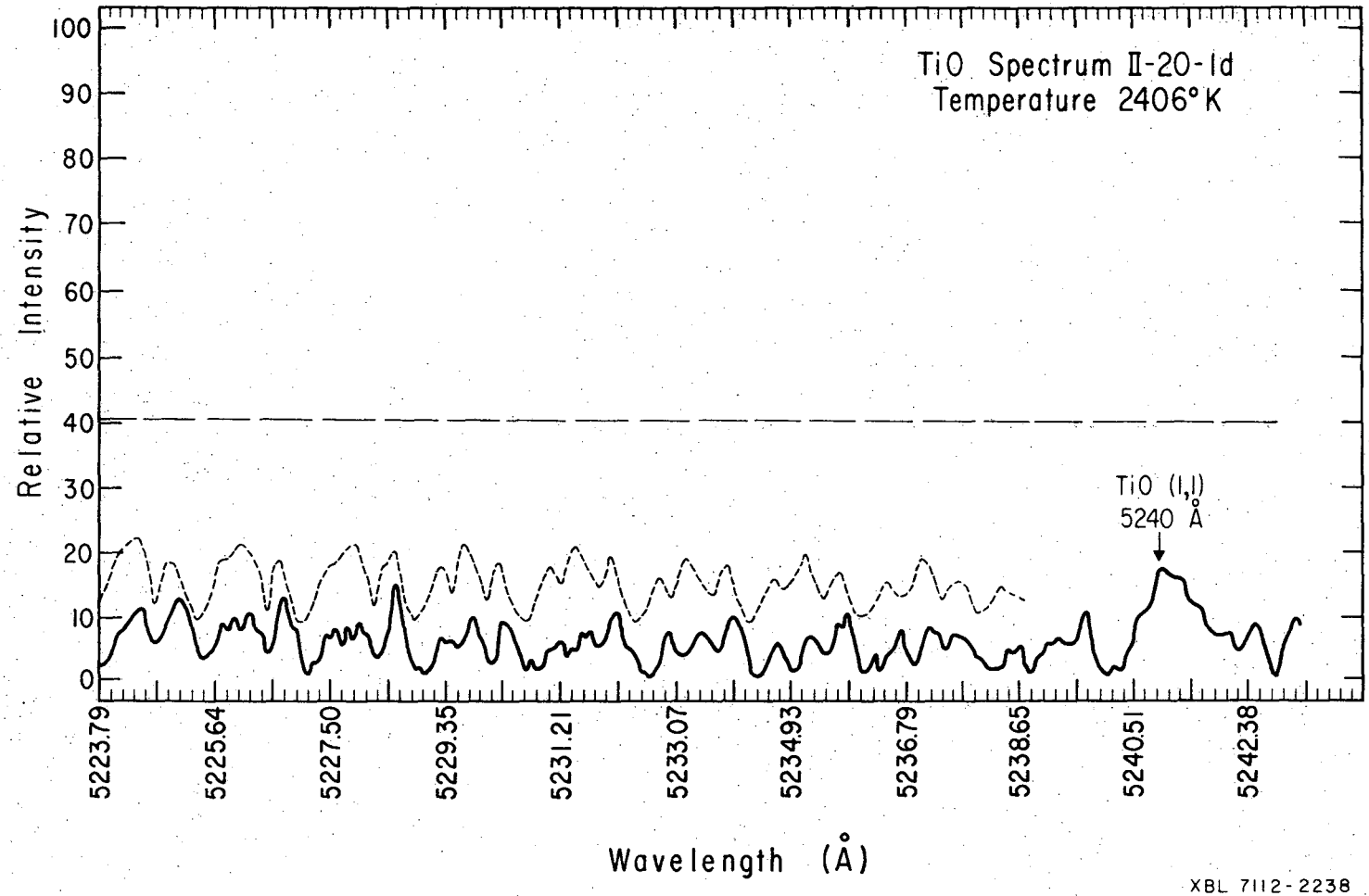

Figure 20 (continued)

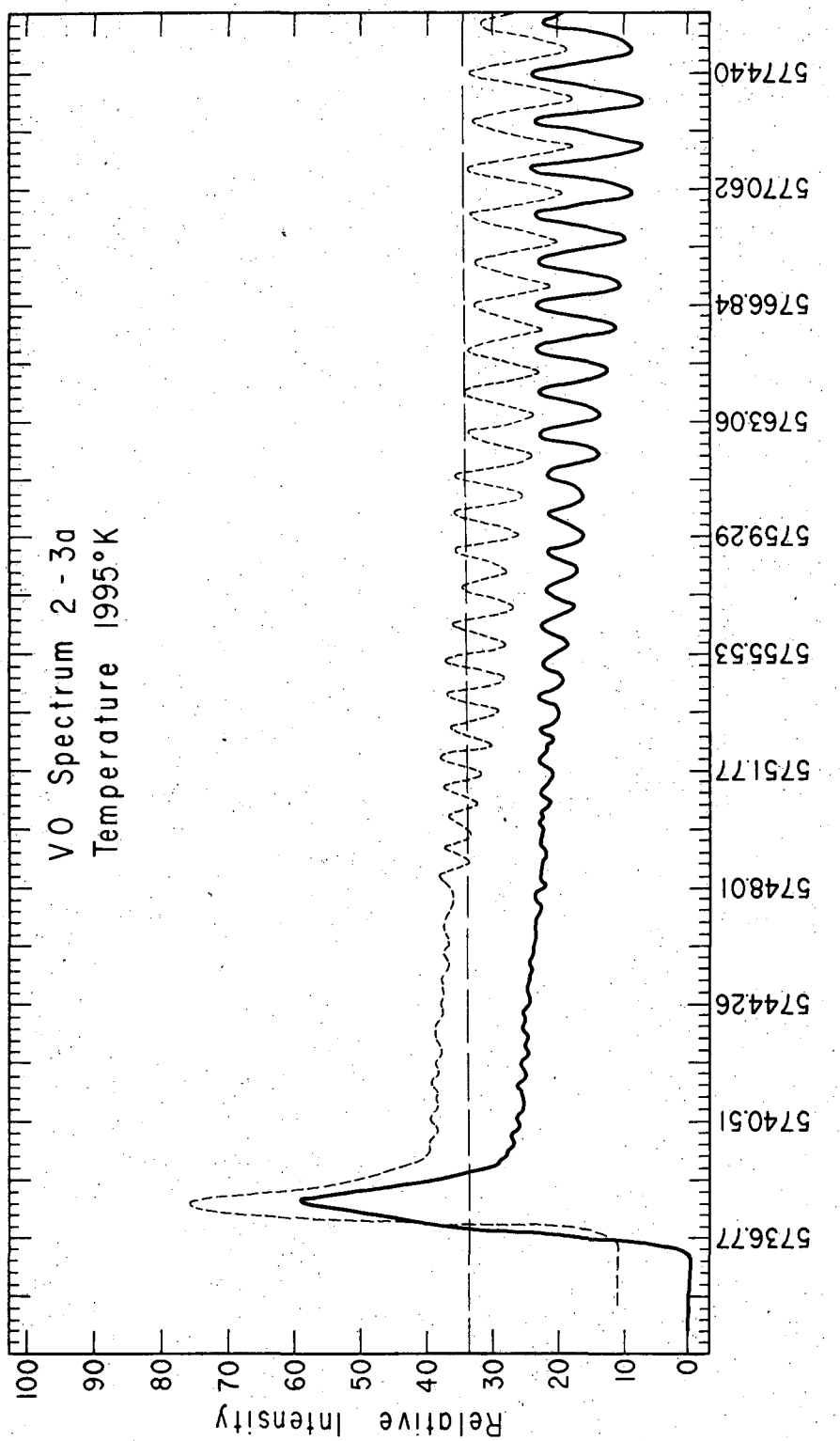
VO Spectrum 2 - 3a
Temperature 1995°K
Relative Intensity
0
10
20
30
40
50
60
70
80
90
100
5736.77
5740.51
5744.26
5748.01
5751.77
5755.53
5759.29
5763.06
5766.84
5770.62
5774.40
Wavelength (Å)
XBL 7112-2247

Figure 21

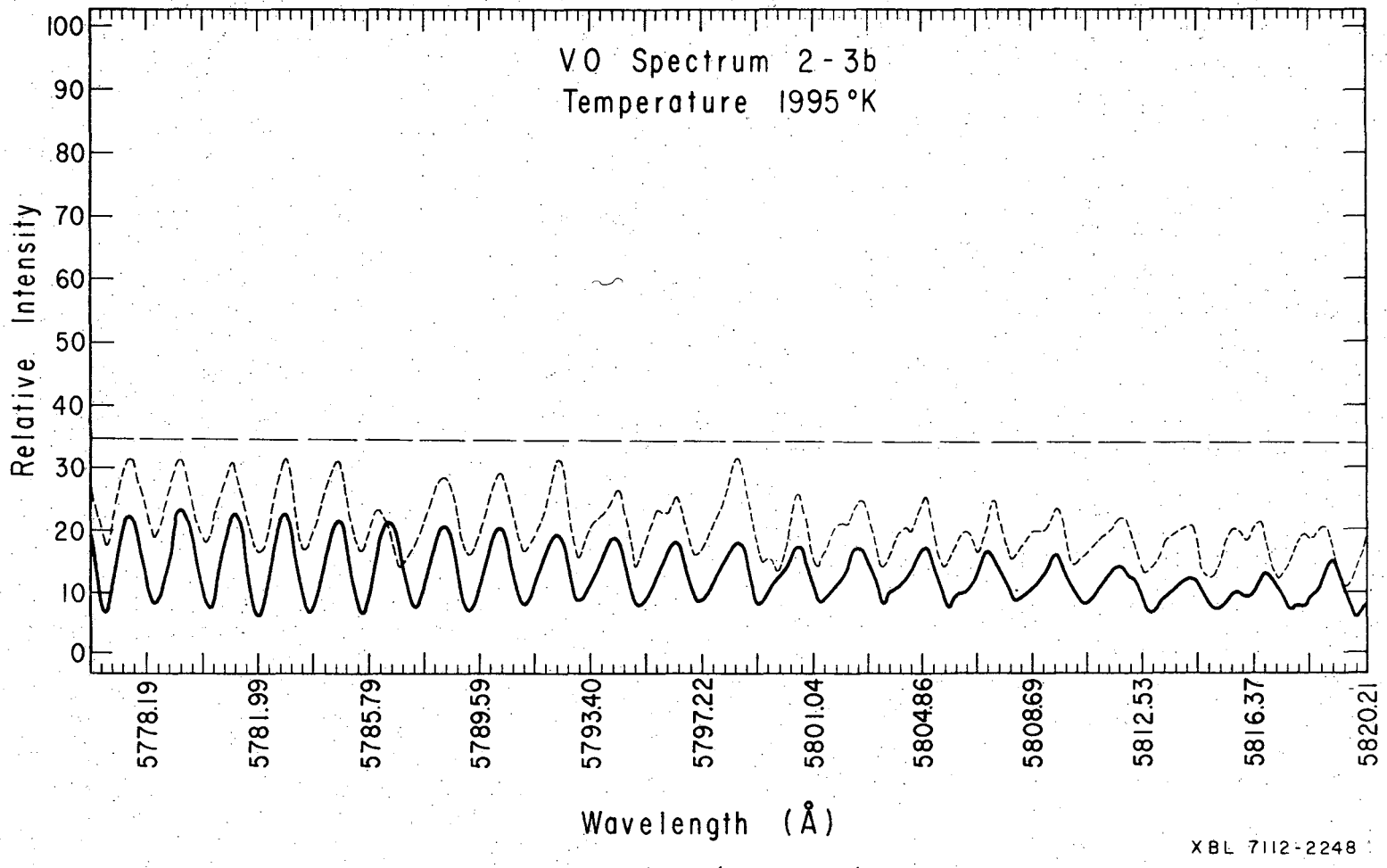

Figure 21 (continued)

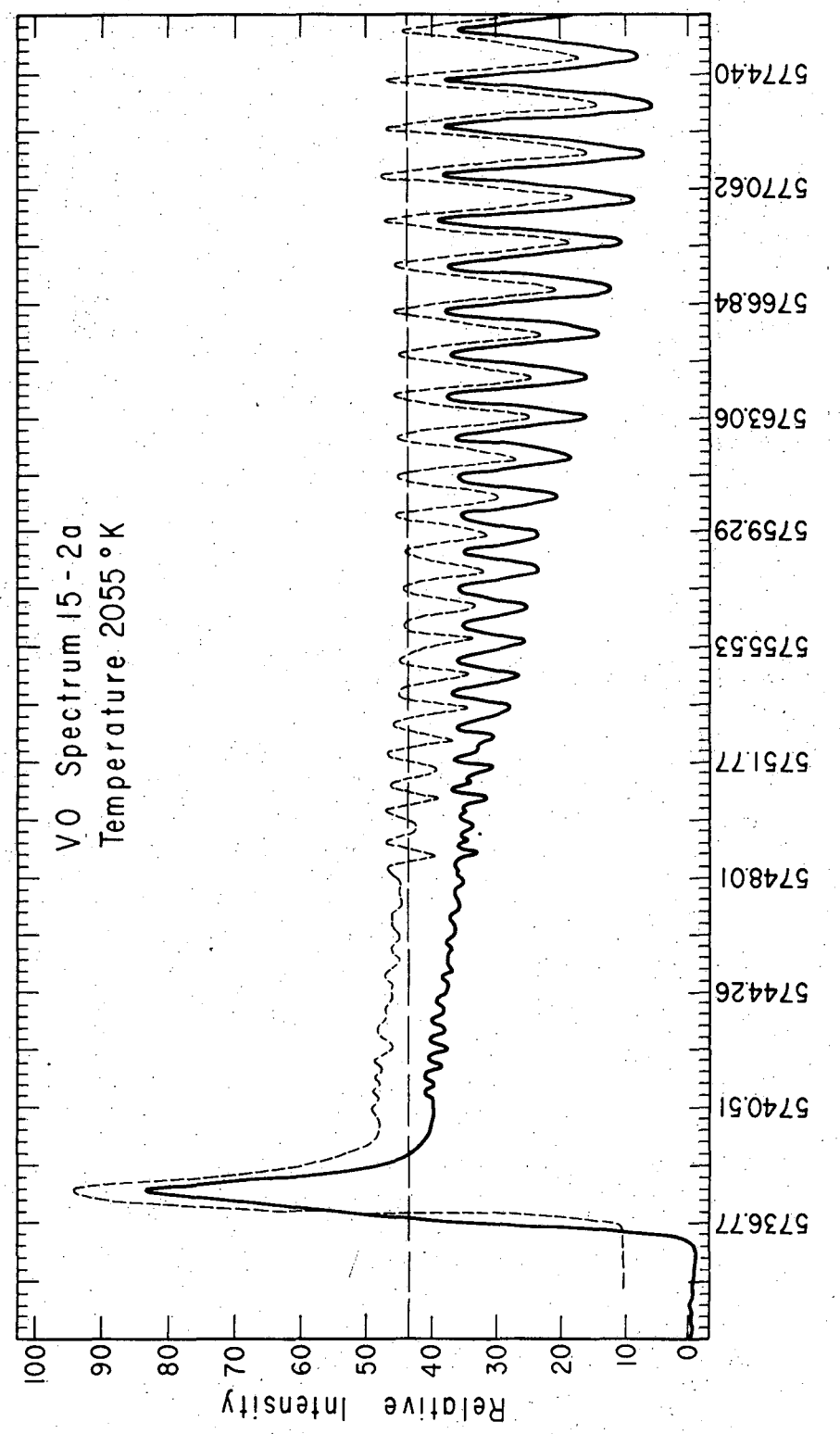
VO Spectrum 15-2a
Temperature 2055 °K
Relative Intensity
0
10
20
30
40
50
60
70
80
90
100
5736.77
5740.51
5744.26
5748.01
5751.77
5755.53
5759.29
5763.06
5766.84
5770.62
5774.40
Wavelength (Å)
XBL 7112-2251

Figure 22

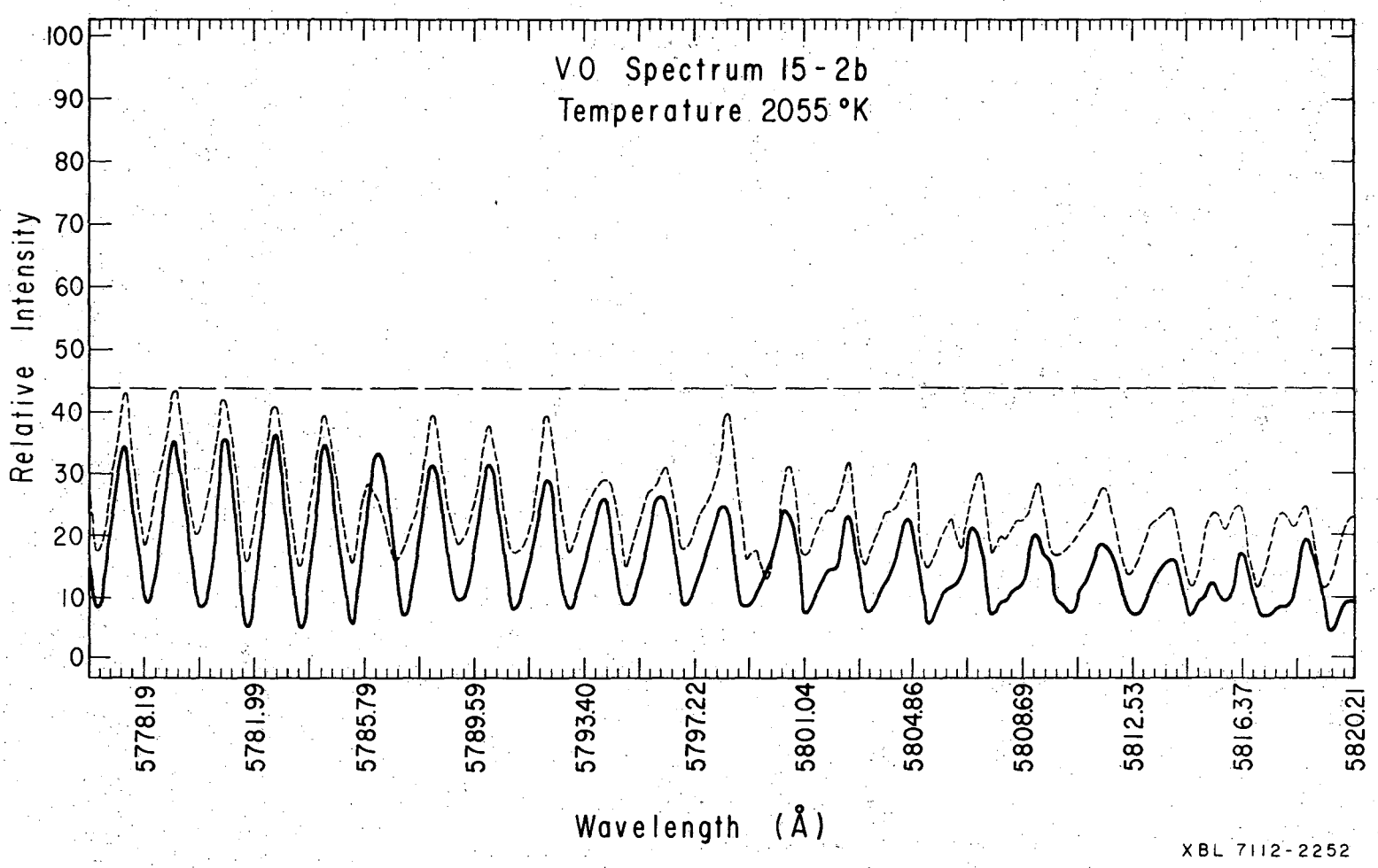

Figure 22 (continued)

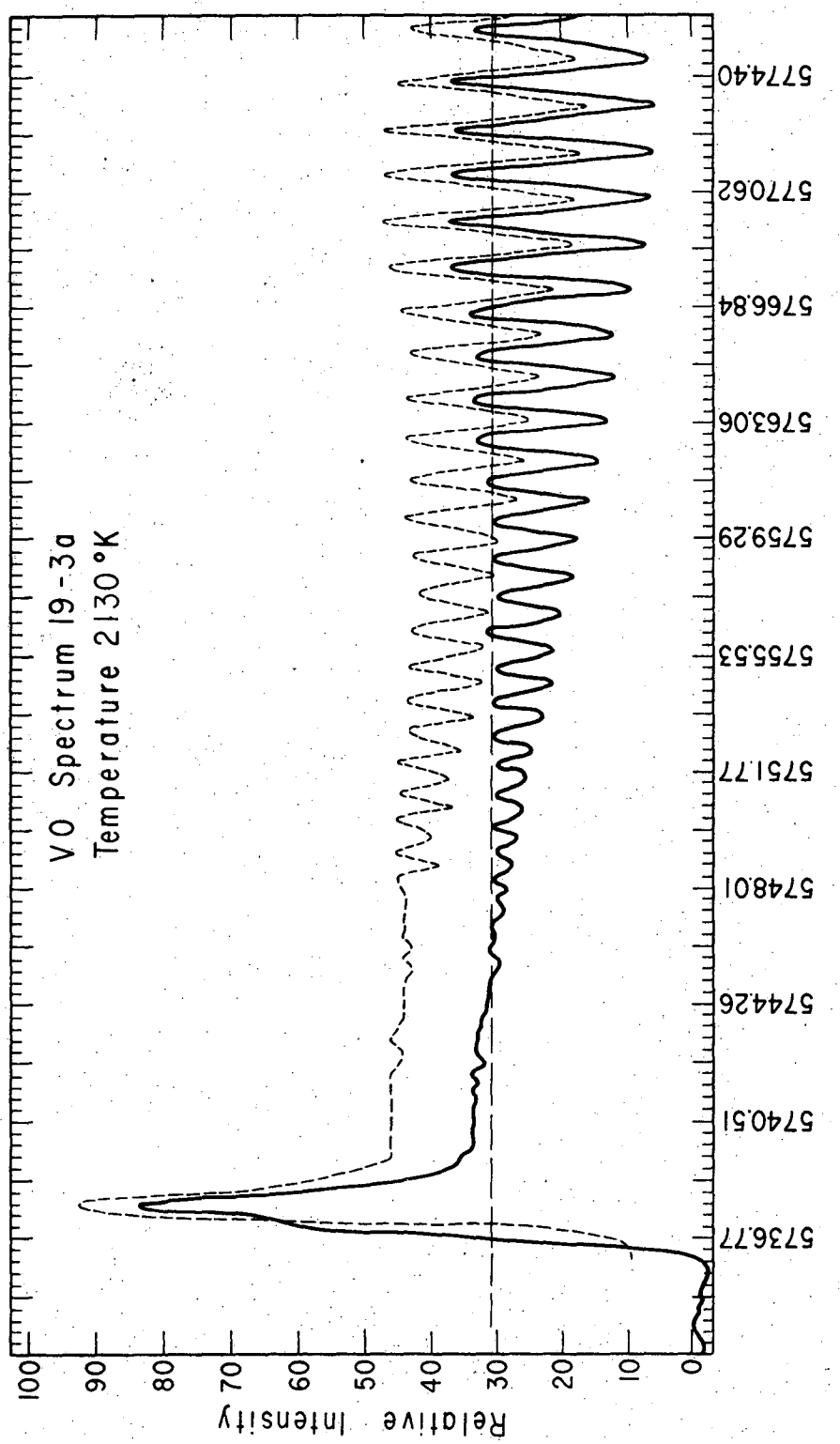
VO Spectrum 19-3a
Temperature 2130 °K
Relative Intensity
100
90
80
70
60
50
40
30
20
10
0
5736.77
5740.51
5744.26
5748.01
5751.77
5755.53
5759.29
5763.06
5766.84
5770.62
5774.40
Wavelength (Å)
XBL 7112-2253

Figure 23

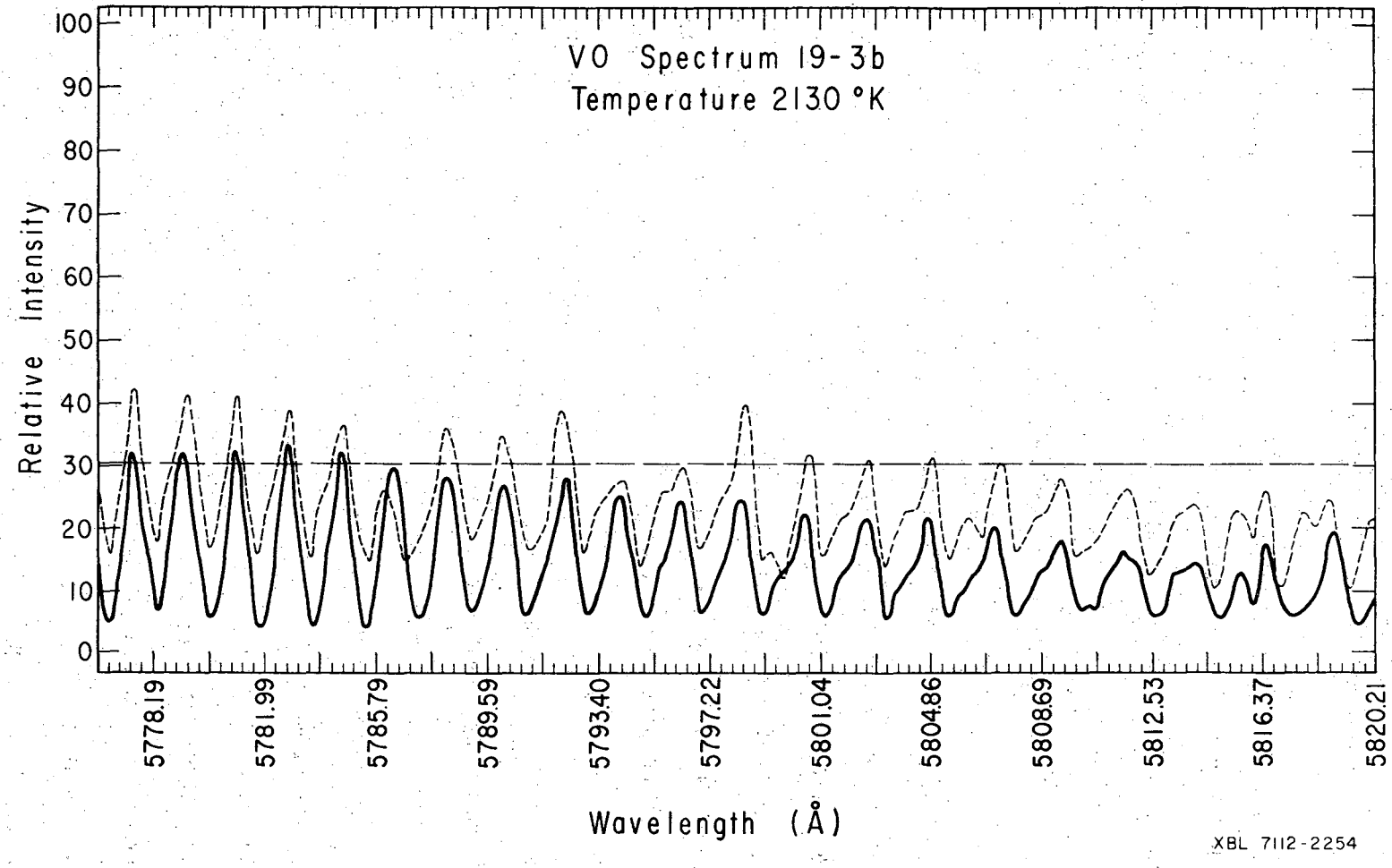

Figure 23 (continued)

VI. DISCUSSION

The vapor pressure of TiO was calculated assuming that the TiO vapor was in thermoequilibrium with the $TiO_{1.6}$ condensed phase. However, the composition of the condensed phase shifts toward the congruent composition (Ti_3O_5 in the solid phase,[74] and between Ti_3O_5-Ti_4O_7 in the liquid phase[87]), when the heating proceeds. The TiO vapor pressure over the solid phase in the range from O/Ti = 1.5 to 1.65 should remain quite steady according to the titanium-oxygen phase diagram (Fig. 11). However the uncertainty in vapor pressure over the liquid phase in such a composition range is present. The vapor pressure of TiO over the liquid phase obtained by extrapolation of the data of the solid phase beyond the melting point should be accurate at the temperatures of this experiment which are only about 100 to 200°K above the melting point. The advantage of using $TiO_{1.6}$ composition lies in the vapor pressure calculation in the previous section. Since the vapor having the maximum proportion of TiO, though not the maximum pressure, arises from the solid composition in the Ti_2O_3 oxygen-rich region (Ti_2O_3 + Ti_3O_5 region). At this composition the vapor pressure of Ti is about the same as that of TiO_2 which has less than ten percent of the vapor pressure of TiO(g). Above more metal rich samples, Ti(g) becomes relatively more important, while above more oxygen rich samples TiO_2(g) becomes relatively more important. Hence, the chosen composition range is the most effective for generating TiO vapor, since it leads to less Ti(g) and TiO_2(g).

The vapor pressures of VO were calculated assuming that the composition of VO in condensed phase changed only slowly when the heating proceeded so that the vapor pressure of VO kept steady for a given temperature during the period of experiment. This assumption might introduce some uncertainty on the calculation of the equilibrium concentration of VO.

The possible source of error due to the composition change during the experiment may be examined by doing a quantitative analysis on the sample residue.[88] It was found that the composition of the condensed phase in the TiO experiment was almost unchanged during the period of experiment. It was difficult to collect clean samples of residue for the VO test as it is necessary to break the heating tube before the residue can be sampled out. In doing so, not only the carbon powder but also the tiny tungsten and tantalum chips will always contaminate the sample residue. However, as reported by Berkowitz et al.,[84] the uncertainty of VO vapor pressure determination due to the change of composition on the VO condensed phase is expected to be very small. This was further proved by the following considerations:

a) The emission radiances of VO vapor which were taken at the same temperature but at different time during the same run did not indicate any sign of decreasing with time.

b) The oscillator strengths of VO calculated from the emission radiances which were taken during the same run, first at a temperature of 2075°K (plate 17), then at a higher temperature of 2130°K (plate 19), and finally at a lower temperature of 2030°K (plate 21) did not indicate the trend of decreasing with time.

At high temperature, the low-lying molecular states are appreciably populated; therefore the precise electronic location of all the excited low-lying molecular states must be known and included in the calculation of the electronic partition function. This is necessary in order to decrease the error when computing the number density of molecules in a certain state. The electronic partition function of TiO was calculated from the electronic states of TiO given by Brewer and Rosenblatt.[16] However, in addition to the states determined by Brewer and Rosenblatt, it is expected that three more molecular states, $^3\Sigma^-$, $^1\Sigma^+$, $^1\Gamma$ from the molecular orbital $d\delta^2$ are low-lying, perhaps in the infrared region. If the $^3\Sigma^-$, $^1\Sigma^+$, $^1\Gamma$ states are included in the calculation of the electronic partition function, the f value of TiO obtained will be higher than that calculated when these three low-lying states are ignored.

The electronic partition function of VO is calculated from the low-lying electronic states of the doubly charged gaseous ion $V^{2+}O^{2-}$ as calculated from the energy levels listed by Moore,[17] since the low-lying electronic states of VO are not well known. This might introduce some error in the determination of the number density of molecules in a specific electronic state because the location of the low-lying electronic states of VO might be somewhat different from those of $V^{2+}O^{2-}$.

At the temperature of this experiment, it is believed that the self-absorption in the emitting gases is negligible for the following reasons:

a) The ratio of the radiance of the most intense feature of the spectrum (i.e. the radiance of the band head) to that of a black body at the same temperature and wavelength is within 0.15 for both TiO and VO. If this ratio is represented by R, then the correction factor, Q, given for monochromatic self-absorption, $Q = -\frac{1}{R}\ln(1 - R)$ by Brewer, Hick and Krikorian[71] is less than 1.075. Here, Q is a factor when it is multiplied by the measured radiance, an "ideal" radiance, a quantity which is directly proportional to the concentration of the emitting state, is obtained. This correction on the band head is clearly not going to seriously affect the results when the total radiance of the whole band is used for calculation.

b) The ratio of the integrated radiance of the whole band to that of a black body at the same temperature and over the same wavelength interval is about 0.03 for TiO and 0.02 for VO. These correspond to no more than 3% correction on the total radiance of a band (compared to the correction factors calculated for the Swan band of C_2 by Hagen[67] and Hick[89]).

c) If self-absorption is appreciable, the observed profile would depart from the theoretical profile more on the features with more intense radiance and less on the features with less intense radiance. However, such a phenomenon is almost undetectable for both TiO and VO spectra (Figs. 12-17 and Figs. 19-21).

Another source of error is due to the determination of the gas temperature. Because of the sufficient number of collisions between the gaseous species and the wall inside the graphite tube, the system can be considered to be in thermoequilibrium during the experiment. Hence, the temperature of the gas can be regarded as the true temperature of the hot zone which is obtained by making the emissivity correction on the brightness temperature of the $TiO_{1.6}$ and the VO condensed phased. However, the presence of temperature gradients within the hot zone of the graphite tube make the determination complicated. The middle of the tube is somewhat hotter than the ends near the buffles. A temperature drop of about 40°K was observed from the tube center to the buffles at around 2500°K. The temperature at the center is used to evaluate the data and the temperature on the buffles is taken as the lower bound. These correspond to a $f_{em} = 0.144$ with 0.205 as the upper bound and a $f_{em} = 0.0058$ with 0.0084 as the upper bound for the TiO (0,0) band α-system and the VO (0,0) band green system respectively. The brightness temperature of the tungsten wall is used as the reference to calculate the absolute integrated radiance of the gas emission.

It is recalled that only those branches (two R and two P branches) analyzed by Lagerqvist and Selin are included in the summation term of Eq.(14) for VO calculation. However, in addition to these lines, Richard and Barrow[28,29] claimed that they have found four more broad line branches, two more R and two more P. As Figs. 19-21 show, not only the trend but also the fine structure of the band in the observed profiles match very well with those of the theoretical profiles which

also include only those branches given by Lagerqvist and Selin. Therefore, the lines claimed by Richard and Barrow must be unable to be resolved from those of Lagerqvist and Selin by our spectrograph. If that is the case, the results of the f_{em} value given for VO must be divided by 2, since we only consider half of the lines in our calculation. The f_{em} should be equal to 0.0029 for the (0,0) band of the VO green system.

The f_{em} value of TiO presented here is about five times larger than that given by Penner et al.[44] from their shock tube experiment. It seems unlikely that the uncertainty of our temperature and concentration determination of the TiO vapor in the present experiment would account for such a discrepancy. A measurement by a concentration independent method would be most valuable to pin down the cause of this discrepancy.

APPENDIX A

Rotational Line Locations of (0,0) Band of TiO α-System and VO Green-System

TiO (0,0) BAND ALPHA SYSTEM HEAD AT 5166.7 Å

J	P1	R1	P2	R2	P3	R3
1	0.	19343.47	0..	19345.52	0.	0.
2	19339.39	19344.17	19341.47	19346.31	0.	0.
3	19338.26	19345.03	19340.17	19340.00	0.	19337.41
4	19336.92	19345.52	19338.87	19347.54	19329.18	19337.90
5	19335.41	19346.15	19337.41	19348.07	19327.76	19338.50
6	19334.07	19346.59	19335.99	19348.48	19326.13	19338.87
7	19332.45	19346.74	19334.30	19348.82	19324.64	19339.38
8	19330.77	19347.00	19332.55	19349.08	19322.74	19339.67
9	19328.94	19347.25	19330.77	19349.12	19320.97	19339.87
10	19327.18	19347.25	19328.94	19349.12	19319.12	19339.87
11	19325.10	19347.25	19326.94	19349.12	19317.19	19339.87
12	19323.06	19347.25	19324.81	19349.08	19315.09	19339.87
13	19320.97	19347.00	19322.61	19348.82	19312.91	19339.67
14	19318.70	19346.74	19320.34	19348.48	19310.60	19339.38
15	19316.40	19346.31	19317.98	19348.07	19308.31	19338.87
16	19313.98	19345.83	19315.52	19347.54	19305.85	19338.50
17	19311.47	19345.29	19312.94	19347.00	19303.40	19337.90
18	19308.93	19344.63	19310.36	19346.31	19300.67	19337.27
19	19306.22	19343.82	19307.64	19345.52	19298.01	19336.47
20	19303.42	19343.00	19304.82	19344.63	19295.25	19335.66
21	19300.62	19342.10	19301.89	19343.69	19292.34	19334.67
22	19297.64	19341.07	19298.90	19342.61	19289.30	19333.70
23	19294.62	19339.87	19295.78	19341.47	19286.25	19332.55
24	19291.47	19338.82	19292.56	19340.17	19283.05	19331.37
25	19288.26	19337.47	19289.30	19338.87	19279.83	19330.09
26	19284.92	19336.02	19285.86	19337.41	19276.46	19328.73
27	19281.52	19334.62	19282.41	19335.98	19273.03	19327.18
28	19278.12	19333.03	19278.85	19334.34	19269.51	19325.69
29	19274.53	19331.37	19275.21	19332.55	19265.87	19323.93
30	19270.81	19329.61	19271.43	19330.77	19262.17	19322.26
31	19267.04	19327.76	19267.56	19328.92	19258.34	19320.34
32	19263.21	19325.84	19263.68	19326.94	19254.47	19318.45
33	19259.27	19323.86	19259.62	19324.81	19250.48	19316.40
34	19255.24	19321.70	19255.49	19322.61	19246.36	19314.29

35	19251.17	19319.50	19251.42	1932.034	19242.26	19312.09
36	19246.92	19317.19	19246.98	19317.98	19237.97	19309.75
37	19242.56	19314.82	19242.59	19315.52	19233.61	19307.38
38	19238.15	19312.30	19238.15	19312.94	19229.11	19304.82
39	19233.61	19309.75	19233.61	19310.36	19224.66	19302.25
40	19229.11	19307.09	19229.04	19307.64	19219.97	19299.58
41	19224.47	19304.32	19224.24	19304.82	19215.25	19296.79
42	19219.68	19301.47	19219.37	19301.89	19210.45	19293.92
43	19214.84	19298.52	19214.44	19298.88	19205.56	19290.96
44	19209.87	19295.50	19209.42	19295.78	19200.57	19287.91
45	19204.87	19292.34	19204.29	19292.57	19195.47	19284.74
46	19199.71	19289.16	19199.08	19289.28	19190.30	19281.52
47	19194.45	19285.84	19193.77	19285.86	19185.02	19278.12
48	19189.14	19282.45	19188.37	19282.41	19179.66	19274.69
49	19183.78	19278.85	19182.90	19278.85	19174.19	19271.21
50	19178.27	19275.23	19177.33	19275.24	19168.66	19267.56
51	19172.69	19271.56	19171.64	19271.43	19163.01	19263.89
52	19167.00	19267.77	19165.88	19267.56	19157.28	19259.98
53	19161.22	19263.89	19160.03	19263.68	19151.46	19256.12
54	19155.34	19259.98	19154.08	19259.62	19145.53	19252.11
55	19149.40	19255.89	19148.04	19255.49	19139.52	19248.05
56	19143.36	19251.70	19141.91	19251.24	19133.44	19243.86
57	19137.21	19247.46	19135.69	19246.92	19127.22	19239.56
58	19130.98	19243.12	19129.35	19242.54	19120.96	19235.18
59	19124.65	19238.69	19122.94	19237.97	19114.52	19230.69
60	19118.22	19234.15	19116.43	19233.40	19108.03	19226.13
61	19111.67	19229.51	19109.83	19228.66	19101.49	19221.43
62	19105.09	19224.73	19103.13	19223.87	19094.82	19216.71
63	19098.40	19219.97	19096.38	19218.97	19088.07	19211.85
64	19091.61	19215.05	19089.52	19213.97	19081.22	19206.90
65	19084.73	19210.02	19082.55	19208.88	19074.30	19201.85
66	19077.75	19204.88	19075.46	19203.71	19067.27	19196.70
67	19070.68	19199.71	19068.28	19198.45	19060.12	19191.47
68	19063.55	19194.45	19061.02	19193.07	19052.89	19186.15
69	19056.27	19189.11	19053.70	19187.58	19045.56	19180.69
70	19048.88	19183.58	19046.25	19182.04	19038.15	19175.17

71	19041.44	19177.98	19038.71	19176.37	19030.58	19169.54
72	19033.86	19172.28	19031.06	19170.63	19023.03	19163.83
73	19026.22	19166.51	19023.34	19164.77	19015.39	19158.00
74	19018.50	19160.64	19015.53	19158.83	19007.61	19152.10
75	19010.71	19154.68	19007.61	19152.84	18999.68	19146.07
76	19002.79	19148.59	18999.68	19146.67	18991.65	19139.95
77	18994.78	19142.43	18991.65	19140.43	18983.62	19133.72
78	18986.69	19136.18	18983.39	19134.08	18975.44	19127.44
79	18978.49	19129.81	18975.13	19127.67	18967.18	19121.01
80	18970.16	19123.36	18966.74	19121.06	18958.84	19114.52
81	18961.74	19116.81	18958.29	19114.52	18950.37	19107.99
82	18953.31	19110.17	18949.68	19107.82	18941.83	19101.25
83	18944.71	19103.39	18941.03	19100.99	18933.16	19094.45
84	18936.03	19096.53	18932.26	19094.06	18924.42	19087.56
85	18927.23	19089.56	18923.40	19087.05	18915.58	19080.55
86	18918.42	19082.57	18914.48	19079.93	18906.67	19073.47
87	18909.38	19075.46	18905.42	19072.72	18897.63	19066.26
88	18900.35	19068.26	18896.31	19065.42	18888.51	19059.02
89	18891.20	19060.87	18887.08	19057.99	18879.30	19051.63
90	18881.94	19053.45	18877.73	19050.54	18869.95	19044.09
91	18872.54	19045.89	18868.30	19042.89	18860.55	19036.47
92	18863.16	19038.17	18858.80	19035.15	18851.05	19028.86
93	18853.63	19030.55	18849.19	19027.37	18841.40	19021.09
94	18844.00	19022.64	18839.47	19019.50	18831.74	19013.22
95	18834.22	19014.77	18829.70	19011.52	18821.94	19005.18
96	18824.41	19006.73	18819.76	19003.45	18812.03	18997.08
97	18814.50	18998.62	18809.76	18995.14	18802.04	0.
98	18804.45	18990.45	18799.68	18986.89	18791.94	18980.60
99	18794.32	18982.04	18789.46	18978.49	18781.76	18972.21
100	18784.12	18973.60	18779.18	18970.07	18771.47	18963.74

VO (0,0) SIGMA-SIGMA TRANSITION

K	RA	PA	RB	PB
1	17419.92	17416.64	17419.92	17416.64
2	17420.80	17415.34	17420.80	17415.34
3	17421.58	17413.93	17421.58	17413.93
4	17422.25	17412.42	17422.25	17412.42
5	17422.81	17410.80	17422.81	17410.80
6	17423.27	17409.07	17423.27	17409.07
7	17423.63	17407.24	17423.63	17407.24
8	17423.88	17405.31	17423.88	17405.31
9	17424.02	17403.27	17424.02	17403.27
10	17424.06	17401.12	17424.06	17401.12
11	17423.99	17398.87	17423.99	17398.87
12	17423.82	17396.51	17423.82	17396.51
13	17423.54	17394.05	17423.54	17394.05
14	17422.92	17394.30	17422.76	17393.99
15	17422.23	17391.78	17422.02	17391.38
16	17421.61	17389.05	17421.15	17388.65
17	17420.81	17386.30	17420.26	17385.87
18	17420.00	17383.44	17419.41	17382.96
19	17418.95	17380.49	17418.32	17380.02
20	17417.81	17377.39	17417.27	17376.92
21	17416.67	17374.12	17415.94	17373.72
22	17415.35	17370.91	17414.61	17370.31
23	17413.96	17367.54	17413.11	17366.86
24	17412.44	17364.05	17411.52	17363.28
25	17410.87	17360.44	17409.93	17359.62
26	17409.08	17356.76	17408.09	17355.95
27	17407.20	17352.93	17406.23	17352.04
28	17405.34	17349.12	17404.24	17348.10
29	17403.23	17345.11	17402.17	17344.06
30	17401.10	17341.00	17399.97	17339.85
31	17398.85	17336.76	17397.67	17335.67
32	17396.49	17332.46	17395.27	17331.27
33	17393.99	17327.97	17392.72	17326.78
34	17391.38	17323.44	17390.09	17322.20
35	17388.65	17318.82	17387.37	17317.50
36	17385.87	17314.10	17384.57	17312.75
37	17382.96	17309.24	17381.61	17307.87
38	17380.02	17304.31	17378.58	17302.81
39	17376.92	17299.21	17375.41	17297.79
40	17373.72	17294.04	17372.13	17292.58
41	17370.31	17288.79	17368.77	17287.23
42	17366.86	17283.34	17365.31	17281.83
43	17363.28	17277.89	17361.74	17376.29
44	17360.00	17272.24	17358.09	17270.70
45	17356.36	17266.51	17354.33	17265.09
46	17352.43	17260.00	17350.41	17259.23
47	17348.43	17255.25	17346.43	17253.26

48	17344.34	17249.15	17342.33	17247.27
49	17340.16	17243.03	17338.11	17241.09
50	17335.94	17241.00	17333.83	17234.84
51	17331.61	17230.47	17329.41	17228.41
52	17327.10	17224.04	17324.88	17221.93
53	17322.45	17217.54	17320.21	17215.00
54	17317.82	17210.90	17315.52	17208.70
55	17312.97	17204.19	17310.72	17201.94
56	17308.14	17197.37	17305.75	17195.09
57	17303.10	17190.46	17300.69	17188.06
58	17298.00	17183.38	17295.52	17181.01
59	17292.80	17176.33	17290.25	17173.90
60	17287.48	17169.10	17284.93	17166.58
61	17282.11	17161.70	17279.43	17159.16
62	17276.54	17154.23	17273.90	17151.63
63	17270.92	17146.68	17268.23	17244.05
64	17265.09	17139.03	17262.45	17136.32
65	17259.23	17131.28	17256.54	17128.56
66	17253.26	17123.40	17250.23	17120.61
67	17247.27	17115.51	17244.46	17112.71
68	17241.09	17107.39	17238.21	17104.57
69	17234.84	17099.36	17231.94	17096.46
70	17228.54	17091.05	17225.58	17088.10
71	17222.10	17082.66	17219.13	17079.70
72	17215.00	17074.21	17212.66	17071.19
73	17208.94	17085.77	17206.36	17062.63
74	17202.29	17057.07	17200.31	17054.08
75	17195.52	17048.33	17191.29	17045.69
76	17188.65	17039.57	17184.48	17037.55
77	17181.72	17030.69	17177.23	17026.41

APPENDIX B

Computer Program Listings

(CDC 6600)

```
      PROGRAM PROTIO(INPUT,CUTPUT)
C     THIS PROGRAM USES THE ACTUAL EXPERIMENTAL LOCATIONS OF THE
C     ROTATICNAL LINES TC CALCULATE AND PLOT THE INTEGRATED INTENSITY
C     PROFILE OF A BAND BY ASSUMING GAUSSIAN LINE SHAPE FCR EVERY
C     ROTATIONAL LINE AND ALSC SUMS THE LINE STRENGTH TIMED BOLTZMAN
C     FACTCR AND WAVENUMBER SQUARE CF THE LINES IN A BANC FOR A GIVEN
C     TEMPERATURE AND RELATIVE ABUNCANCE
C     THE PROGRAM IS WRITTEN FOR THE TRIPLET CELTA-TRIPLET CELTA
C     TITANIUM MCNOXIDE TRANSITICN . HERE, CNLY P AND R BRANCHES ARE
C     CONSIDERED. THE PROGRAM CAN BE EASILY MCCIFIED FOR CTHER TYPE
C     TRANSITION
      DIMENSION SIGP3(2CC),SIGR3(200),SIGP2(200),SIGR2(2CC)
      DIMENSION SIGP1(2CC),SIGR1(200),TITLE(16),WORDS(16),ARRAY(6)
      DIMENSION SR3(2CO),SP3(200),SR2(200),SP2(200),SR1(2CO),SP1(200)
      DIMENSION GRAPH(14C), PRDP1(2CC),PRCP2(200),PRDP3(2CO),PRDR1(200)
      DIMENSION PRDR2(2CC),PRDR3(200),BLTZ(200)
      DATA ARRAY/2HP1,2HR1,2HP2,2HR2,2HP3,2HR3/
      DATA BLANK/4H    /
      READ 14,K42
      READ 5, BLANK,ONE,SYMB
      READ 88, T, ABUND, HFWD, DISP, START, STCP
C     HERE, K42 IS THE MAXIMUM ROTATICNAL QUANTUM NUMBER INVOLVEC
C     IN THE COMPUTATIONS, TEMPERATURE IN DEGREE KELVIN, HALF-WICTH OF
C     LINES IN ANGSTRCNS, DISPERSION IN ANGSTRCNS PER ONE SIXTH INCH,
C     WAVELENGTH START AND STOP IN ANGSTRCNS
      READ 1, (WORDS(I),I =1,16)
      PRINT 2
      PRINT 1, (WORDS(I), I=1,16)
    1 FORMAT (16A5)
    2 FORMAT (1H1)
    5 FORMAT (3A1)
      DO 216 I=1,200
      SIGP1(I)=C.C
      SIGR1(I)=C.C
      SIGP2(I)=C.C
      SIGR2(I)=C.C
      SIGP3(I)=C.C
      SIGR3(I)=C.C
  216 CONTINUE
   12 FORMAT (19X,F8.2,1X,I7,I3,1X,I3,I7,I3,1X,I3,I7,I3,1X,I3)
   14 FORMAT (I4)
   10 READ 12, SIGWVN,MP1,MAR1,MBR1,MP2,MAR2,MBR2,MP3,MAR3,MBR3
      IF (SIGWVN.EQ.0) GO TC 95
   81 IF (MP1.NE.0) SIGP1(MP1)=SIGWVN
   82 IF (MAR1.NE.0) SIGR1(MAR1)=SIGWVN
      IF (MBR1.NE.0) SIGR1(MBR1)=SIGWVN
   83 IF (MP2.NE.0) SIGP2(MP2)=SIGWVN
   84 IF (MAR2.NE.0) SIGR2(MAR2)=SIGWVN
      IF (MBR2.NE.0) SIGR2(MBR2)=SIGWVN
   85 IF (MP3.NE.0) SIGP3(MP3)=SIGWVN
   86 IF (MAR3.NE.0) SIGR3(MAR3)=SIGWVN
      IF (MBR3.NE.0) SIGR3(MBR3)=SIGWVN
   87 GO TO 10
   95 PRINT 15
   15 FORMAT (1HO,103H  J        P1                  R1                  P2
     1                 R2                  P3                  R3//)
```

```
      DO 16 M=1,K42
   16 PRINT 18,M,SIGP1(M),SIGR1(M),SIGP2(M),SIGR2(M),SIGP3(M),SIGR3(M)
   18 FORMAT (I4,F13.2,5F18.2)
   88 FORMAT (6F12.5)
      PRINT 210, T
      PRINT 211, ABUND
      PRINT 212, HFWD
      PRINT 213, DISP
      PRINT 214, START
      PRINT 215, STOP
  210 FORMAT (1H1, 4X,11HTEMPERATURE 7X, F12.5)
  211 FORMAT ( 5X, 9HABUNDANCE 9X, F12.5)
  212 FORMAT (5X, 10HHALF WIDTH 8X, F12.5)
  213 FORMAT (5X, 10HDISPERSION 8X, F12.5)
  214 FORMAT (5X, 14HINITIAL LAMBDA 4X, F12.5)
  215 FORMAT (5X, 12HFINAL LAMBDA 6X, F12.5)
      K43=K42+3
      DO 580 M=1,K43
      BLTZ(M)=EXP(-1.4388*0.4889*M*(M+1)/T)
  580 CONTINUE
      END=10.**8/STOP
      SUMP3=0
      SUMR3=0
      SUMP2=0
      SUMR2=0
      SUMP1=0
      SUMR1=0
C     THE FOLLOWING PART OF THE PROGRAM SUMS THE LINE STRENGTH TIMED
C     BOLTZMAN FACTOR AND WAVENUMBER SQUARE OF THE ROTATIONAL LINES
  700 DO 5C0 M=2,K42
      IF (SIGR3(M+1).LT.END) GO TO 701
      SR3(M+1)=(((M+2)**2-9.0)/(M+2))*BLTZ(M+1)*SIGR3(M+1)**2
      SUMR3=SUMR3+SR3(M+1)
  50C CONTINUE
  7C1 DO 5C1 M=2,K42
      IF (SIGP3(M+2).LT.END) GO TO 702
      SP3(M+2)=(((M+2)**2-9.0)/(M+2))*BLTZ(M+2)*SIGP3(M+2)**2
      SUMP3=SUMP3+SP3(M+2)
  5C1 CONTINUE
  702 DO 5C2 M=1,K42
      IF (SIGR2(M).LT.END) GO TO 703
      SR2(M)=(((M+1)**2-4.0)/(M+1))*BLTZ(M)*SIGR2(M)**2
      SUMR2=SUMR2+SR2(M)
  5C2 CONTINUE
  7C3 DO 5C3 M=1,K42
      IF (SIGP2(M+1).LT.END) GO TO 704
      SP2(M+1)=(((M+1)**2-4.0)/(M+1))*BLTZ(M+1)*SIGP2(M+1)**2
      SUMP2=SUMP2+SP2(M+1)
  503 CONTINUE
  704 DO 5C4 M=1,K42
      IF (SIGR1(M).LT.END) GO TO 705
      SR1(M)=(((M+1)**2-1.0)/(M+1))*BLTZ(M)*SIGR1(M)**2
      SUMR1=SUMR1+SR1(M)
  5C4 CONTINUE
  705 DO 5C5 M=1,K42
      IF (SIGP1(M+1).LT.END) GO TO 706
```

```
      SP1(M+1)=(((M+1)**2-1.0)/(M+1))*BLTZ(M+1)*SIGP1(M+1)**2
      SUMP1=SUMP1+SP1(M+1)
  505 CONTINUE
  706 PRINT 600
  600 FORMAT (1H0,105H  J          SP1                  SR1                  SP2
     1                  SR2                  SP3                  SR3//)
      DO 610 M=1,K42
      PRINT 650,M,SP1(M),SR1(M),SP2(M),SR2(M),SP3(M),SR3(M)
  650 FORMAT (I4,6F18.3)
  610 CONTINUE
  506 SUMT=SUMR3+SUMP3+SUMR2+SUMP2+SUMR1+SUMP1
      PRINT 550,SUMR3,SUMP3,SUMR2,SUMP2,SUMR1,SUMP1,SUMT
  550 FORMAT (1H0,5X,* SUMR3  =  *,F18.3,30X,* SUMP3  =  *F18.3,/
     15X,* SUMR2  =  *,F18.3,30X,* SUMP2  =  *F18.3,/
     25X,* SUMR1  =  *,F18.3,30X,* SUMP1  =  *F18.3,/
     35X,* SUMT   =  *,F18.3)
C     THE FOLLOWING PART OF THE PROGRAM CALCULATES AND PLOTS THE
C     INTEGRATED INTENSITY PROFILE OF A BAND
      DO 100 M = 1,K42
      PRDR3(M+1)=((SIGR3(M+1)/10000.0)**4)*(((M+2)**2-9.0)/(M+2))*
     1BLTZ(M+1)
      PRDP3(M+2)=((SIGP3(M+2)/10000.0)**4)*(((M+2)**2-9.0)/(M+2))*
     1BLTZ(M+2)
      PRDR2(M)=((SIGR2(M)/10000.0)**4)*(((M+1)**2-4.0)/(M+1))*BLTZ(M)
      PRDP2(M+1)=((SIGP2(M+1)/10000.0)**4)*(((M+1)**2-4.0)/(M+1))*
     1BLTZ(M+1)
      PRDR1(M)=((SIGR1(M)/10000.0)**4)*(((M+1)**2-1.0)/(M+1))*BLTZ(M)
  100 PRDP1(M+1)=((SIGP1(M+1)/10000.0)**4)*(((M+1)**2-1.0)/(M+1))*
     1BLTZ(M+1)
      STRTN = 10000000.0/START
      STOPN = 10000000.0/STOP
      SCALE = STRTN/START
      HFWDN = HFWD*SCALE
      DISPN = DISP*SCALE
      DO 561 I11 = 20,100
  561 GRAPH (I11) = ONE
      PRINT 67, (GRAPH(I11), I11 = 20,100)
   67 FORMAT (1H1,1HZ, 18X,81A1)
   68 FORMAT ( 1HZ,18X,81A1)
      KNTLN = 1
      SUMWV = 0.0
      WVNUM = STRTN
  207 DO 91 I21 = 20,100
   91 GRAPH (I21) = BLANK
      DO 101 I31 = 20,100,80
  101 GRAPH (I31) = ONE
      DO 111 I81 = 2,K42
      IF (WVNUM+1.5*HFWDN-SIGP1(I81)) 111,111,121
  121 IF (WVNUM-1.5*HFWDN-SIGP1(I81)) 131,141,141
  131 IF (SIGP1(I81) - WVNUM) 151,161,161
  151 WVINT = WVNUM - SIGP1(I81)
      GO TO 171
  161 WVINT = SIGP1(I81) - WVNUM
  171 GSNP1=(0.93952/HFWDN)*EXP(-2.77309*WVINT**2/HFWDN**2)
      SUMWV=SUMWV+GSNP1*PRDP1(I81)
  111 CONTINUE
```

```
141 DO 112 I82 = 1,K42
    I83 = I82 + 1
    IF (SIGR1(I82).EQ.SIGR1(I83)) GO TO 182
    IF (SIGR1(I82).LT.SIGR1(I83)) GO TO 182
    IF (WVNUM+1.5*HFWDN-SIGR1(I82)) 112,112,122
122 IF (WVNUM-1.5*HFWDN-SIGR1(I82)) 132,142,142
182 IF (WVNUM-1.5*HFWDN-SIGR1(I82)) 192,112,112
192 IF (WVNUM+1.5*HFWDN-SIGR1(I82)) 112,112,132
132 IF (SIGR1(I82) - WVNUM) 152,162,162
152 WVINT = WVNUM - SIGR1(I82)
    GO TO 172
162 WVINT = SIGR1(I82) - WVNUM
172 GSNR1=(0.93952/HFWDN)*EXP(-2.77309*WVINT**2/HFWDN**2)
    SUMWV=SUMWV+GSNR1*PRDR1(I82)
112 CONTINUE
142 DO 113 I83 = 2,K42
    IF (WVNUM+1.5*HFWDN-SIGP2(I83)) 113,113,123
123 IF (WVNUM-1.5*HFWDN-SIGP2(I83)) 133,143,143
133 IF (SIGP2(I83) - WVNUM) 153,163,163
153 WVINT = WVNUM - SIGP2(I83)
    GO TO 173
163 WVINT = SIGP2(I83) - WVNUM
173 GSNP2=(0.93952/HFWDN)*EXP(-2.77309*WVINT**2/HFWDN**2)
    SUMWV=SUMWV+GSNP2*PRDP2(I83)
113 CONTINUE
143 DO 114 I84 = 1,K42
    I85 = I84 + 1
    IF (SIGR2(I84).EQ.SIGR2(I85)) GO TO 184
    IF (SIGR2(I84).LT.SIGR2(I85)) GO TO 184
    IF (WVNUM+1.5*HFWDN-SIGR2(I84)) 114,114,124
124 IF (WVNUM-1.5*HFWDN-SIGR2(I84)) 134,144,144
184 IF (WVNUM-1.5*HFWDN-SIGR2(I84)) 194,114,114
194 IF (WVNUM+1.5*HFWDN-SIGR2(I84)) 114,114,134
134 IF (SIGR2(I84) - WVNUM) 154,164,164
154 WVINT = WVNUM - SIGR2(I84)
    GO TO 174
164 WVINT = SIGR2(I84) - WVNUM
174 GSNR2=(0.93952/HFWDN)*EXP(-2.77309*WVINT**2/HFWDN**2)
    SUMWV=SUMWV+GSNR2*PRDR2(I84)
114 CONTINUE
144 DO 115 I85 = 3,K42
    IF (WVNUM+1.5*HFWDN-SIGP3(I85)) 115,115,125
125 IF (WVNUM-1.5*HFWDN-SIGP3(I85)) 135,145,145
135 IF (SIGP3(I85) - WVNUM) 155,165,165
155 WVINT = WVNUM - SIGP3(I85)
    GO TO 175
165 WVINT = SIGP3(I85) - WVNUM
175 GSNP3=(0.93952/HFWDN)*EXP(-2.77309*WVINT**2/HFWDN**2)
    SUMWV=SUMWV+GSNP3*PRDP3(I85)
115 CONTINUE
145 DO 116 I86 = 2,K42
    I87 = I86 + 1
    IF (SIGR3(I86).EQ.SIGR3(I87)) GO TO 186
    IF (SIGR3(I86).LT.SIGR3(I87)) GO TO 186
    IF (WVNUM+1.5*HFWDN-SIGR3(I86)) 116,116,126
126 IF (WVNUM-1.5*HFWDN-SIGR3(I86)) 136,146,146
```

```
  186 IF (WVNUM-1.5*HFWDN-SIGR3(I86)) 196,116,116
  196 IF (WVNUM+1.5*HFWDN-SIGR3(I86)) 116,116,136
  136 IF (SIGR3(I86) - WVNUM) 156,166,166
  156 WVINT = WVNUM - SIGR3(I86)
      GO TO 176
  166 WVINT = SIGR3(I86) - WVNUM
  176 GSNR3=(0.93952/HFWDN)*EXP(-2.77309*WVINT**2/HFWDN**2)
      SUMWV=SUMWV+GSNR3*PRDR3(I86)
  116 CONTINUE
  146 I41 = 20. + (SUMWV*ABLND)
      IF (I41.GT.105) GO TO 209
      GRAPH (I41) = SYMB
  209 IF (KNTLN.EQ.10) GO TO 201
      PRINT 202, ( GRAPH(I101), I101 = 20,100)
      GO TO 203
  201 REFRN=1+6432.8/10**8+2949810/(146*10**8-WVNUM**2)+
     12554C/(41*10**8-WVNUM**2)
      WVLG=10.**8/REFRN/WVNUM
C     EDLENS FORMULA,J.OPT.SOC.AM.43,339(1953)  IS USED TO CONVERT THE
C     WAVELENGTH (ANGSTROMS) IN AIR TO WAVENUMBER (KAISER) IN VACUUM
      PRINT 204, WVLG, (GRAPH(I101), I101 = 20,100)
  202 FORMAT (1HZ, 18X, 81A1)
  204 FORMAT (1HZ, F15.3, 3X, 81A1)
      KNTLN = 0
  203 KNTLN = KNTLN + 1
      SUMWV = 0.0
      WVNUM = WVNUM - DISPN
      IF (WVNUM - STOPN) 205,205,206
  206 GO TO 207
  205 DO 208 I102 = 20,100
  208 GRAPH (I102) = ONE
      PRINT 68,(GRAPH(I102), I102 = 20,100)
      STOP
      END
```

```
      PROGRAM PROVO (INPUT,CUTPUT)
C     THIS PROGRAM PLOTS THE INTEGRATED PROFILE AND ALSO SUMS THE LINE
C     STRENGTH TIMED BOLTZMAN FACTOR AND WAVENUMBER SQUARE OF THE
C     ROTATIONAL LINES IN A BAND OF QUARTET SIGMA - QUARTET SIGMA ,
C     VANADIUM MONOXIDE TRANSITION.  PARTS OF THE LOCATION OF ROTATIONAL
C     LINES ARE DETERMINED BY LAGERQVIST AND SELIN AND THE REST ARE
C     CALCULATED FROM EQUATIONS BY USING THEIR ROTATIONAL CONSTANT
      DIMENSION WORDS(16),FA2(20),FA1(20),FB2(20),FB1(20)
      DIMENSION SIGPA(200),SIGPB(200),SIGRA(200),SIGRB(200),TITLE(16)
      DIMENSION GRAPH(140),PRDPA(200),PRDPB(200),PRDRA(200),PRDRB(200)
      DIMENSION BLTZ(200),ARRAY(6),SPA(200),SPB(200),SRA(200),SRB(200)
      DATA ARRAY/2HPA,2HRA,2HPB,2HRB/
      DATA BLANK/4H    /
      READ 999,K42
      READ 998, BLANK,ONE,SYMB
   40 READ 5, SIGMA,SIGMB,VPR,VDPR
   42 READ 1, (WORDS(I),I=1,16)
      PRINT 2
      PRINT 1,(WORDS(I),I=1,16)
      READ 3, B1,D1,H1,B2,D2,H2
      READ 4, W1,W1X1,W1Y1,W1Z1,W2,W2X2,W2Y2,W2Z2
      PRINT 6
      PRINT 8, B1,B2
      PRINT 9, D1,D2
      PRINT 10,H1,H2
      PRINT 12,W1,W2
      PRINT 13, W1X1,W2X2
      PRINT 14, W1Y1,W2Y2
      PRINT 15, W1Z1,W2Z2
      PRINT 25, SIGMA
      PRINT 26, SIGMB
      DO 216 I=1,200
      SIGPA(I)=0.0
      SIGPB(I)=0.0
      SIGRA(I)=0.0
      SIGRB(I)=0.0
  216 CONTINUE
      VPR1=VPR+0.5
      VDPR1=VDPR+0.5
      HUGE=W1*VPR1-W1X1*VPR1**2+W1Y1*VPR1**3-W1Z1*VPR1**4-W2*VDPR1
     1+W2X2*VDPR1**2-W2Y2*VDPR1**3+W2Z2*VDPR1**4
      K43=K42+3
      DO 17 K=1,14
      FA2(K)=B2*K*(K+1)-D2*K**2*(K+1)**2+H2*K**3*(K+1)**3
      FB2(K)=B2*K*(K+1)-D2*K**2*(K+1)**2+H2*K**3*(K+1)**3
      FA1(K)=B1*K*(K+1)-D1*K**2*(K+1)**2+H1*K**3*(K+1)**3
      FB1(K)=B1*K*(K+1)-D1*K**2*(K+1)**2+H1*K**3*(K+1)**3
   17 CONTINUE
      FA2(0)=0.0
      FB2(0)=0.0
      DO 18 K=1,13
      SIGPA(K)=SIGMA+HUGE+FA1(K)-FA2(K+1)
      SIGPB(K)=SIGMB+HUGE+FB1(K)-FB2(K+1)
   18 CONTINUE
      DO 19 K=1,13
      SIGRA(K)=SIGMA+HUGE+FA1(K)-FA2(K-1)
```

```
      SIGRB(K)=SIGMB+HUGE+FB1(K)-FB2(K-1)
   19 CONTINUE
      K43=K42+3
      DO 2C K=14,K43
      READ 7,K,SIGRA(K),SIGPA(K),SIGRB(K),SIGPB(K)
      IF (K.EQ.C) GO TO 22
   2C CONTINUE
   22 PRINT 11
      DO 23 K=1,K42
   23 PRINT 7,K,SIGRA(K),SIGPA(K),SIGRB(K),SIGPB(K)
      GO TC 43
    1 FORMAT (16A5)
    2 FORMAT (1H1)
    3 FORMAT (2(F9.C,2E9.C))
    4 FORMAT (8F9.0)
    5 FORMAT (2F1C.2,2F4.C)
    6 FORMAT (1HO,34H        UPPER STATE     LCWER STATE//)
    7 FORMAT (I5,4(4X,F8.2))
    8 FORMAT (3H B   6X, 2(F10.5, 6X))
    9 FORMAT (2H D 7X, 2(1PE10.3, 6X))
   10 FORMAT (2H H 7X, 2(1PE10.3, 6X))
   11 FORMAT (1HO,49H   J        RA           PA           RB           PB/)
   12 FORMAT (3H WE  6X,F10.3,  6X, F10.3)
   13 FORMAT (5H WEXE 4X, F10.3,  6X, F10.3)
   14 FORMAT (5H WEYE 4X, F10.3, 6X, F10.3)
   15 FORMAT (5H WEZE 4X, F10.3, 6X, F10.3)
   25 FORMAT (6H SIGEA 1CX, F12.3)
   26 FORMAT (6H SIGEB 1CX, F12.3)
  998 FORMAT (3A1)
  999 FORMAT (I4)
   43 READ 88, T, ABUND,HFWD,DISP, START, STOP
C     HERE, K42 IS THE MAXIMUM ROTATIONAL QUANTUM NUMBER INVOLVED
C     IN THE COMPUTATIONS, TEMPERATURE IN DEGREE KELVIN, HALF-WIDTH OF
C     LINES IN ANGSTROMS, DISPERSION IN ANGSTROMS PER ONE SIXTH INCH,
C     WAVELENGTH START AND STOP IN ANGSTROMS
   88 FORMAT (6F12.5)
      PRINT 210, T
      PRINT 211, ABUND
      PRINT 212, HFWD
      PRINT 213, DISP
      PRINT 214, START
      PRINT 215, STOP
  210 FORMAT (1H1, 4X,11HTEMPERATURE 7X, F12.5)
  211 FORMAT ( 5X, 9HABUNDANCE 9X, F12.5)
  212 FORMAT (5X, 1CHHALF WIDTH 8X, F12.5)
  213 FORMAT (5X, 1CHDISPERSICN 8X, F12.5)
  214 FORMAT (5X, 14HINITIAL LAMBDA 4X, F12.5)
  215 FORMAT (5X, 12HFINAL LAMBDA 6X, F12.5)
      DO 58C M=1,K43
      BLTZ(M)=EXP(-1.4388*0.4889*M*(M+1)/T)
  58C CONTINUE
      ENC=1C.**8/STOP
      SUMPA=0
      SUMRA=0
      SUMPB=0
      SUMRB=0
```

```
C      THE FOLLOWING PART OF THE PROGRAM SUMS THE LINE STRENGTH TIMED
C      BOLTZMAN FACTOR AND WAVENUMBER SQUARE OF THE ROTATIONAL LINES
  700  DO 500 M=1,K42
       IF (SIGRA(M).LT.END) GO TO 701
       SRA(M)=M*BLTZ(M)*SIGRA(M)**2
       SUMRA=SUMRA+SRA(M)
  500  CONTINUE
  701  DO 501 M=1,K42
       IF (SIGPA(M).LT.END) GO TO 702
       SPA(M)=(M+1)*BLTZ(M)*SIGPA(M)**2
       SUMPA=SUMPA+SPA(M)
  501  CONTINUE
  702  DO 502 M=1,K42
       IF (SIGRB(M).LT.END) GO TO 703
       SRB(M)=M*BLTZ(M)*SIGRB(M)**2
       SUMRB=SUMRB+SRB(M)
  502  CONTINUE
  703  DO 503 M=1,K42
       IF (SIGPB(M).LT.END) GO TO 704
       SPB(M)=(M+1)*BLTZ(M)*SIGPB(M)**2
       SUMPB=SUMPB+SPB(M)
  503  CONTINUE
  704  PRINT 600
  600  FORMAT (1HO,70H   J          SPA                  SRA                  SPB
     1                  SRB//)
       DO 610 M=1,K42
       PRINT 650,M,SPA(M),SRA(M),SPB(M),SRB(M)
  650  FORMAT (I4,4F18.3)
  610  CONTINUE
  506  SUMT=SUMRA+SUMPA+SUMRB+SUMPB
       PRINT 550,SUMRA,SUMPA,SUMRB,SUMPB,SUMT
  550  FORMAT (1HO,5X,* SUMRA  =  *,F18.3,30X,* SUMPA  =  *F18.3,/
     15X,* SUMRB  =  *,F18.3,30X,* SUMPB  =  *F18.3,/
     25X,* SUMT   =  *,F18.3)
C      THE FOLLOWING PART OF THE PROGRAM CALCULATES AND PLOTS THE
C      INTEGRATED INTENSITY PROFILE OF A BAND
       DO 620 M=1,K42
       PRDPA(M)=((SIGPA(M)/10000.0)**4)*(M+1)*BLTZ(M)
       PRDRA(M)=((SIGRA(M)/10000.0)**4)*M*BLTZ(M)
       PRDPB(M)=((SIGPB(M)/10000.0)**4)*(M+1)*BLTZ(M)
       PRDRB(M)=((SIGRB(M)/10000.0)**4)*M*BLTZ(M)
  620  CONTINUE
       STRTN = 1000000C0.0/START
       STOPN = 100C000C0.0/STOP
       SCALE = STRTN/START
       HFWDN = HFWD*SCALE
       DISPN = DISP*SCALE
       DO 561 I11 = 20,1C0
  561  GRAPH (I11) = ONE
       PRINT 67, (GRAPH(I11), I11 = 2C,100)
   67  FORMAT (1H1,1HZ, 18X,81A1)
   68  FORMAT ( 1HZ,18X,81A1)
       KNTLN = 1
       SUMWV = 0.0
       WVNUM = STRTN
  2C7  DO 91 I21 = 20,10C
```

```
 91 GRAPH (I21) = BLANK
    DO 101 I31 = 20,100,80
101 GRAPH (I31) = ONE
    DO 111 I81=1,K42
    IF (WVNUM+1.5*HFWDN-SIGPA(I81)) 111,111,121
121 IF (WVNUM-1.5*HFWDN-SIGPA(I81)) 131,141,141
131 IF (SIGPA(I81)-WVNUM) 151,161,161
151 WVINT=WVNUM-SIGPA(I81)
    GO TO 171
161 WVINT=SIGPA(I81)-WVNUM
171 GSNPA=(0.93952/HFWDN)*EXP(-2.77309*WVINT**2/HFWDN**2)
    SUMWV=SUMWV+GSNPA*PRDPA(I81)
111 CONTINUE
141 DO 112 I82 = 1,K42
    I83 = I82 + 1
    IF (SIGRA(I82).EQ.SIGRA(I83)) GO TO 182
    IF (SIGRA(I82).LT.SIGRA(I83)) GO TO 182
    IF (WVNUM+1.5*HFWDN-SIGRA(I82)) 112,112,122
122 IF (WVNUM-1.5*HFWDN-SIGRA(I82)) 132,142,142
182 IF (WVNUM-1.5*HFWDN-SIGRA(I82)) 192,112,112
192 IF(WVNUM+1.5*HFWDN-SIGRA(I82)) 112,112,132
132 IF (SIGRA(I82)-WVNUM) 152,162,162
152 WVINT=WVNUM-SIGRA(I82)
    GO TO 172
162 WVINT=SIGRA(I82)-WVNUM
172 GSNRA=(0.93952/HFWDN)*EXP(-2.77309*WVINT**2/HFWDN**2)
    SUMWV=SUMWV+GSNRA*PRDRA(I82)
112 CONTINUE
142 DO 113 I83=1,K42
    IF (WVNUM+1.5*HFWDN-SIGPB(I83)) 113,113,123
123 IF (WVNUM-1.5*HFWDN-SIGPB(I83)) 133,143,143
133 IF (SIGPB(I83)-WVNUM) 153,163,163
153 WVINT=WVNUM-SIGPB(I83)
    GO TO 173
163 WVINT=SIGPB(I83)-WVNUM
173 GSNPB=(0.93952/HFWDN)*EXP(-2.77309*WVINT**2/HFWDN**2)
    SUMWV=SUMWV+GSNPB*PRDPB(I83)
113 CONTINUE
143 DO 114 I84 = 1,K42
    I85 = I84 + 1
    IF (SIGRB(I84).EQ.SIGRB(I85)) GO TO 184
    IF (SIGRB(I84).LT.SIGRB(I85)) GO TO 184
    IF (WVNUM+1.5*HFWDN-SIGRB(I84)) 114,114,124
124 IF (WVNUM-1.5*HFWDN-SIGRB(I84)) 134,146,146
184 IF (WVNUM-1.5*HFWDN-SIGRB(I84)) 194,114,114
194 IF (WVNUM+1.5*HFWDN-SIGRB(I84)) 114,114,134
134 IF (SIGRB(I84)-WVNUM) 154,164,164
154 WVINT=WVNUM-SIGRB(I84)
    GO TO 174
164 WVINT=SIGRB(I84)-WVNUM
174 GSNRB=(0.93952/HFWDN)*EXP(-2.77309*WVINT**2/HFWDN**2)
    SUMWV=SUMWV+GSNRB*PRDRB(I84)
114 CONTINUE
146 I41 = 20. + (SUMWV*ABLND)
    IF (I41.GT.105) GO TO 209
    GRAPH (I41) = SYMB
```

```
  209 REFRN=1+6432.8/10**8+2949810/(146*10**8-WVNUM**2)+
     12554C/(41*10**8-WVNUM**2)
      WVLG=10.**8/REFRN/WVNUM
      IF (KNTLN.EQ.10) GO TO 201
      PRINT 202, (GRAPH(I1C1),I101=2C,100),WVLG,I41
C     EDLENS FORMULA,J.OPT.SOC.AM.43,339(1953)  IS USED TO CONVERT THE
C     WAVELENGTH (ANGSTROMS) IN AIR TO WAVENUMBER (KAISER) IN VACUUM
      GO TO 203
  201 PRINT 204, WVNUM,(GRAPH(I101),I101=20,100),WVLG,I41
  202 FORMAT (1HZ, 18X, 81A1,5X,F10.3,5X,I4)
  204 FORMAT (1HZ, F15.3,3X,81A1,5X,F10.3,5X,I4)
      KNTLN = 0
  203 KNTLN = KNTLN + 1
      SUMWV = 0.0
      WVNUM = WVNUM - DISPN
      IF (WVNUM - STOPN) 205,205,206
  206 GO TO 207
  205 DO 208 I102 = 2C,1CC
  208 GRAPH (I1C2) = CNE
      PRINT 68,(GRAPH(I1C2), I102 = 20,100)
      STOP
      ENC
```

Input Data for Figures 15-23

TiO

Plate	Temp. (°K)	Abundance	Half Width (Å)	Dispersion (Å/ $\frac{1}{6}$ inch)	Initial Wavelength (Å)	Final Wavelength (Å)
I-30-3	2152	0.0590	0.72	0.37587	5165.0	5245.0
I-26-2	2237	0.070	0.72	0.37587	5165.0	5245.0
I-34-3	2323	0.0575	0.72	0.37587	5165.0	5245.0
II-22-1	2292	0.053	0.41	0.1810	5165.0	5245.0
II-25-1	2328	0.052	0.41	0.1810	5165.0	5245.0
II-20-1	2406	0.046	0.40	0.1810	5165.0	5245.0

VO

2-3	1995	0.095	0.65	0.3735	5735.0	5822.0
15-2	2055	0.125	0.645	0.3735	5735.0	5822.0
19-3	2130	0.120	0.650	0.3735	5735.0	5822.0

ACKNOWLEDGEMENTS

I am deeply grateful to Professor Leo Brewer for directing my graduate research training and for guiding this work. The opportunity for exposure to his broad and deep scientific insight and perspective has been exciting. I have profitted very much from many discussions with him. It has been really a great pleasure to work with him under his charming personality.

I am indebted to all of the members of the research group with whom I have had the chance to exchange ideas about research. Their acquaintance has enhanced my experience as a graduate student.

I wish to thank Professor Sumner P. Davis and Professor John G. Phillips for their kind and helpful advice and for the use of their equipment.

I owe special thanks to my wife, Judy, for typing the manuscript of the thesis and for her understanding, encouragement and patience during my graduate studies. Finally I wish to thank my parents for their concern in every respect from the day I was born. It was their sacrifice over my past years that made my studies toward an advanced degree possible.

This research was performed under the auspices of the United States Atomic Energy Commission.

REFERENCES

1. A. Christy, Phys. Rev. 33, 701 (1929).
2. F. Lowater, Proc. Phys. Soc. 41, 557 (1929).
3. J. G. Phillips, Astrophys. J. 114, 152 (1951).
4. A. Budo, Z. Physik 96, 219 (1935).
5. U. Uhler, Dissertation, University of Stockholm, Sweden (1954).
6. J. G. Phillips, Astrophys. J. 157, 449 (1969).
7. J. G. Phillips, Astrophys. J. 111, 314 (1950).
8. P. P. Dobronravin, C. R. Acad. Sic. U.S.S.R. 17, 399 (1937).
9. K. Wurm and H. J. Meister, Z. Astrophys. 13, 199 (1937).
10. A. V. Pettersson, Ark. Fys. 16, 185 (1959).
11. A. V. Pettersson and B. Lindgren, Ark. Fys. 22, 491 (1962).
12. C. M. Pathak and H. B. Palmer, J. Mol. Spect. 33, 137 (1970).
13. N. S. McIntyre, K. R. Thompson and W. Weltner, Jr., J. Phys. Chem. 75, 3243 (1971).
14. L. Brewer and D. W. Green, High Temp. Sci. 1, 26 (1969).
15. C. K. Jorgensen, Mol. Phys. 7, 417 (1964).
16. L. Brewer and G. Rosenblatt, Advances in High Temperature Chemistry Vol. 2 (Academic Press, New York and London, 1969), p. 1.
17. C. E. Moore, Atomic Energy Levels Vol. 1, National Bureau of Standards Circular 467, 1949.
18. L. Brewer and D. F. Mastick, J. Am. Chem. Soc. 73, 2045 (1951).
19. G. Herzberg, Spectra of Diatomic Molecules (D. Van Nostrand Company, Inc., Princeton, New Jersey, 1950).

20. I. Kovacs, Rotational Structures in the Spectra of Diatomic Molecules (Adam Hilger LTD, London, 1969).

21. R. de L. Kronig, Z. Physik 50, 347 (1928).

22. J. H. Van Vleck, Physic. Rev. 33, 467 (1929).

23. R. Mecke, Phys. Z. 28, 514 (1927).

24. W. F. C. Ferguson, Bur. Stand. J. Res. Wash. 8, 382 (1932).

25. P. C. Mahanti, Proc. Phys. Soc. London 47, 433 (1935).

26. A. Lagerqvist and L. E. Selin, Ark. Fys. 12, 553 (1957).

27. K. D. Carlson and C. Moser, J. Chem. Phys. 44, 3259 (1966).

28. D. Richards and R. F. Barrow, Nature 217, 842 (1968).

29. D. Richards and R. F. Barrow, Nature 219, 1244 (1968).

30. P. H. Kasai, J. Chem. Phys. 49, 4979 (1968).

31. P. C. Keenan and L. W. Schroeder, Astrophys. J. 115, 82 (1952).

32. A. Lagerqvist and L. E. Selin, Ark. Fys. 11, 429 (1957).

33. E. W. Foster, Rept. Prog. Phys. 27, 469 (1964).

34. R. G. Bennett, Rev. Sci. Instr. 31, 524 (1963).

35. R. J. Wolff, (Ph.D. Thesis), University of California, Berkeley (1967).

36. R. J. Wolff and S. P. Davis, J. Opt. Soc. Am. 48, 490 (1968).

37. L. Brewer, C. G. James, R. G. Brewer, F. E. Stafford, R. A. Berg and G. Rosenblatt, Rev. Sci. Instr. 33, 1450 (1962).

38. L. Brewer, R. A. Berg and G. Rosenblatt, J. Chem. Phys. 38, 1381 (1963).

39. A. Chutjian, J. Link and L. Brewer, J. Chem. Phys. 46, 2666 (1967).

40. P. T. Cunnunghan, (Ph.D. Thesis), University of California, Berkeley, UCRL-18419 (Nov. 1968).

41. G. M. Lawrence, J. Quant. Spectrosc. Radiat. Transfer 5, 359 (1965).

42. N. R. Tawde and P. V. Chandratreya, Ind. J. Phys. 29, 388 (1955).

43. J. A. Harrington, A. P. Modica and D. R. Libby, J. Chem. Phys. 44, 3380 (1966).

44. M. L. Price, K. G. P. Sulzmann and S. S. Penner, J. Quant. Spectrosc. Radiat. Transfer 11, 427 (1971).

45. L. Brewer, W. T. Hicks and O. H. Krickorian, J. Chem. Phys. 36, 182 (1962).

46. L. Brewer and L. G. Hagen, to be published.

47. J. G. Phillips, Astrophys. J. 118, 274 (1953).

48. P. A. Fraser, W. R. Jarmain and R. W. Nicholls, Astrophys. J. 118, 286 (1953).

49. E. Hutchisson, Phys. Rev. 36, 410 (1930).

50. F. S. Ortenberg, Optics and Spectros. 9, 80 (1960).

51. P. A. Fraser and W. R. Jarmain, Proc. Phys. Soc. A66, 1145 (1953).

52. S. S. Prasad, Proc. Phys. Soc. 79, 1078 (1962).

53. S. S. Prasad, Proc. Phys. Soc. 82, 419 (1963).

54. C. Linton and R. W. Nicholls, J. Phys. B2, 490 (1969).

55. C. Linton and R. W. Nicholls, J. Quant. Spectrosc. Radiat. Transfer 10, 311 (1970).

56. S. S. Prasad, Ind. J. Phys. 37, 457 (1963).

57. N. S. Murthy, T. K.S. Setty and K. V. Sumathi, Indian J. Phys. 38, 428 (1964).

58. R. Ladenberg and F. Reiche, Ann. Physik 42, 181 (1913).

59. A. Einstein, Physik Z. 18, 121 (1917).

60. C. W. Allen, Astrophysical Quantities, 2nd Ed., (Oxford Univ. Press, New York, 1963).

61. R. Mulliken, J. Chem. Phys. 7, 14 (1939).

62. J. B. Tatum, Astrophys. J. Suppl. Ser. XVI (124), 21 (1967).

63. M. Born and R. Oppenheimer, Ann. Physik 84, 457 (1927).

64. U. Condon and G. H. Shorley, The Theory of Atomic Spectra (Cambridge University Press, Cambridge, 1951).

65. A. C. Mitchell and M. W. Zemansky, Resonance Radiation and Excited Atoms (Cambridge University Press, New York, 1961), pp. 94, 170.

66. L. Brewer, P. W. Gilles and F. A. Jenkins, J. Chem. Phys. 16, 797 (1948).

67. L. G. Hagen, (Ph.D. Thesis), University of California, Berkeley, UCRL-10620 (March 1963).

68. The International Practical Temperature Scale of 1968, Metrotogia 5, 35 (1969).

69. T. B. Douglas, J. Research NBS 73A, 451 (1969).

70. F. H. Morgan, J. Appl. Physics 22, 108 (1951).

71. L. Brewer, W. T. Hicks and O. H. Krikorian, J. Chem. Phys. 36, 182 (1962).

72. W. O. Groves, M. Hock and H. L. Johnston, J. Phys. Chem. 59, 127 (1955).

73. J. Berkowitz, W. A. Chupka and M. G. Inghram, J. Phys. Chem. 61, 1569 (1957).

74. P. J. Hampson and P. W. Gilles, J. Chem. Phys. 55, 3712 (1971).

75. P. G. Wahlbeck and P. W. Gilles, J. Am. Ceram. Soc. 49, 180 (1966).

76. D. R. Stull and H. Prophet, JANAF Thermochemical Tables, Second Edition, NSRDS-NBS-37, U.S. Govt. Printing Office, Washington, D.C.

77. G. N. Lewis, M. Randall, K. S. Pitzer and L. Brewer, Thermodynamics 2nd ed., McGraw-Hill, New York (1961).

78. J. G. Phillips, Private communication.

79. W. Jevous, Report on Band-Spectra of Diatomic Molecules, (Cambridge University Press, Cambridge, Engl., 1932), p. 134.

80. R. A. Sawyer, Experimental Spectroscopy, (Prentice-Hall, New York, 1946).

81. H. G. Beutler, J. Opt. Soc. Am. 35, 311 (1945).

82. O. H. Krikorian, (Ph.D. Thesis), University of California, Berkeley, UCRL-2888 (April 1955).

83. W. Rostoker and A. S. Yamamoto, Trans. ASM, 47, 1002 (1955).

84. J. Berkowitz, W. A. Chupka and M. G. Inghram, J. Chem. Phys. 27, 87 (1957).

85. R. L. Orr, J. Am. Chem. Soc. 76, 857 (1954).

86. K. S. Rao, Ind. J. Phys. 27, 368 (1953).

87. P. W. Gilles, H. F. Franzen, G. D. Stone, and P. G. Wahlbeck, J. Chem. Phys. 48, 1938 (1968).

88. W. F. Hillebrand, G. E. F. Lundell, H. A. Bright and J. I. Hoffman, Applied Inorganic Analysis, 2nd ed., (John Wiley & Sons, Inc., New York, 1955).

89. W. T. Hicks, (Ph.D. Thesis), University of California, Berkeley, UCRL-3696 (Feb. 1957).

TECHNICAL INFORMATION DIVISION
LAWRENCE BERKELEY LABORATORY
UNIVERSITY OF CALIFORNIA
BERKELEY, CALIFORNIA 94720